PARP inhibitors in combination with chemotherapeutics target the underlying genetic phenotype of Ewing's sarcoma and osteosarcoma to induce cell death or synthetic lethality

Dissertation

zur Erlangung des Doktorgrades

der Naturwissenschaften

vorgelegt beim Fachbereich Biochemie, Chemie und Pharmazie

der Johann Wolfgang Goethe-Universität

in Frankfurt am Main

von

Florian Engert

aus Heppenheim

Frankfurt 2016

(D30)

vom Fachbereich 14 der

Johann Wolfgang Goethe - Universität als Dissertation angenommen.

Dekan: Prof. Dr. Michael Karas

Erster Gutachter: Prof. Dr. Volker Dötsch

Zweiter Gutachter: Prof. Dr. Simone Fulda

Datum der Disputation:

Table of Contents

Abstract

Recently, two of the most common types of bone cancers in children and young adults have been proven to exhibit vulnerability to poly(ADP)-ribose polymerase, (PARP) inhibitors (e.g. olaparib, talazoparib). Ewing's sarcoma (ES) are reported to harbor a fusion gene *EWS-FLI1* (85%), inducing tumorigenesis. Additional, as the fusion gene acts as aberrant transcription factor, it similarly induces elevated PARP expression levels sensitizing ES to PARP inhibition. Second, by an exome sequencing approach in a set of primary osteosarcomas (OS) we identified mutation signatures being reminiscent of BRCA deficiency. Therefore, the sensitivity of a panel of OS cell lines to either talazoparib single treatment or in combination with several chemotherapeutic drugs was investigated.

To screen ES tumor cell lines against PARP inhibitors we applied four different PARP inhibitors (talazoparib, olaparib, niraparib and veliparib) that are frequently being used for clinical studies. We combined those PARP inhibitors with a set of chemotherapeutics (temozolomide (TMZ), SN-38, etoposide, ifosfamide, doxorubicin, vincristine and actinomycin D) that are part of the first-line therapy of ES patients. Here, we demonstrate how PARP inhibitors synergize with TMZ or SN-38 to induce apoptosis, whereas the combination of PARP inhibitors with the other drugs are not favorable. By investigation of key checkpoints in the molecular mechanisms of cell death, the pivotal role of the mitochondrial pathway of apoptosis mediating the synergy between olaparib and TMZ was revealed.

Employing talazoparib monotherapy in combination with or without several chemotherapeutic drugs (TMZ, SN-38, cisplatin, doxorubicin, methotrexate and etoposide/carboplatin), the correlation between homologous recombination (HR) repair deficiency (BRCAness) and the response to talazoparib as prototypical PARP inhibitor was validated in different OS cell lines. By calculation of combination indices (CI) and fraction affected (Fa) values, we identified TMZ as the most potent chemotherapeutic drug in combination with talazoparib inducing the mitochondrial apoptotic pathway in OS.

In our studies of two independent tumor entities with contrary genetic background we identified the combination of PARP inhibitor and TMZ as being most effective. Our studies point out that after TMZ induced DNA methylation and concomitant PARP trapping, DNA damage-imposed checkpoint kinase activation consequently induces G_2-cell cycle arrest. Subsequent, PARP inhibitor/TMZ causes MCL-1 degradation, followed by activation of BAK and BAX, succeeding in loss of mitochondrial outer membrane potential (LMMP) and activation of downstream effector-caspases in mitochondrial apoptosis. Our findings emphasize the importance of PARP inhibition in order to chemosensitize ES, which express high PARP levels, or OS that bear features of BRCAness.

I Introduction

I.1 Cancer

Cancer is a collection of various diseases that is able to occur in every part of the human body. Main features of cancer cells are their ability to undergo uncontrolled growth, to break their resident growth in a controlled tissue environment and to evade cell death. In 2011, Hanahan and Weinberg termed ten different critical hallmarks leading to and fostering cancer (Figure 1, (1)). One of the hallmarks is enhanced proliferation. Cancer cells ensure their proliferative capabilities by excessive production of growth signals in an autocrine manner or by stimulating the tumor associated stroma in order to excrete growth factors, which lead to tumor growth and to a collapse of normal tissue function, homeostasis and architecture (2,3). Another hallmark is the ability of cancer cells to evade growth suppression. Two of the most important tumor suppressors are the retinoblastoma 1 (RB1) and tumor protein 53 (p53) protein that are important regulators of two crucial cellular programs, which decide between proliferation, senescence or cell death (4,5). Healthy cells stop cell cycle progression upon high doses of radiation, for instance, whereas cancer cells keep cycling, often due to mutation of p53 (6). Two further hallmarks by which cancer cells create a niche for preferable survival are masking against the immune system (7) and creating an inflammatory microenvironment (8,9). Furthermore, cancer cells interact with adjacent tissue or the host body, respectively, where they induce angiogenesis in order to ensure nutrient and oxygen supply and cancer cells are able to undergo epithelial-mesenchymal transition, EMT, leading to invasion and metastasis (10–12). Moreover, tumor cells harbor the ability to enable replicative immortality by activating telomerases, specialized DNA polymerases that add telomere repeat segments to the DNA (13,14). In healthy cells, telomere ends shorten by every cell cycle guiding to a point in which they are no longer able to conserve the chromosomal DNA, finally leading to a high number of end-to-end fusions that culminate in senescence and apoptosis (13,15). Genomic instability and mutations are further characteristics in tumorigenesis. Tumors which harbor such genomic alterations often carry a selection advantage in contrast to the healthy tissue environment and the growth of adjacent cells (16,17). Resistance to cell death, especially apoptosis, is another key feature of cancer cells. It is accompanied by upregulation of antiapoptotic BCL-2 family proteins, such as BCL-2, BCL-X_L or MCL-1. These changes in the expression of antiapoptotic BCL-2 family proteins promote cancer cells' survival when exposed to physiological stresses during tumorigenesis (18). Deregulation of cellular energetics with the ability to change glucose metabolism in favor of glycolysis and to generate energy under hypoxic conditions also supports tumor persistence (19). Taken together, not only one, but often a combination of various cancer hallmarks lead to malignancy.

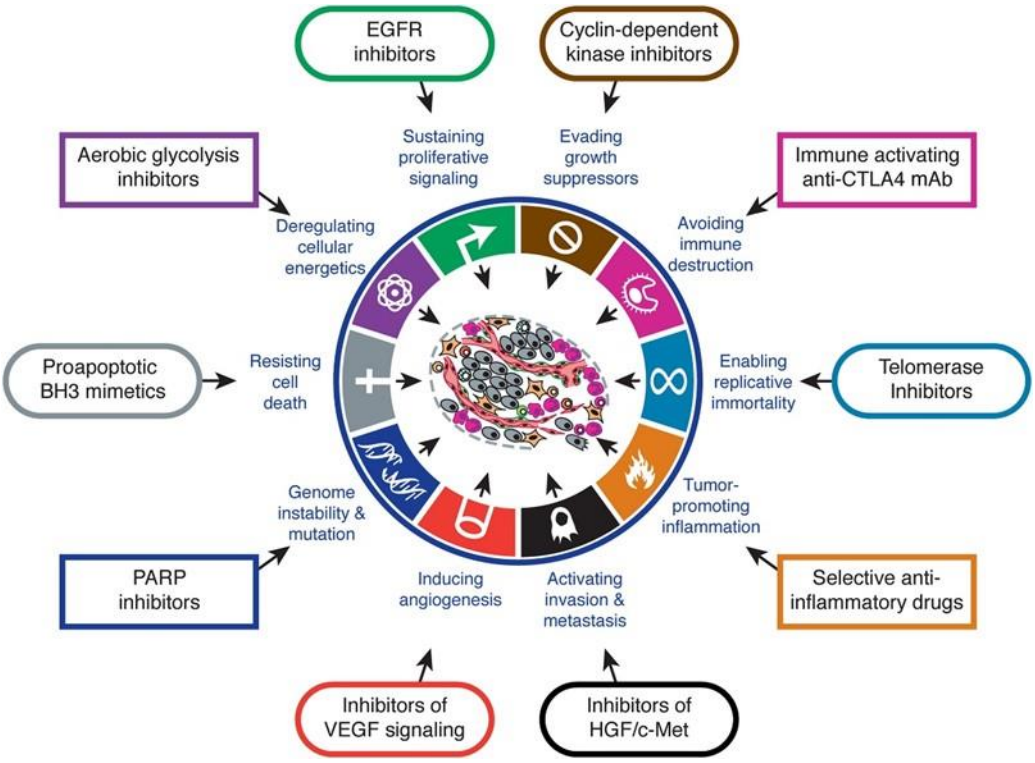

Figure 1: Hallmarks of cancer.

In tumor development ten different hallmarks are described, which play an important role for tumorigenesis and support tumor persistence. The most promising pharmacological treatment options to overcome a given hallmark and fight cancer are displayed; figure adapted from (1).

I.1.1 Ewing's sarcoma

Ewing's sarcoma (ES), first described by James Ewing in the year 1921 (20), is the second most common primary bone tumor in children and young adults with an incidence of about 3 new cases in 1 000 000 per year (21). It is prevalent in the Caucasian population with a slight predominance in males (22). The tumor origin is yet not fully understood, nevertheless is believed to be originated from mesenchymal stem/progenitor cells (23). Treatment of ES is difficult since its tendency to form metastases in early stages, preferable in the lungs, bone and bone marrow (22). Besides surgery and irradiation, treatment of Ewing's sarcoma consists of classical chemotherapy most often containing VIDE (vincristine, irinotecan, doxorubicin and etoposide) and temozolomide (22,24). Five-year survival rates range from 75% for patients with local tumors to 30% for patients with metastases (25). ES and peripheral primitive neuroectodermal tumor (pPNET) belong to the Ewing's sarcoma family of tumor (ESFT), which are characterized by a chimeric fusion protein (26). In 85% of the cases this fusion protein originates from a translocation of the chromosome 11 and 22 creating the *EWS-FLI1* fusion gene t(11;22)(q24:q12) (27). The second most common chromosome translocation (10%) is found between chromosome 21 and 22 leading

to the *EWS-ERG* fusion gene t(21;22)(q22;q12) (28). The chimeric fusion protein functions as an aberrant transcription factor disturbing the cell metabolism leading to oncogenic transformation (29,30). In 2012, Garnett *et al.* foremost implicated that there might be a vulnerability of Ewing's sarcoma against PARP inhibitors, unless their BRCA wildtype status (31). Later, Brenner *et al.* could clearly demonstrate the association between the chimeric fusion protein EWS-FLI1 and EWS-ERG, respectively and *PARP1* mRNA expression levels (32). In a *EWS-FLI1* positive xenograft model, they did show a convincing reduction of tumor volume upon PARP inhibition (olaparib) and TMZ treatment. Yet, the underlying molecular mechanisms still remained elusive (32).

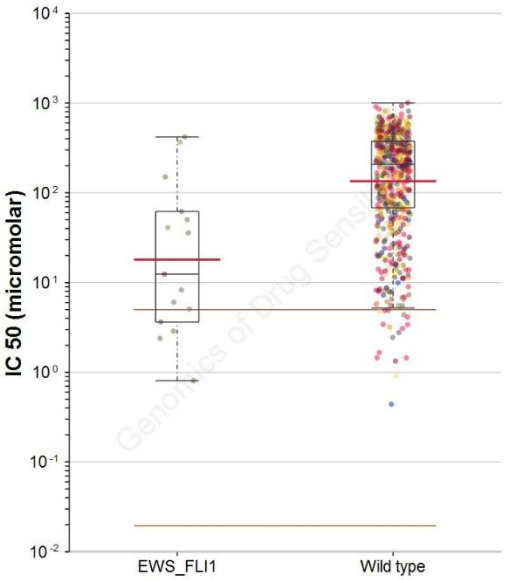

Figure 2: IC_{50} scatter plot of 648 human cell lines treated with olaparib.

Cell lines carrying the *EWS-FLI1* fusion gene are significantly more sensitive to olaparib than wild type cells. Figure was created online (33).

I.1.1.1 Ewing's sarcoma cell lines

Obtaining ES cell lines from primary samples follows a general procedure: After surgical resection the patient biopsy is mechanically reduced, rinsed and plated into complete culture media under humidified and sterile settings at 37 °C and 5% CO_2 (34). Under these conditions ES cell lines form an adherent cell monolayer. Importantly, the previous mentioned chimeric fusion proteins can also be found in the ES cell lines A4573 and SK-ES-1 (full list in Table 7), making them a perfect model for studying pharmacological treatment possibilities for Ewing's sarcoma patients (35,36).

I.1.2 Osteosarcoma

Osteosarcoma (OS) is the most common form of primary bone cancer in children and young adults with an incidence of about 30 in 1 000 000 per year (37). It shows a slight elevated risk for boys with a taller physique (38). OS arises from mesenchymal cells and the emergence peaks at the age of 15-19 years (23). The massive demand for optimizing the treatment options for OS patients is because, approximately 15-20% of patients have metastasis developed at the time of diagnosis, most commonly found in the lung. Micro-metastases that can evolve 6-36 months after diagnosis, further urges treatment optimization (39). Current disease management incorporates surgery and combinational chemotherapy of doxorubicin, cisplatin and methotrexate (MTX), which leads to a cure in about 70% of the patients (40). However the five-year survival rates is less than 30% in patients who already have metastases (41). Most frequently

somatic mutations, likewise in *TP53* and *RB1* are reported for OS (42–44). Despite the general genomic instability, osteosarcoma also demonstrates a high frequency (33%) of chromothripsis (45), a catastrophic incident resulting in massive genomic rearrangements and chromosome remodeling, and around 50% of all osteosarcomas show patterns of localized hypermutations, named kataegis (44). Summarizing, OS shows few targetable overlapping mutations, and current trials of targeted compounds have overall been disappointing (37). Recently, by performing exome sequencing we showed that osteosarcomas harbor features of BRCAness (46), defects in the HR pathway either due to direct *BRCA1/2* gene mutation or due to BRCA-associated gene mutations in *PTEN*, *ATM*, *CHEK2* or *BARD1,* for instance, which might lead to sensitivity against PARP inhibitors (47). Precisely, we showed that on average a representative OS carries 17 mutations in BRCA genes and their central interaction partners (e.g. *FANCD2*, *CHEK2* or *ATM*) (46). Nonetheless, this does not rule out the general view of OS as being a monoclonal expansion of an initial *TP53* mutant cell, but elucidates how the vulnerability to chromosomal damage is persistent and suspects OS to be sensitive towards PARP inhibition, as we investigated in the present study (46).

I.1.2.1 Osteosarcoma cell lines

The creation of OS cell lines follows the procedure as explained above (48). Cells grow adherently as a cell monolayer. About 42% of the OS cell lines show a loss of the tumor suppressor gene *CDKN2A/B* and *TP53* mutation in about 47% of all OS cell lines (49,50). Every OS cell lines tested in the present study, revealed a differential homologous recombination mutational profile, providing a suitable model system for investigating the vulnerability to PARP inhibition (Table 1). Homologous recombination deficiency (HRD)-loss of heterozygosity (LOH) score is a DNA-based measure of genomic instability describing BRCAness (51).

Table 1: List of osteosarcoma cell lines with their characteristic genetic background.

Cell Line	HRD-LOH	Ploidy	Mutational profile	Talazoparib IC_{50}
MG63	positive	triploid	*BAP1* ↓, *FANCA* ↓, *FANCD2* ↓	0.448 µM
ZK-58	positive	diploid	*BARD1* ↓, *FANCD2* ↑	0.115 µM
SaOS-2	borderline	triploid	*TP53* ↓, *CHEK2* ↓	33.57 µM
MNNG-HOS	positive	triploid	*ATM* ↓, *PTEN* ↑, *FANCD2* ↑	87.56 µM
U2OS	negative	diploid or tetraploid	*TP53* ↓, *BRCA2* ↓	> 100 µM

Homologous recombination deficiency - loss of heterozygosity (HRD-LOH) score indicating BRCAness, copy-number alterations (losses ↓, disruptive gains ↑), IC_{50} values of OS cell lines determined by MTT assay and SigmaPLOT™

I.2 Programmed Cell Death

Programmed cell death (PCD) comprises apoptosis, autophagy and necroptosis (programmed necrosis) (52). The purpose of PCD is to manage tissue homeostasis and to eliminate cells bearing fatal damages, thereby restricting cancer (1). Main forms of PCD can be easily distinguished by their morphological features: Type I programmed cell death, called apoptosis, is characterized by cell shrinkage, nuclear condensation, DNA fragmentation, loss of membrane integrity and the loss of cell adhesion (53). Autophagy, or type II PCD, respectively, can be characterized by the formation of autophagosomes, that are double membrane structures capsuling macromolecules and cell organelles targeting them for recycling (54). Type III PCD is termed programmed necrosis, further assigned as necroptosis, involves cell swelling, dysfunction of cell organelles and cell lysis (52). Besides the three main forms of PCD additionally, a lot of rather unknown and scarcely explored forms of cell death exist, e.g. parthanatos and ferroptosis (55). Parthanatos takes place after a decrease of NAD^+ and ATP levels and is dependent on PARP as executioner (56), whereas ferroptosis is often pharmacologically induced and results in decreased levels of glutathione (57). Both pathways lead to dysregulation of redox homeostasis and finally culminate in necroptosis (55).

I.2.1 Apoptosis

Apoptosis covers the intrinsic, mitochondrial pathway and the extrinsic, death receptor mediated pathway. Intrinsic apoptosis, triggered for example by DNA damage, and extrinsic apoptosis, triggered for instance by growth factor withdrawal, both culminate in the activation of caspases (58,59). Caspases are cysteine proteases subdivided into initiator and executioner caspases. Initiator caspases, such as caspase-9 form protein platforms that cleave, regulate and thereby activate downstream executioner caspases-3 and -7, further promoting the apoptotic process (52). A tightly regulated process called MOMP (mitochondrial outer membrane permeabilization), upstream of caspase-9 processing determines whether a cell undergoes apoptosis (60). As MOMP is considered to be the point of no return in apoptosis, it is excessively regulated by the BCL-2 family of proteins, which regulate how strong a cell is primed to death (61,62). A cell, which is highly primed to death needs lower levels of stress stimuli, for instance DNA damage, whereas a non-primed cell is able to cope with a high amount of DNA damage (63). The BCL-2 protein family exhibit distinct molecular features: multi-domain proapoptotic, multi-domain antiapoptotic and BH3-only proapoptotic proteins (64). The first group covers BAK, BAX and BOK, which undergo conformational changes upon activation and regulate/induce pore formation within the outer mitochondrial membrane, subsequently leading to release of apoptosis inducing factors from the mitochondria (60,65). The antiapoptotic BCL-2 proteins are BCL-2, BCL-X_L, MCL-1, BCL-W and A1 (60). One

of their main function is to bind to the pore forming proapoptotic proteins as well as to BH3-only proteins (60,65). The more BH3-only proteins are bound, the less the cell is primed for apoptosis (61,62,66). Upon binding to BAK and BAX they block pore formation, MOMP and therefore induction of apoptosis (65). Counteracting the antiapoptotic BCL-2 proteins, BH3-only proteins can bind to all multi domain BCL-2 proteins (67,68). They can be subdivided into activators, such as BID, BIM and PUMA, which are directly able to bind BAK and BAX and into sensitizers, for example NOXA, BMF and HRK, which sequester antiapoptotic BCL-2 proteins, then releasing BAK and BAX (61,68). Pore formation leads to release of cytochrome c and SMAC/DIABLO into the cytoplasm, subsequently activating caspase-9 (52,60). The extrinsic (or death receptor) pathway of apoptosis can be triggered by binding of death receptor ligands such as FasL or TNF-α to the death receptor family (53). Further, those death stimuli activate caspase-8 via FAS associated death domain protein (FADD) and TNFR associated death domain protein (TRADD) (52,69). Activated caspase-8 subsequently cleaves executioner caspases-3 and -7 as well as the BH3 only protein BID, which then translocates to the mitochondria, thereby co-activating the intrinsic pathway, converging both pathways (52).

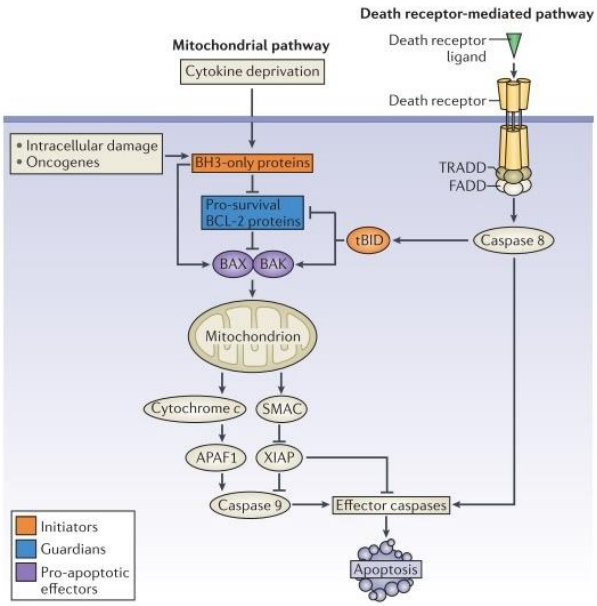

Figure 3: Apoptotic signaling pathways.

Apoptosis is mediated via two distinct pathways, *i.e*. the extrinsic (death receptor) pathway and the intrinsic (mitochondrial) pathway, which both lead to activation of caspases as cell death effector molecules. Engagement of the mitochondrial pathway results in mitochondrial outer membrane permeabilization (MOMP) accompanied by the release of mitochondrial intermembrane space proteins such as cytochrome c into the cytosol, which in turn results in caspase activation and apoptosis. The death receptor pathway can be triggered by FasL or TNF-α, leading to caspase-8 activation and subsequent BID cleavage, translocating to the mitochondria converging both pathways. MOMP is tightly controlled by various factors including proteins of the BCL-2 family. BCL-2 family proteins consist of both antiapoptotic members, e.g. BCL-2, BCL-X_L and MCL-1, and proapoptotic molecules such as the multi-domain proteins BAK and BAX and BH3-only domain proteins, e.g. BIM, PUMA and NOXA; figure adapted from (52).

I.3 PARP inhibitors and BRCAness

First findings about DNA repair capabilities of PARP1 and the possibility that blockage of PARP might support cytotoxic, alkylating agents range back to the 1980s (72). Employing a differential scanning fluorimetry binding assay Wahlberg *et al.* performed a family-wide profiling of PARP and tankyrase inhibitors (73). Of note, PARP inhibitors were presented to selectively bind PARP1-4. Moreover, they observed that olaparib, veliparib and rucaparib, originally designed as PARP1 inhibitors, induced stabilization of PARP1, PARP2, PARP3 and PARP4 (73). Therefore, while mentioning PARP inhibitors it is referred to PARP1-4 as binding partners to these inhibitors. PARP inhibition was first broadly recognized as it was proven, that inhibition of PARP in *BRCA1* or *BRCA2* negative tumors, omits cytotoxicity in cell lines (74,75) and human tumors (76). This accelerated the development of PARP inhibitors to treat tumors harboring genetic lesions in DNA repair pathways and more precisely defects in double strand break (DSB) repair due to *BRCA1/2* deficiency. Such deficiency results in cells that are contingent on PARP and base excision repair (BER) to repair DNA lesions and sustain genomic integrity (77). The loss of BRCA function has been termed “BRCAness” and could recently be reassessed in a way that cells, which show alterations

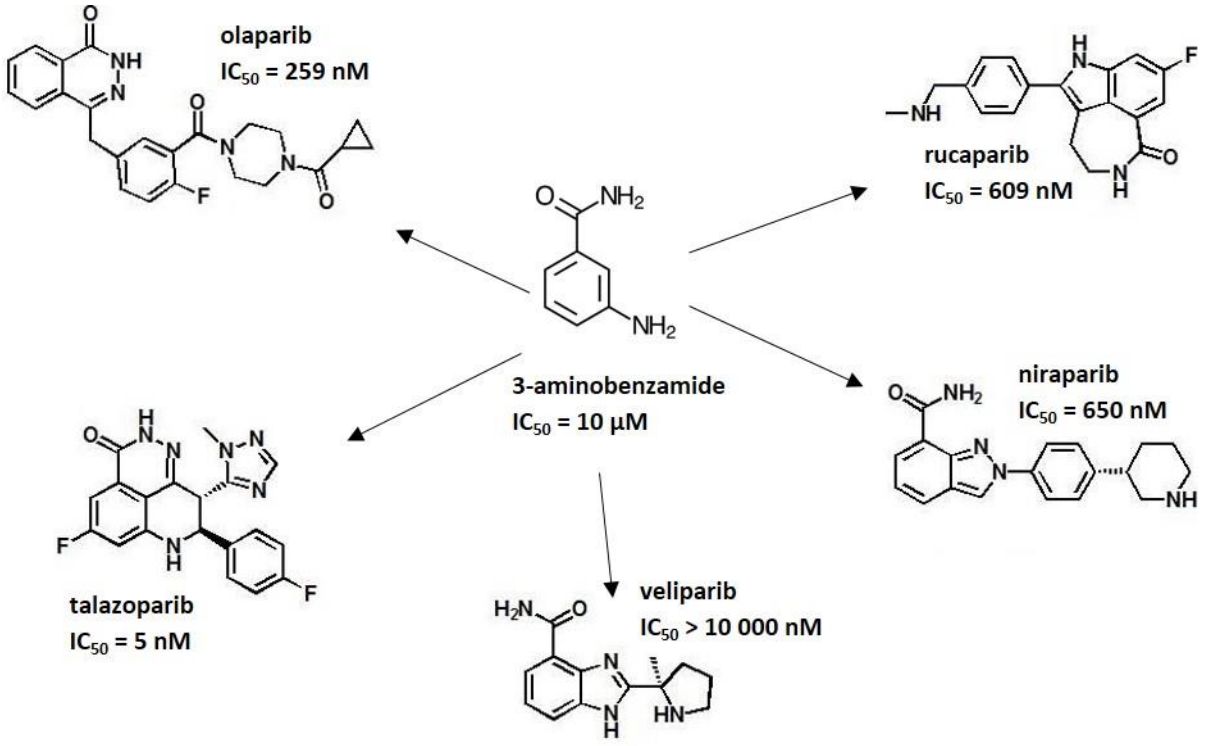

Figure 4: Molecule structures and associated IC_{50} values of PARP inhibitors.

Structure of 3-aminobenzamide (middle) as one of the first PARP inhibitors together with the recent poly (ADP-ribose) polymerase inhibitors (olaparib, talazoparib, veliparib, niraparib and rucaparib). To ensure comparability of the IC_{50} values the single agent cytotoxicity of the recent PARP inhibitors was measured in human *BRCA1/2* deficient Capan-1 cells (70). Molecule structures adapted from (71).

in HR genes, not only *BRCA1/2*, also show features of BRCAness, when homologous recombination is impaired (46,47). Therefore, it was figured out that BRCAness does not only account to a small fraction of ovarian and breast cancer, but also to a significant proportion of prostate cancer, pancreatic tumors (47) as well as osteosarcomas (46). In case of BRCAness with non-functional HR repair and blockage of BER due to PARP inhibition, cells are not able to repair thousands of DNA lesions. Those lesions basally result from genotoxic stress or are potentiated by chemotherapeutic drugs, ultimately resulting in synthetic lethality. Under resting and proliferative conditions, PARP promotes the clearance of those lesions during BER (78). However, when those lesions are not repaired, they result in increased DNA double-strand breaks and cells undergo cell death (74,75). Until then, the primary mechanism for PARP inhibitors to exert their cytotoxicity has been attributed to this accumulation of unrepaired single-strand breaks (SSB) resulting from catalytic PARP inhibition (79). But recently, Pommier *et al.* discovered that besides the catalytic PARP inhibition, selected PARP inhibitors lead to trapping of PARP1 and PARP2 on damaged DNA (79–81). This trapping prevents DNA replication and transcription, killing cancer cells more efficiently than solely by catalytic inhibition. They also provided evidence that PARP inhibitor cytotoxicity primarily results from PARP trapping rather than enzyme inhibition (79–81). Taking together, all PARP inhibitors shown distinct PARP trapping activities, whereas they represent similar efficacy in catalytic inhibition. Allosteric trapping of PARP to the DNA explains the 100 - 10 000-fold differences in cytotoxicity (70,80,81). First studies of PARP inhibitors were performed with 3-aminobenzamide, a non-selective inhibitor with low potency in comparison to current pharmacological inhibitors (82). Nevertheless, it demonstrated an enhanced radiosensitivity when PARP was inhibited, guiding the way to more structure-based inhibitors (83). Till today, five important PARP inhibitors (olaparib, talazoparib, veliparib, niraparib and rucaparib) are still under investigation in more than 170 clinical trials (> 60 active trials) as monotherapy, as combination therapy with chemotherapy and as combination with radiotherapy in multiple tumor types (full overview in (84) and (85)). In the following a more detailed description of the most commonly used PARP inhibitors is given, taking into account their capability in catalytically inhibiting PARP as well as trapping PARP onto the DNA.

I.3.1 Olaparib

Olaparib (AZD-2281, AstraZeneca), an orally administered, small molecule poly(ADP-ribose) polymerase inhibitor was the first PARP inhibitor getting FDA approval (86). In December 2014, olaparib got approval for treatment of *BRCA* mutated ovarian cancer and recently designated breakthrough therapy as monotherapy in castration-resistance prostate cancer (CRPC), harboring *BRCA* or *ATM* gene mutation (87). Phase III studies in gastric cancer (NCT01924533), pancreatic cancer (NCT02677038) and breast cancer

(NCT02032823) are ongoing together with additional studies in soft tissue sarcomas and further solid tumors (85). In Capan-1 cells, olaparib has been shown to be the second most potent binding partner to PARP1/2 with an IC_{50} of 5 nM for PARP1 and 1 nM for PARP2, respectively. Furthermore, it inhibits cells' PARylation, evaluated via an assay that measures poly(ADP-ribose) formation and estimates catalytic PARP activity, at concentrations of 3.6 nM (70).

I.3.2 Talazoparib

Talazoparib (BMN-673, Medivation) is reported to oppose the highest PARP trapping ability accompanied by the highest potency to suppress tumor growth (80). The most advanced clinical trial is currently in phase III, assessing the efficacy in *BRCA* mutated breast cancer (NCT01945775) (84). Additionally, talazoparib is being tested in various other clinical trials involving childhood solid tumors (NCT02392793), ovarian cancer (NCT02326844, NCT01989546) and cancer patients with alterations in *BRCA1/2*, mutations/deletions in *PTEN* or *PTEN* loss, mutations/deletions in HR pathway genes (e.g. *ATM*, *PALB2*, Fanconi Anemia genes) and individuals with *BRCA* mutations who do not suffer from breast or ovarian cancer (NCT02286687) (85). It demonstrated the highest binding affinity to PARP molecules with K_i = 1.2 nM for PARP1 and 0.9 nM for PARP2, respectively, resulting in the best PARP trapping capabilities being ~ 100-fold more efficient than olaparib, niraparib and rucaparib and ~ 10 000-fold more efficient than veliparib in trapping PARP to DNA (80). In cell PARylation assays it showed the highest cytotoxicity among the tested PARP inhibitors with an IC_{50} of 2.5nM (70).

I.3.3 Veliparib

In present, the most promising clinical trial of Veliparib (ABT-888, AbbVie) is a phase III study of veliparib in glioblastoma multiforme with or without TMZ treatment (NCT02152982). Additionally, it is tested in numerous malignancies including ovarian (NCT02483104), breast (NCT02158507) and pancreatic cancer (NCT01908478) (85). It binds PARP1 with a K_i of 5.2 nM and PARP2 with a K_i of 2.9 nM (70), respectively. Pommier *et al.* have shown that veliparib has the lowest PARP trapping capability, lacking PARP-DNA complexes, thereby barely blocking DNA replication and transcription (79–81). This fits together with the high IC_{50} of > 10 000 nM of veliparib exhibited in Capan-1 cells and other cell types (70,79,81). However, for catalytic inhibition, veliparib demonstrates an IC_{50} of 5.9 nM in the PARylation assay, which is comparable to the results obtained with the other presented PARP inhibitors (83). This emphasizes the prior mentioned hypothesis, which describes the creation of PARP-DNA complexes as primary mechanism for PARP inhibitor cytotoxicity, rather than inhibition of the enzyme function of PARP (fully discussed in IV.1) (70,79–81,88).

I.3.4 Niraparib

Niraparib (MK-4827, TESARO) is currently tested in phase III clinical trials for ovarian cancer (NCT02354131, NCT02354586) and *BRCA* mutation positive breast cancer (NCT01905592) (85). Additionally, it is tested in other studies comprising a phase I study in prostate cancer (NCT02500901) and a phase I study in formerly treated, incurable Ewing's sarcoma (NCT02044120) (85). With a K_i of 3.2 nM for PARP1 and 4.0 nM for PARP2 and an IC_{50} of 650 nM in Capan-1 cells it shows comparable cytotoxicity to olaparib, being ~ 100-fold more potent than veliparib and ~ 100-fold less potent than talazoparib (70).

I.4 Chemotherapeutics

In the last decades, chemotherapy has evolved to one of the most important cancer treatment options, besides surgery and radiotherapy. Chemotherapeutics mainly act by inducing DNA damage or hindering the DNA damage response. Therefore, primarily fast replicating cancer cells are sensitized towards chemotherapeutics (84). Chemotherapeutic agents can mainly be divided into groups based on their mode of action or their chemical structure. The main groups consist of alkylating agents, antimetabolites, anthracyclines, topoisomerase I and, -II inhibitors, microtubule inhibitors and corticosteroids further described in more detail (see Figure 5) (89).

I.4.1 Alkylating agents

TMZ is a monoalkylating drug, which largely induces cytotoxicity by methylating the DNA (90). In combination with PARP inhibitors, it elicits its cytotoxicity through its N^3-methyladenine and N^7-methylguanine that induce PARP trapping, double-strand breaks and replication fork stalling (91). By comparison, TMZ as single agent induces cytotoxicity mainly through O^6-methylguanine followed by futile cycles of mismatch repair, pointing to different mechanisms of cytotoxicity for TMZ monotherapy or in combination with PARP inhibitors (92). It is mainly tested for treatment of glioblastoma, melanoma or soft tissue sarcoma, e.g. Ewing's sarcoma (22,85). Platinum salts such as cisplatin and

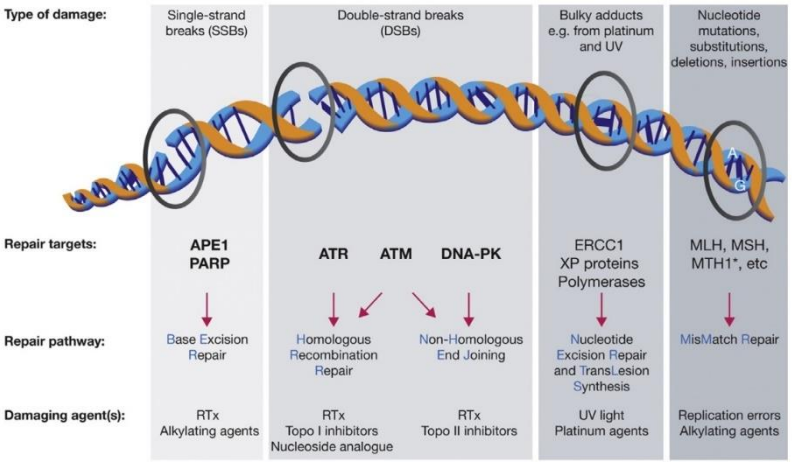

Figure 5: Different modes of DNA damage with associated repair pathways.
DNA damage response target pathways modified from (84), RTx = radiotherapy. Single-strand breaks are reported to be the most common form of DNA damage, whereas double-strand breaks are most cytotoxic (84).

carboplatin, are commonly used alkylating agents in chemotherapy of ovarian cancer, head and neck cancer as well as osteosarcoma (39,93) These drugs are generally classified as alkylating agents, even though they do not alkylate DNA, but rather induce cytotoxicity in a way of generating covalent cross-links between DNA bases (94). Ifosfamide on the other hand, is a nitrogen mustard that mainly acts through modifying and cross-linking purine bases in the DNA (95). Active intermediates are created after its activation in the liver (96). Ifosfamide is often used in the treatment of, for example breast or ovarian cancers, lymphomas or sarcomas (24,96). Summarizing, inhibition of DNA, RNA and protein synthesis by alkylating agents rapidly leads to apoptosis in heavily proliferating cells (93).

I.4.2 Topoisomerase I inhibitors

SN-38, an active metabolite of irinotecan, acts trough topoisomerase I inhibition (97). It causes DNA single strand breaks and covalent topoisomerase I DNA complexes, which trigger PARP activation and requires PARP during base excision repair (BER) (98). Binding of topoisomerase I to DNA and subsequent hindering of the replication fork or other DNA processing events is important for exhibiting concomitant cytotoxicity, as compounds that solitary block access of topoisomerases to DNA do not demonstrate clinical efficacy (99,100). Topoisomerase I inhibitors, such as SN-38, are mainly included in the treatment of soft tissue sarcomas and osteosarcoma (88,99).

I.4.3 Topoisomerase II inhibitors

Doxorubicin is an anthracycline and nonspecific DNA-intercalating agent, which induces protein-associated strand breaks by binding topoisomerase II covalently to DNA (101,102). Etoposide (VP-16) on the other hand, is supposed to be the most selective topoisomerase II inhibitor currently used in the clinic (98). Analogous to topoisomerase I inhibitors, topoisomerase II inhibitors are cytotoxic mainly during DNA processing events, as this culminates in severe DNA editing failures (98). Topoisomerase II inhibitors are mostly included in treatment protocols of breast cancer, small-cell lung cancer and soft tissue sarcomas (93).

I.4.4 Microtubule inhibitors

Vincristine, a well described microtubule inhibitor, displays its cytotoxic effects by interfering with microtubule formation and mitotic spindle dynamics (103). It ultimately leads to mitotic arrest and finally apoptosis (104). Agents targeting microtubules are widely described for treatment of various cancers, including ovarian, breast, leukemia and soft tissue sarcomas (24,103).

I.4.5 Anthracyclines

Actinomycin D is an anthracycline antibiotic which intercalates into the DNA (105). In 1971, it was reported to be one of the first small molecules being able to target DNA and to demonstrate sequence selectivity (106). Actinomycin D is still widely used for a variety of cancers including sarcomas, for example Ewing's sarcoma (93).

I.4.6 Antimetabolites

Antimetabolites, such as methotrexate (MTX), interfere with cell metabolism. For instance, MTX interferes in the metabolism of folic acid by binding dihydrofolate reductase (107). Through binding, MTX inhibits DNA synthesis as folic acid is required for synthesis of thymidine (107). It is often applied in pediatric sarcomas (37,108) and for treatment of rheumatoid arthritis (109).

I.5 Aim of the study

In order to explore potentially clinically relevant combination treatments, the general aim of these studies was to systematically evaluate the efficiency of PARP inhibitors in combination with chemotherapeutics to treat ES and OS. Of note, PARP inhibitors were presented to selectively bind PARP1-4. Four different PARP inhibitors (talazoparib, olaparib, niraparib and veliparib) were studied in combination with seven different chemotherapeutics of different classes and systematic combination regimens in this detail have not been performed before. Second, since little is yet known about the molecular cell death mechanisms underlying PARP inhibitor-mediated cytotoxicity, we aimed to thoroughly investigate the molecular pathways of apoptosis and to reveal potential checkpoints in olaparib/TMZ mediated apoptosis.

In OS, displaying BRCAness as recently described (46), we first aimed to investigate the vulnerability of several OS cell lines with varying mutational profiles in HR-associated genes to PARP inhibitor talazoparib monotherapy. Furthermore, we explored the effects of clinically applied drugs for OS therapy in combination with talazoparib to identify the most potent drug synergy. As PARP inhibitors are currently not considered clinically for treatment of OS, our findings may comprise new possible drug combinations for optimizing treatment strategies. A genetic background of BRCAness, as observed in a high percentage of OS (46), could offer vulnerability of OS to PARP inhibitors alone or in combination with selected chemotherapeutics. Second, we wanted to validate our prior elucidated cell death mechanisms in ES for the OS model system, as well, bearing a differential genetic background (Figure 6).

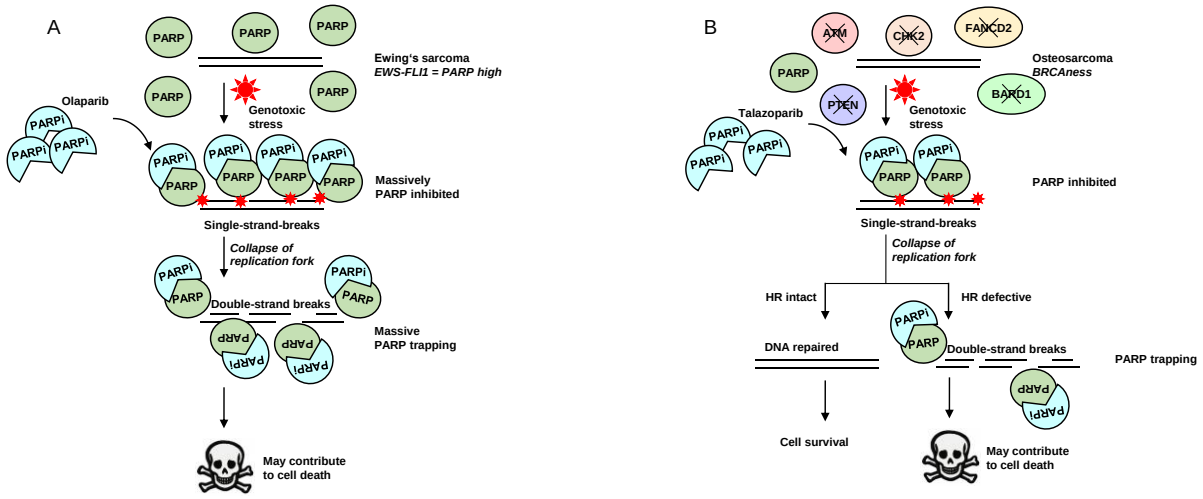

Figure 6: The role of PARP inhibitors in PARP trapping and synthetic lethality.

Different genetic backgrounds justifying PARP inhibitor therapies. **(A)** Ewing's sarcoma exhibits high levels of PARP protein by the tumorigenic fusion protein and concomitant massive PARP trapping by combination treatment of PARP inhibitor and chemotherapeutics leads to cytotoxicity. However, molecular cell death mechanism are not fully understood. **(B)** Osteosarcoma cells, recently described susceptible to harbor BRCAness, depend on PARP for maintaining their DNA integrity. Combination of PARP inhibitors and chemotherapeutics in homologous recombination (HR) defective cells triggers synthetic lethality.

II Material and methods

The materials used in this work are listed in the appendix (page 82 ff.).

II.1 Maintenance of cells

Ewing's sarcoma cell lines A4573, TC-32 and TC-71 were cultured in RPMI 1640 medium, supplemented with 10% fetal calf serum, 1% penicillin/streptomycin and 1 mM sodium pyruvate. SK-ES-1 cells were cultured in and DMEM GlutaMAX™-I, supplemented with 10% fetal calf serum, 1% penicillin/streptomycin, 1 mM sodium pyruvate. All osteosarcoma cell lines (MG63, ZK-58, SaOS-2, MNNG-HOS and U2OS) were cultured in RPMI 1640 medium, supplemented with 10% fetal calf serum, 1% penicillin/streptomycin and 1 mM sodium pyruvate. Entire cell lines were adherently growing and maintained in cell culture flasks (T175 cm^2 for regular culture) in a humidified atmosphere at 37 °C under 5% CO_2 conditions and were passaged twice a week by trypsinization with trypsin/EDTA.

II.2 Treatment of adherent cell lines

II.2.1 Plating of adherent cell lines

Prior to treatment, all of the adherent cell lines have been plated 18 to 24 hours in selected cell culture plates (6-, 24- or 96-well plates) or in selected cell culture dishes (6, 10 or 14.5 cm dishes) depending on the desired experiment. Therefore, old cell culture medium was removed and confluent cell layers were washed briefly with warmed, sterile PBS. Afterwards, trypsin/EDTA was added to the monolayer and cell culture flasks were set to rest for 5 min at 37 °C. Then, trypsinization was evaluated under the microscope and if all cells detached, trypsinization was stopped adding fresh complete medium. The number of viable cells per ml cell suspension was determined using Casy Cell Counter. Depending on the cell line and experiment to be performed, cell suspension was further diluted and cells were then seeded with a density of 10 000-20 000 cells/cm^2 in fresh medium. 5/10/20 ml of cell suspension was given into 6/10/14.5 cm dishes and 3000/500/100 µl of cell suspension per well was given into 6-/24-/96-well plates, correspondingly.

II.2.2 Treatment of adherent cell lines

Treatment of cells (drug- and inhibitor-treatments) followed 18 to 24 hours after seeding, to ensure that cells were adherent and proliferating again. To do so, cell culture medium was aspirated and chemotherapeutic drug or pharmacological inhibitor, diluted in designated concentrations in cell culture medium, was given to the cells for displayed times.

II.3 Flow cytometric analysis (fluorescence activated cell sorting, FACS)

II.3.1 Determination of apoptosis

Cells undergoing apoptosis were assessed by measuring DNA fragmentation of nuclei as characteristic marker of cell death using flow cytometry. Hence, we performed nuclear staining using the fluorogenic compound propidium iodide (PI). Cells were plated as mentioned in II.2.1 in 24-well plates in between 18 and 24 hours prior treatment. Afterwards, drug treatment was performed as mentioned in II.2.2 and cells were maintained at 37 °C, 5% CO_2 up to 72 hours under treatment conditions. Later, cell supernatant together with the trypsinized cells was transferred to corresponding and labeled FACS tubes. Next, cell suspension was centrifuged for 5 min at 4 C with 1800 rpm. Subsequently, supernatant was discarded and the remaining cell pellet, each in its corresponding tube, was suspended with 100 µl PI-buffer (hypotonic propidium iodide buffer, see page 89). After incubation for at least 1 hour, samples underwent flow cytometric analysis of a hypodiploid peak (termed sub-G_1), equivalent to the fragmented DNA content of the cells. Apoptotic cells, appearing in this sub-G_1-fraction were recorded and calculated in the red (PE) fluorescence channel.

II.3.2 Cell cycle analysis

To investigate the replication status of a cell population, nuclear PI-staining was performed as described above (II.3.1). Because hypodiploid cells can be easily discriminated from normal (G_1) or diploid (G_2) cells, cell cycle analysis was recorded in the histogram of the PE fluorescence channel. Then, FACS raw data files were exported and final cell cycle analysis was done using FlowJo™ software, stringently gating on the living cell population.

II.3.3 Determination of changes of the mitochondrial membrane potential (JC-1 staining)

During the onset of apoptosis, active mitochondria are being disrupted, displaying alterations in the mitochondrial membrane potential (also referred as LMMP). We used two different dyes ($TMRM^+$ and JC-1) to monitor these changes, since those dyes accumulate within mitochondria, depending on the mitochondrial potential. $TMRM^+$ (100 nM final concentration) accumulates in polarized mitochondria and is decreasing upon loss of mitochondrial membrane potential. JC-1 (2 µM final concentration) changes its fluorescence emission status from red, 590 nm as JC-1 aggregates in intact mitochondria, to green, 529 nm as JC-1 monomer upon depolarization of mitochondria. Briefly, we measured those two phenomena's using FACS analysis on cells plated and treated in 24-well plates as previously described

above in II.3.1. Except, before transfer to corresponding FACS tubes, cells were stained for 30 minutes with the employed dye at 37 °C and supernatant, containing dead cells, was discarded. FCCP treatment (18 h with 1 µM) was used as positive control for mitochondrial depolarization. FACS raw data files were analyzed using FlowJo™ software, solitary gating on the living cell population.

II.3.4 Determination of cell death using PI staining

Measurement of cell death using PI staining was performed as described in II.3.1 with the exception that instead of a hypotonic PI-staining buffer we added 1 µg/µl of PI dye immediately before acquisition. Cell death was assessed by PI positive cell population in the red (PE) fluorescence channel.

II.4 Microscopic analysis

II.4.1 Caspase activity assay

For determination of caspase activity cells were plated and treated (as described in II.2) in 96 well plates together with 2 µM of CellEvent™ Caspase-3/-7 Green Detection Reagent. After 48 hours of incubation, cell nuclei were stained with 2 µM Hoechst-33342 and incubated for 5 minutes. Then fluorescence (460 nm - 490 nm) was measured immediately to discriminate single cells using the ImageXpress MicroXLS system. Directly afterwards, emission in the green channel (530 nm), fluorescence by the detection reagent triggered by active caspases, was measured. During analysis, caspase activity was calculated for each cell (green fluorescence > background threshold/ cell) and is expressed in the following as percentage of caspase-3/-7 activity in the whole cell population.

II.5 Determination of cell viability and clonogenic survival

II.5.1 MTT assay

We performed measurements of cell viability by incubating cells with 3-(4,5-dimethylthiazol-2-yl)-2,5-diphenyltetrazolium bromide (MTT). Cells were seeded in 96-well plates and treated with indicated drug concentrations for indicated periods as described in II.2. After treatment for indicated times, medium was removed by flipping the plates on tissue paper and 100 µl/well of 1x MTT solution (see VIII.9) was added. Before the addition of 100 µl of 100% 2-propanol per well, cells were incubated at 37 °C for 3 hours. To ensure formazan resuspension, the volume was repeatedly pipetted up and down and a supplementary incubation step on a rocking shaker at RT for 30 minutes was added. Lastly, absorbance at 550 nm was measured by using the Infinite M100 microplate reader. Cell viability was always expressed as percentage of non-treated control samples of the corresponding experiment.

II.5.2 Crystal violet assay

Additional to MTT assay, we determined cell viability by cell density, which was assessed by crystal violet staining. Therefore, cells were seeded into 24-well plates and treated with indicated drug concentrations for indicated periods as described in II.2. Shortly, old cell culture medium was removed and cell layer was rinsed by warmed PBS. Afterwards the cells were stained with crystal violet solution (consisting of 0.5% crystal violet, 30% ethanol, 3% formaldehyde) for 10 min. Then, plates were rinsed with water to remove the dye and 400 µl of 1% SDS solution was added to the wells overnight in order to solubilize incorporated crystal violet dye. Finally, we measured absorbance (550 nm) by using the Infinite M100 microplate reader. The quantity of incorporated formazan dye and thereby the optical density measured, correlated with cell quantity and cell viability. For displaying the results, cell viability of treated samples was expressed as percentage of corresponding, untreated control samples.

II.5.3 Colony formation assay

To investigate the clonogenic survival of Ewing's sarcoma and osteosarcoma cells we performed colony formation assay. To do so, cells were treated for 24 hours as described in II.2. Afterwards, old cell culture medium containing drug treatment was discarded and cells were rinsed with sterile PBS. Then, cells were trypsinized for 5 min and counted to determine the cell number of the living cell suspension. Next, 100 cells/well were plated for each corresponding treatment condition to determine their ability to form colonies. After additional 10 to 12 days of incubation at 37 °C and 5% CO_2, cells were fixed and stained with crystal violet solution as described above (II.5.2). At last, fixed and stained colonies were counted macroscopically and colony formation of treated samples was normalized to the experiment corresponding, untreated control. For additional evaluation, colonies were scanned and displayed as images next to the figures.

II.6 Transfection of eukaryotic cells

II.6.1 Lipofectamine transfection

For transfection of mammalian cell lines we used Lipofectamine 2000. Therefore, 12 µl of Lipofectamine 2000 reagent or 4 µg of plasmid DNA was diluted in 150 µl Opti-MEM medium. Then, DNA solution was added to transfection solution, mixed gently by inverting the Eppi and incubated for 20 minutes. The complete DNA-Lipofectamine 2000-mix was subsequently added dropwise to 20 000 cells/cm^2 plated in 6-well plates 18 to 24 hours prior to transfection. After 6 hours of transfection the medium was exchanged, by replacing transfection medium with complete growth medium of the corresponding cell line.

II.6.2 RNAiMAX transfection

In contrast to the Lipofectamine transfection protocol described above, cell lines were transfected using Lipofectamine RNAiMAX during seeding of up to 30 000 cells/cm² cells (so called "reverse" siRNA transfection). Therefore 1.5 µl of Lipofectamine RNAiMAX or 5 pmol of siRNA were diluted in 25 µl Opti-MEM before adding the siRNA mix to the Lipofectamine mix. After 5 minutes of incubation, the transfection-mix was distributed to the wells of a 24-well plate (50 µl/well) before seeding the cells on top (450 µl cell suspension/well). Alternatively, to check for knockdown of desired proteins via Western blot, 500 µl of transfection-mix was given to 6 cm dishes and 3500 µl of cell suspension was added per dish

II.7 Generation of genetically modified cell lines

II.7.1 Isolation of plasmid DNA

For the generation of genetically modified cell lines we first transformed one Shot TOP10 chemically competent *E. coli* by a heat shock reaction with 50 ng of plasmid DNA. Then, competent bacteria was thawed on ice, gently mixed with plasmid DNA and incubated for 30 minutes (cold). Afterwards, we performed another heat shock at 42 °C for 40 seconds and cooled the cells on ice for another 2 minutes, before adding 1 ml of pre-warmed S.O.C. medium. Following incubation at 37 °C for 1 hour and 120 rpm in a bacteria shaker we plated the cells on LB agar containing antibiotics for selection (ampicillin for pMSCV plasmids, kanamycin for pCMB Tag3B plasmids – both in concentration of 100 µg/ml). LB agar plates were inverted and incubated overnight at 37 °C. The next day, single clones were picked and transferred into 3 ml LB medium containing the plasmid corresponding antibiotic and incubated them for 3 hours, 37 °C and 120 rpm. To upstream bacterial cultures we transferred the cultures in 250 ml LB medium containing antibiotics and incubated them again overnight at 37 °C. Isolation of plasmid DNA was performed afterwards using the PureLink HiPure plasmid Filter Maxiprep kit following the manufacturer's instructions. The amount of plasmid DNA was determined by the NanoDrop 1000 spectrophotometer.

II.7.2 Retroviral transduction

Genetically stable A4573 and SK-ES-1 ES cell lines were generated performing retroviral transduction of plasmid DNA (BCL-2). Therefore Phoenix cells were used as retrovirus producer, plated 48 hours prior to transduction and transfected with plasmids. One day before retroviral transduction ES cell lines were plated in 6-well plates with a density of 10 000 cells/cm². Supernatant of Phoenix cells, containing the retrovirus, was collected via centrifugation, sterile filtered (0.45 µm) and 8 µg/µl polybrene was added. Then, we performed spin-transduction with 1 ml of retrovirus solution at 37 °C, 90 minutes and 1 300 rpm. After incubation of transduced cells for 8 hours, the medium was replaced by complete growth medium.

Five days after the cells could recover from transductional stress, we carried out antibiotic selection with 20 µl/ml blasticidine for additional 2-3 weeks.

II.7.3 Transient overexpression & selection for stable clones

For generation of stably transfected cells, transiently overexpressing non-degradable, phospho-defective MCL-1 4A mutant (4A = S64A/S121A/S159A/T163A), we transfected A4573 and SK-ES-1 cells with 4 µg of pCMV-Tag3B plasmid according to the procedure described in II.6.1. Afterwards, cells were selected with 500 µg/ml of Geneticin (G418) for at least 2 weeks before using them for further experiments.

II.8 RNA interference (RNAi)

II.8.1 Transient knockdown

For transient knockdown of BAK,BAX or NOXA, ES and OS cells were reversely transfected with 5 pmol, respectively 10 pmol for combined knockdown experiments, of Silencer Select control siRNA (named as siCtrl) or gene of interest targeting siRNA (e.g. siNOXA) using the Lipofectamine RNAiMAX protocol as described in II.6.2. SiRNA constructs used in this study are listed in VIII.5.

II.9 SDS-PAGE & Western blot analysis

II.9.1 Protein extraction

For Western blot analysis cell pellets of treated or untreated cells were collected by scraping tissue culture dishes after indicated periods of time. Then, dishes were washed once with ice cold PBS and the volume was transferred to the corresponding, prior labeled falcon tubes. After centrifugation at 4 °C, 5 minutes and 1 800 rpm, supernatant was discarded and cell pellets were lysed with lysis buffer (containing 30 mM TrisHCl, 150 nM NaCl, 1% Triton X-100, 10% Glycerol, 0.5 nM PMSF, 2 mM DTT, 1x protease inhibitor cocktail, 1 mM sodium orthovanadate, 1 mM β-glycerolphosphate, 5 mM sodium fluoride) on ice for 25 minutes. Then, lysed cells were centrifuged for additional 20 minutes at 4 °C and 14 000 rpm in order to remove cell debris. The supernatant of the last centrifugation step, containing all cellular proteins, was immediately stored at -20 °C or directly taken for protein determination by BCA Protein Assay Kit.

II.9.2 Protein determination

For protein determination of whole cell lysates we used Pierce BCA Protein Assay Kit according to the manufacturer's instructions. Shortly, BSA standard (up to 2 mg/ml) was used as reference to measure sample protein concentration in triplicates at 550 nm absorbance with the Infinite M100 microplate reader.

II.9.3 Preparation of polyacrylamide gels

Polyacrylamide gels were casted up to one week before running the protein samples. The polyacrylamide gels were comprised of a 5% stacking gel (consisting of 5% polyacrylamide, 125 mM TrisHCl pH 6.8, 0.1% SDS, 0.1% APS, 0.1% TEMED ad ddH_2O) and a 12% or 15% resolving gel (consisting of 12% or 15% polyacrylamide, 250 mM TrisHCl pH 8.8, 0.1% SDS, 0.1% APS, 0.04% TEMED ad ddH_2O) depending on the desired grade of separation.

II.9.4 SDS-PAGE

We performed SDS-polyacrylamide gel electrophoresis. Therefore, first 50 µg of protein sample were diluted in 1x SDS loading buffer (see VIII.9) ad 18 µl ddH_2O and denaturated for 5 minutes at 96 °C using Thermomixer. Already prepared protein samples were either stored at -20 °C overnight or directly loaded onto casted polyacrylamide gels. For running of gel electrophoresis we used 1x running buffer (see VIII.9) and a constant voltage of 100 Volt for the staking gel (~ 20 minutes) and 140 Volt for the resolving gel (~ 3-4 hours depending on 12% or 15% gels). Gel electrophoresis was monitored regularly and electrophoresis was stopped when the desired separation (indicated by protein ladder) was reached.

II.9.5 Western blot

For blotting procedure the separated proteins were transferred onto nitrocellulose membranes using the semi-dry blotting technique. Therefore we stacked two filter papers soaked in blotting buffer (see VIII.9), moistened nitrocellulose membrane, polyacrylamide gel and another two filter papers soaked in blotting buffer. This package was then put onto the anode of the semi-dry blotting system in the described order to ensure transfer of the proteins from the gel to the membrane. Transfer of the proteins was performed with a constant current (1 mA per cm^2 nitrocellulose membrane) for a different time, depending on the size of the proteins (proteins > 25 kDa = 90 minutes, small proteins < 25 kDa = 65 minutes).

II.9.6 Detection of target proteins

For detection of the targeted proteins we first blocked the membrane after blotting with 5% skimmed milk powder in PBS-T for 60 minutes to diminish unspecific antibody binding. After blocking, the membranes were washed three times for at least 5 minutes with PBS-T before incubation with the primary antibody at 4 °C overnight on an orbital shaker (full list of the used primary antibodies under VIII.4). The next day, primary antibody was stored at -20 °C for later use and the membrane was washed again at least three times for 5 minutes with PBS-T. Then, secondary antibodies were diluted as described in VIII.4 and incubated together with the membrane for at least 1 hour at room temperature on an orbital shaker. Horseradish peroxidase (HRP)-conjugated secondary antibodies were detected with enhanced

chemiluminescence (ECL) following the manufacturer's protocol and using developing solutions in a photo laboratory. IRDye-labelled secondary antibodies were detected using the infrared Odyssey imaging system.

II.10 Determination of BAK/BAX activation

For immunoprecipitation of active BAK and BAX conformation specific antibodies were used (listed in VIII.4). First, cells were harvested as described above in II.9.1 and then lysed using CHAPS buffer (1% CHAPS, 150 mM NaCl, 10 mM HEPES pH 7.4, supplemented with 1x protease inhibitor cocktail (PIC)) for 25 minutes on ice. Then, samples were centrifuged at 4 °C for 25 minutes with 14 000 rpm to remove cell debris. For immunoprecipitation (IP) 500 µg of protein was incubated at 4 °C overnight on a rotational wheel together with either 0.5 µg anti-BAK or 8 µg anti-BAX antibody and 10 µl pan mouse IgG Dynabeads. After incubation, beads were washed at least three time with CHAPS buffer using a magnetic rack by which the beads remained in the reaction tube. Then, beads were mixed with 15 µl of 1x SDS loading buffer and denaturated for 5 minutes at 96 °C. Active BAK and BAX was then analyzed by Western blot following the prior described procedure beginning in II.9.4 with the primary antibodies for BAK and BAX described in VIII.4.

II.11 Isolation of peripheral blood lymphocytes

For isolation of peripheral blood lymphocytes (PBL's) we used blood, drawn from two independent donors. Freshly drawn blood was mixed 1:1 with PBS and EDTA to avoid agglutination. Then 30 ml of blood/PBS mixture was overlayed above 15 ml Biocoll solution in a 50 ml Falcon tube, carefully taking care of not to mix both solutions. Afterwards, density gradient centrifugation (35 minutes with 3 500 rpm) was performed to separate the different components of the blood. Finally, peripheral blood lymphocytes were collected from the interphase, seeded in 96-well plates and treated with indicated concentrations of the drugs/ inhibitors.

II.12 Statistical analysis

For statistical certainty we performed each experiment for at least three different times in independent repetitions including at least triplicates for each condition. Testing for statistical significance, when comparing two different groups within one experiment, we performed Student's t-Test (equal variance, two-sample, two-sided distribution) by using Microsoft Excel. All data were expressed as mean +/- standard deviation (SD). Statistical significance for groups with a calculated p-value as followed: p-value < 0.05 (significant, *), p-value < 0.01 (very significant, **) and p-value < 0.001 (extremely significant, ***).

II.13 Calculation of Combination Index (CI)

Combination indices (CI) and Fraction affected (Fa) values (in cases were CI alone was not meaningful enough) were calculated by using CalcuSyn software, described previously by Chou *et al.* (110).

For ES studies the following subclassification of CI values according to the CalcuSyn manual were used: (CI < 0.1 very strong synergism; 0.1 – 0.3 strong synergism; 0.3 – 0.7 synergism; 0.7 – 0.85 moderate synergism; 0.85 – 0.9 slight synergism; 0.9 – 1.1 nearly additive; 1.1 – 1.2 slightly antagonistic; 1.2 – 1.45 moderate antagonistic and CI > 1.45 antagonism.

For the studies in OS we displayed CI values together with the Fraction affected (Fa) in self-generated CI/Fa plots to allow to discriminate among highly synergistic (CI < 0.2, Fa > 0.5), intermediate synergistic (CI > 0.2 < 0.9, Fa > 0.5) and weakly synergistic (CI > 0.2 < 0.9, Fa > 0.3 < 0.5) drug combinations.

III Results

III.1 PARP inhibitors in Ewing's sarcoma

III.1.1 Screening for synergistic drug interactions of PARP inhibitors and chemotherapeutic drugs

Ewing's sarcoma (ES) has previously been indicated to be susceptibility towards PARP inhibition due to high PARP expression levels by a transcriptional feedback loop of the tumor specific fusion protein ESW-FLI1 (31,111). In this regard, two ES cell lines A4573 and SK-ES-1 were tested for sensitivity towards a set of different PARP inhibitors (Figure 7).

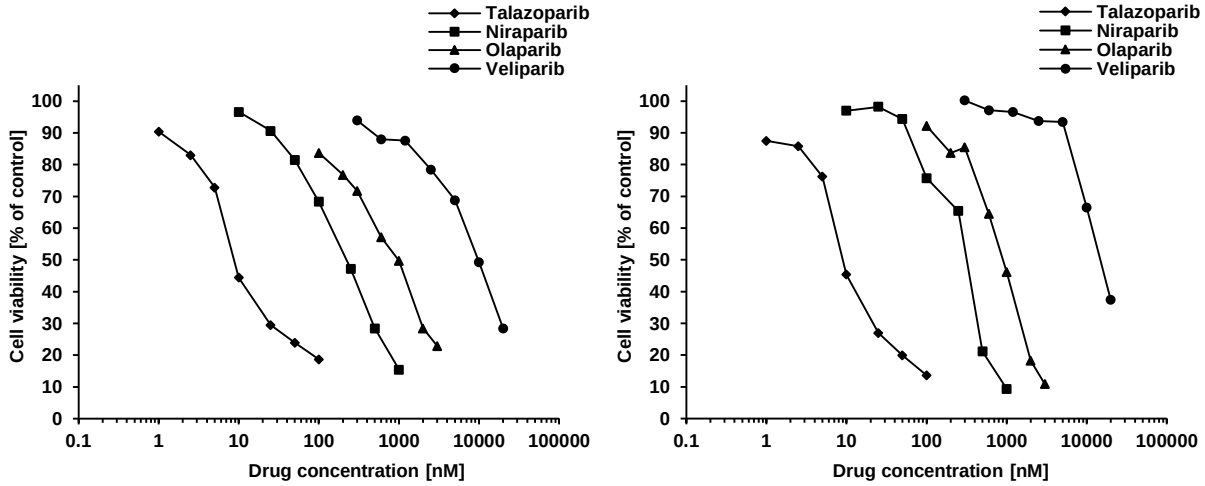

Figure 7: Single agent cytotoxicity of different PARP inhibitors in Ewing's sarcoma cell lines A4573 and SK-ES-1.
A4573 (left) and SK-ES-1 (right) cells were treated for 72 hours with increasing concentrations of four different PARP inhibitors talazoparib, niraparib, olaparib and veliparib for determination of IC_{50} values. Cell viability was assessed by crystal violet staining and is shown as percentage of control (raw data obtained by Cornelius Schneider).

Indeed, both ES cell lines showed a reduction in cell viability in a concentration dependent manner upon treatment with all four PARP inhibitors. Among the PARP inhibitors talazoparib was most potent, with reduction of cell viability in the nanomolar concentration range, followed by niraparib, olaparib and veliparib. Calculation of IC_{50} values in ES cells determined talazoparib to be roughly 30-times more cytotoxic than niraparib, about 100-times more

Table 2: Determination of IC_{50} toxicity in Ewing's sarcoma.

A4573	IC_{50} Value [nM]	SK-ES-1	IC_{50} Value [nM]
Talazoparib	8.87	Talazoparib	7.70
Niraparib	336.93	Niraparib	243.83
Olaparib	978.27	Olaparib	1254.62
Veliparib	10335.70	Veliparib	21538.64

IC_{50} toxicity was generated graphically with Origin™ using the raw data given by quantification of cell viability shown in Figure 7.

cytotoxic than olaparib and around 1 000-times more cytotoxic as veliparib (Table 2). Next, we aimed to investigate whether PARP inhibitors increased the sensitivity of ES cell lines A4573 and SK-ES-1 towards different chemotherapeutics used in therapy of ES (24,112). To screen for synergistic drug interaction we used suboptimal drug concentrations of PARP inhibitors (Figure 8) and genotoxic drugs (Figure 9) that led to a reduction of 20 – 40% of cell viability when added as monotherapy in comparison to untreated controls (Figure 10, Figure 11).

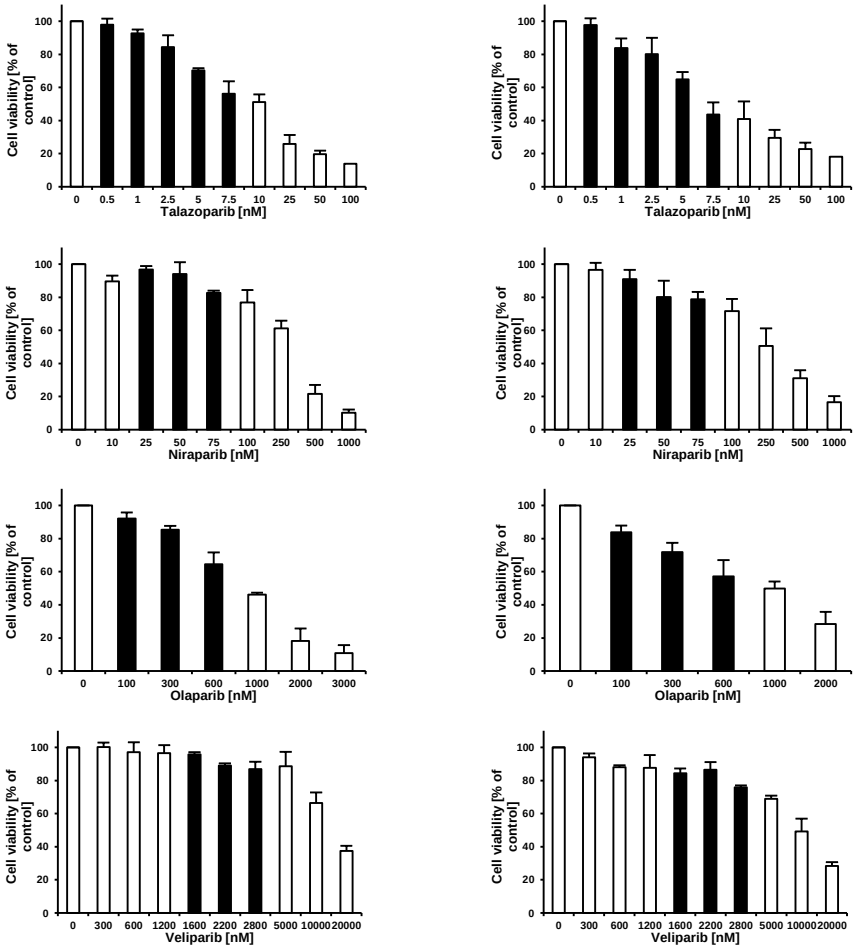

Figure 8: Determination of toxicity of PARP inhibitors in Ewing's sarcoma cell lines.

A4573 (left panel) and SK-ES-1 (right panel) ES cells were treated for 72 hours with indicated concentration of PARP inhibitors and cell viability was assessed by crystal violet staining (raw data obtained by Cornelius Schneider). Black bars indicate the concentrations which were used for combination treatment approaches. Data are shown as mean +/- SD of three independent experiments performed in triplicate.

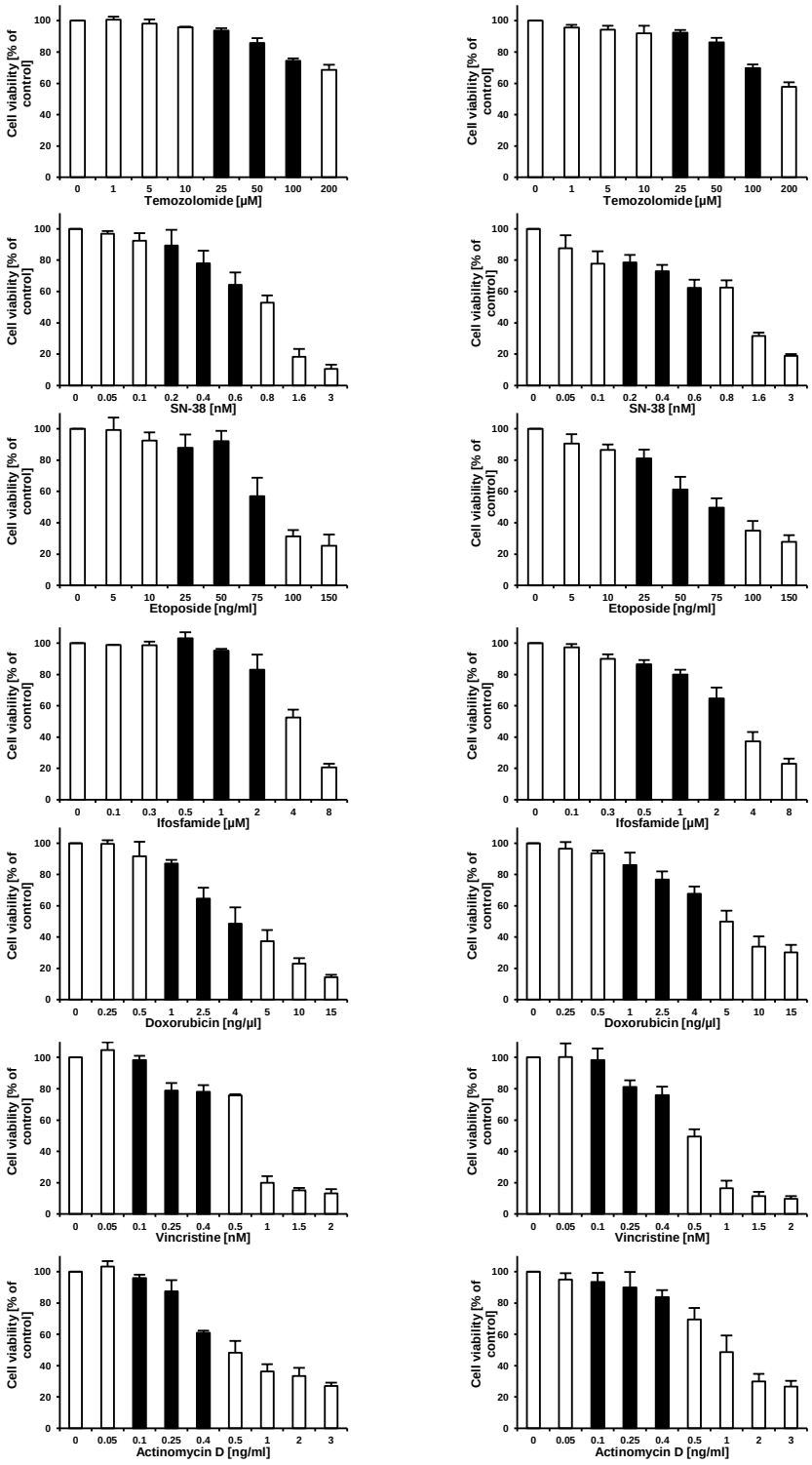

Figure 9: Determination of toxicity of chemotherapeutics in Ewing's sarcoma.

A4573 (left panel) and SK-ES-1 (right panel) ES cells were treated for 72 hours with indicated concentration of chemotherapeutics and cell viability was assessed by crystal violet staining (raw data obtained by Cornelius Schneider). Black bars indicate the concentrations which were used for combination treatment approaches. Data are shown as mean +/- SD of three independent experiments performed in triplicate.

Figure 10: Combination treatment of PARP inhibitors and chemotherapeutics used to determine synergism in A4573.

A4573 cells were treated for 72 hours with indicated concentration of PARP inhibitors (talazoparib, niraparib, olaparib and veliparib) in combination with different chemotherapeutics (temozolomide, SN-38, etoposide, ifosfamide, doxorubicin, vincristine and actinomycin D) and cell viability was assessed by crystal violet staining (performed by Cornelius Schneider) and is expressed as percentage of untreated cells. With given raw data CI-values were calculated and used for heat map generation (**Figure 12**). Data are shown as mean +/- SD of at least three independent experiments performed in triplicate.

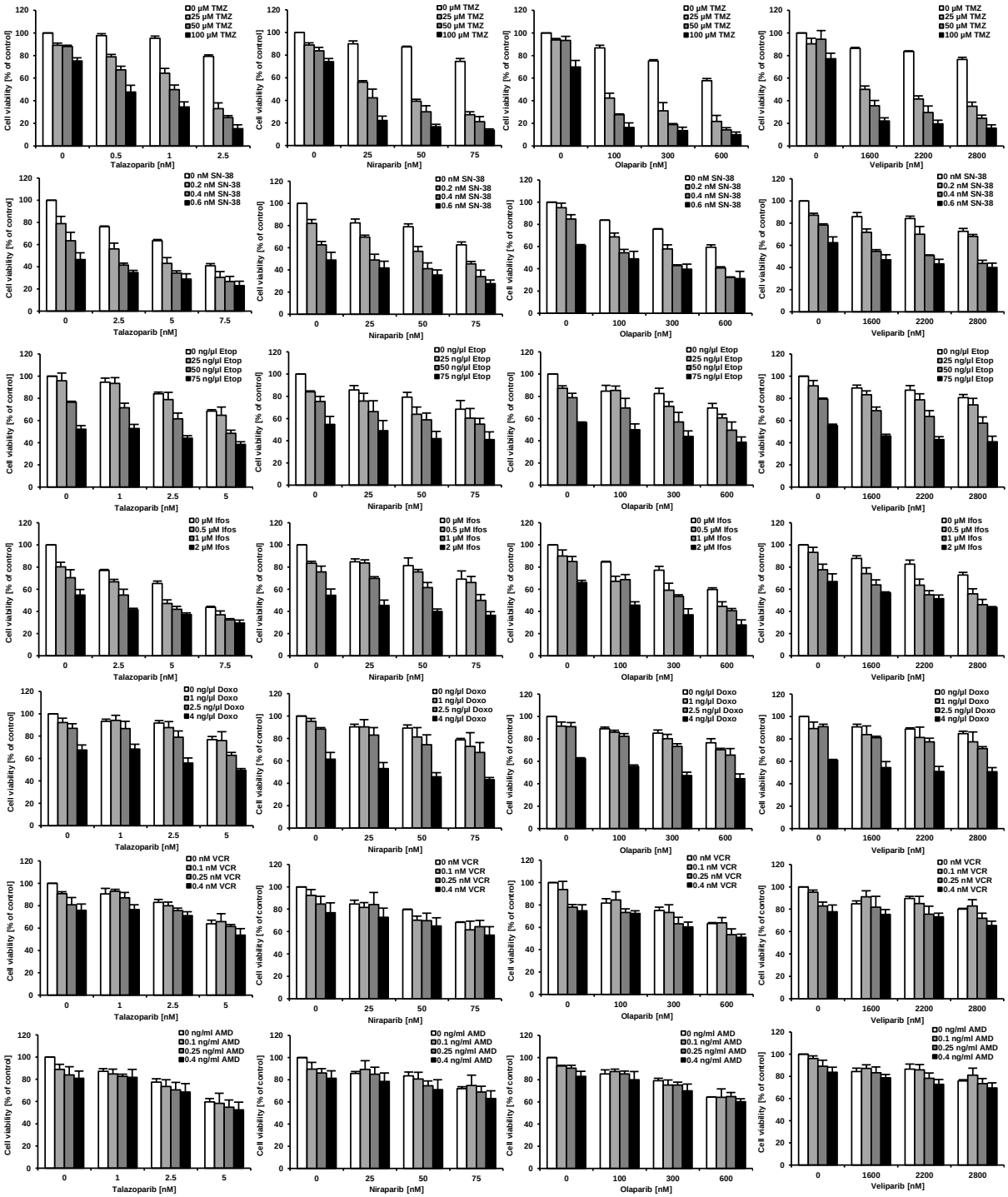

Figure 11: Combination treatment of PARP inhibitors and chemotherapeutics used to determine synergism in SK-ES-1.

SK-ES-1 cells were treated for 72 hours with indicated concentration of PARP inhibitors (talazoparib, niraparib, olaparib and veliparib) in combination with different chemotherapeutics (temozolomide, SN-38, etoposide, ifosfamide, doxorubicin, vincristine and actinomycin D) and cell viability was assessed by crystal violet staining (performed by Cornelius Schneider) and is expressed as percentage of untreated cells. With given raw data CI-values were calculated and used for heat map generation (**Figure 12**). Data are shown as mean +/- SD of at least three independent experiments performed in triplicate

Synergistic, additive or antagonistic CI values for combinatorial drug effects were calculated as previously described by Chou *et al.* (110) (Table 3). CI values were utilized to generate a heat-map of drug interactions according to the subclassification in the software manual (Figure 12). We observed the strongest synergism of all different PARP inhibitors in combination with the alkylating drug TMZ (Figure 10, Figure 11, Figure 12 and Table 3), followed by combination with the topoisomerase I inhibitor SN-38 as second best combination (Figure 10, Figure 11, Figure 12 and Table 3). Of note, we recognized, that talazoparib (lowest PARP inhibitor concentration needed) and olaparib (best CI values) combined with TMZ resulted in the most pronounced combinatory effect (Figure 12). For PARP inhibitors together with the topoisomerase II inhibitors doxorubicin or etoposide and the alkylating drug ifosfamide we observed a less consistent enhanced cytotoxicity in the combinations (Figure 12). The DNA intercalant actinomycin D and

Table 3: Synergistic induction of apoptosis by combination treatment of PARP inhibitors and chemotherapeutics.

A4573		Talazoparib [nM]					Niraparib [nM]			Olaparib [µM]			Veliparib [µM]		
		0.5	1	2.5	5	7.5	25	50	75	100	300	600	1600	2200	2800
TMZ [µM]	25	0.785	0.402	0.164			0.342	0.187	0.115	0.064	0.045	0.024	0.364	0.278	0.277
	50	0.471	0.210	0.088			0.287	0.174	0.118	0.005	0.005	0.006	0.140	0.103	0.080
	100	0.219	0.130	0.086			0.206	0.169	0.131	0.003	0.005	0.007	0.091	0.080	0.074
SN38 [nM]	0.2			1.315	0.856	0.613	1.188	0.766	0.628	0.626	0.480	0.425	1.241	0.949	0.814
	0.4			0.701	0.597	0.484	0.866	0.555	0.363	0.518	0.389	0.301	0.495	0.534	0.464
	0.6			0.634	0.564	0.464	0.346	0.277	0.242	0.474	0.493	0.290	0.587	0.558	0.507
Etoposide [ng/ml]	25		1.123	0.848	0.566		1.126	0.735	0.622	0.796	0.708	0.717	1.300	1.300	1.451
	50		1.188	0.927	0.689		1.032	0.776	0.602	0.833	0.651	0.610	1.270	1.097	1.151
	75		1.050	0.852	0.694		0.813	0.690	0.582	0.715	0.653	0.583	0.952	0.883	0.895
Ifosfamide [µM]	0.5			1.463	1.117	1.031	0.838	1.103	0.788	0.897	0.928	0.638	1.230	1.305	1.325
	1			1.155	0.937	0.786	0.685	0.716	0.566	1.191	1.060	0.839	1.182	1.103	1.139
	2			0.904	0.752	0.715	0.962	0.740	0.573	0.598	0.477	0.332	1.302	1.342	1.329
Doxo [ng/µl]	1		1.469	1.314	1.240		1.706	1.176	0.937	1.652	1.209	0.977	1.610	1.507	1.322
	2.5		1.353	1.161	1.027		1.213	0.919	0.808	1.162	0.993	0.933	1.322	1.318	1.265
	4		0.925	0.868	0.851		0.864	0.751	0.718	0.878	0.846	0.804	0.905	0.871	0.868
Vincristine [nM]	0.1		1.917	1.707	1.269		1.289	1.233	1.025	1.950	1.371	0.866	2.378	2.506	1.702
	0.25		2.060	1.774	1.532		1.898	1.773	1.443	2.034	1.562	1.062	1.723	1.578	1.358
	0.4		1.472	1.475	0.928		1.198	1.169	0.876	1.311	1.139	0.750	1.395	1.312	1.112
AMD [ng/ml]	0.1		2.185	1.533	1.158		2.005	1.885	1.291	3.619	2.470	1.481	1.904	1.793	1.500
	0.25		1.773	1.454	1.319		2.343	1.621	1.293	1.325	1.334	1.195	1.813	1.536	1.500
	0.4		1.328	1.231	1.070		1.130	0.988	0.863	1.198	1.240	1.098	1.382	1.343	1.156

SK-ES-1		Talazoparib [nM]					Niraparib [nM]			Olaparib [µM]			Veliparib [µM]		
		0.5	1	2.5	5	7.5	25	50	75	100	300	600	1600	2200	2800
TMZ [µM]	25	0.463	0.327	0.252			0.198	0.147	0.114	0.159	0.182	0.181	0.222	0.215	0.208
	50	0.367	0.239	0.201			0.141	0.111	0.088	0.139	0.13	0.132	0.139	0.14	0.137
	100	0.225	0.171	0.137			0.068	0.061	0.059	0.143	0.144	0.131	0.085	0.093	0.088
SN38 [nM]	0.2			0.898	0.924	0.817	1.006	0.826	0.664	0.626	0.687	0.493	0.939	1.059	1.164
	0.4			0.847	0.911	0.877	0.81	0.733	0.634	0.661	0.609	0.528	0.774	0.797	0.722
	0.6			0.896	0.933	0.898	0.92	0.827	0.669	0.833	0.77	0.692	0.803	0.796	0.789
Etoposide [ng/ml]	25		1.663	1.165	1.159		0.96	0.745	0.828	1.614	0.713	0.519	1.167	1.099	1.041
	50		1.03	1.034	1.006		1.021	0.912	0.917	0.883	0.573	0.468	1.047	0.969	0.872
	75		1.175	1.106	1.159		0.802	0.672	0.728	0.725	0.599	0.506	0.843	0.815	0.809
Ifosfamide [µM]	0.5			1.064	0.843	0.828	1.734	1.436	1.08	0.458	0.573	0.445	0.929	0.85	0.83
	1			0.912	0.838	0.788	1.158	0.979	0.691	0.743	0.568	0.45	0.94	0.869	0.801
	2			0.809	0.916	0.851	0.728	0.646	0.602	0.484	0.416	0.328	1.172	1.143	1.031
Doxo [ng/µl]	1		2.101	1.53	1.019		2.388	1.46	1.142	0.989	0.993	0.657	0.903	0.903	0.818
	2.5		1.702	1.295	0.771		1.359	1.128	0.997	1.25	0.938	0.766	1.178	1.039	0.802
	4		0.931	0.657	0.609		0.784	0.696	0.688	0.594	0.481	0.461	0.339	0.326	0.363
Vincristine [nM]	0.1		2.633	1.326	1.12		1.043	0.856	0.716	1.816	1.33	1.097	3.053	1.417	1.288
	0.25		2.291	1.415	1.107		1.902	1.036	1.015	1.015	0.873	0.719	1.292	0.904	0.778
	0.4		1.422	1.408	0.926		1.157	0.997	0.825	1.359	0.994	0.807	1.188	1.12	0.809
AMD [ng/ml]	0.1		1.208	1.012	0.909		2.45	1.266	1.099	1.529	1.056	0.858	1.586	1.822	1.59
	0.25		1.472	0.963	0.801		1.812	0.881	0.796	1.538	1.183	0.954	1.546	1.355	1.236
	0.4		1.762	0.946	0.741		1.034	0.774	0.576	1.066	0.864	0.744	1.434	1.232	1.21

Combination indices (CI) were calculated as described in materials and methods for cell viability induced by combined treatment for 72 hours with indicated concentrations of PARP inhibitors and chemotherapeutics.

the microtubule vincristine resulted in little to no synergy (Figure 12). We identified cotreatment of olaparib and TMZ or SN-38 to be the most potent combinations in our screening approach of testing different PARP inhibitors together with different chemotherapeutics. Therefore, we focused on further validation experiments of these combinations.

CI-Values		
< 0,1		Very strong synergism
0,1-0,3		Strong synergism
0,3-0,7		Synergism
0,7-0,85		Moderate synergism
0,85-0,9		Slight synergism
0,9-1,1		Nearly additive
1,1-1,2		Slight antagonistic
1,2-1,45		Moderate antagonistic
>1,45		Antagonism
		Not calculated

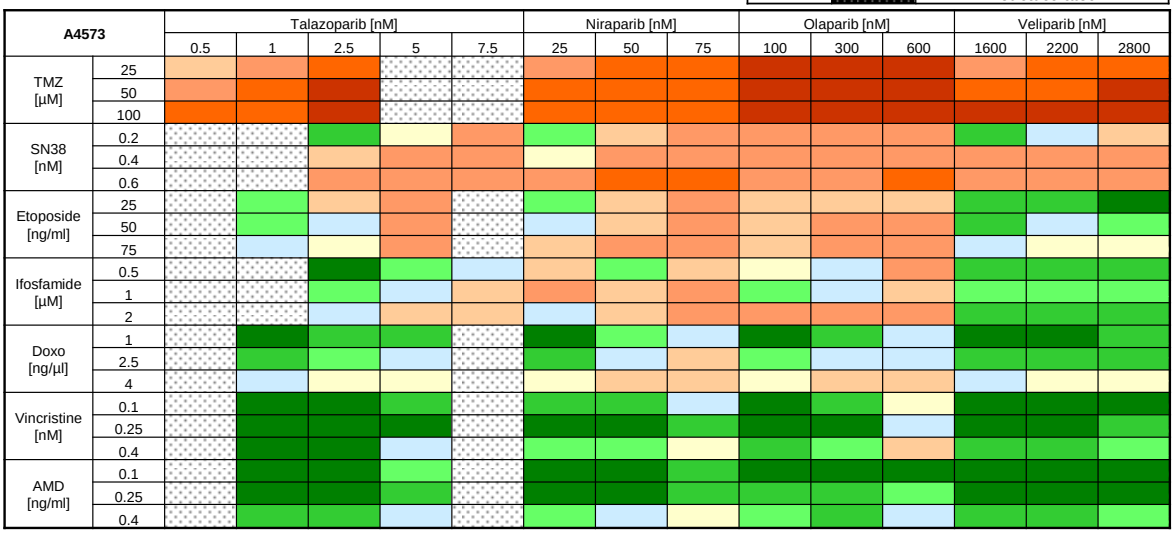

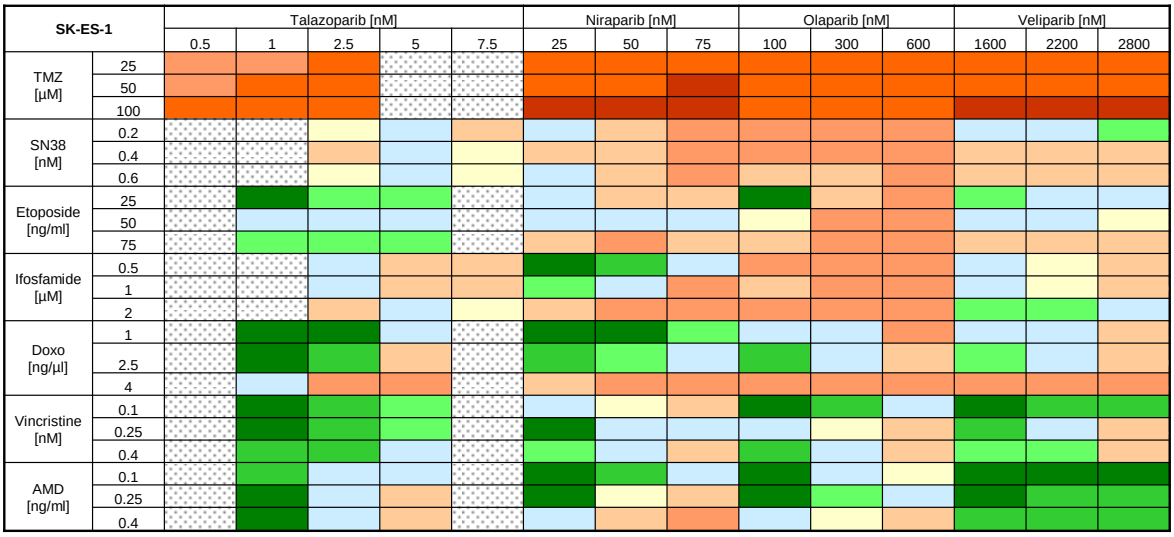

Figure 12: Heat map for synergistic drug induction of PARP inhibitors and chemotherapeutics in ES cell lines.

A4573 and SK-ES-1 cells were treated for 72 hours with different PARP inhibitors (*i.e*. talazoparib, niraparib, olaparib and veliparib) in combination with different cytostatic drugs (*i.e*. TMZ, SN-38, etoposide, ifosfamide, doxorubicin, vincristine and actinomycin D). Synergistic, additive or antagonistic drug interactions were calculated by CI. CI values were then used to generate a heat map of drug interactions according to the classifications provided by the software's manual.

III.1.2 Olaparib synergizes with TMZ and SN-38 to induce cell death in ES cells

To validate the potency of olaparib/TMZ combination treatment, we extended our study to four additional ES cell lines, A4573, SK-ES-1, TC-32 and TC-71. To demonstrate whether treatment of ES cell lines with a combination of olaparib and TMZ or SN-38 can also trigger cell death induction, we additionally assessed DNA fragmentation, as a typical marker of apoptosis. Of note, combination treatment acted together to significantly increase DNA fragmentation and reduce cell viability compared to either treatment alone (Figure 13). Additionally, combination treatment of olaparib/SN-38 likewise induced an increase in DNA

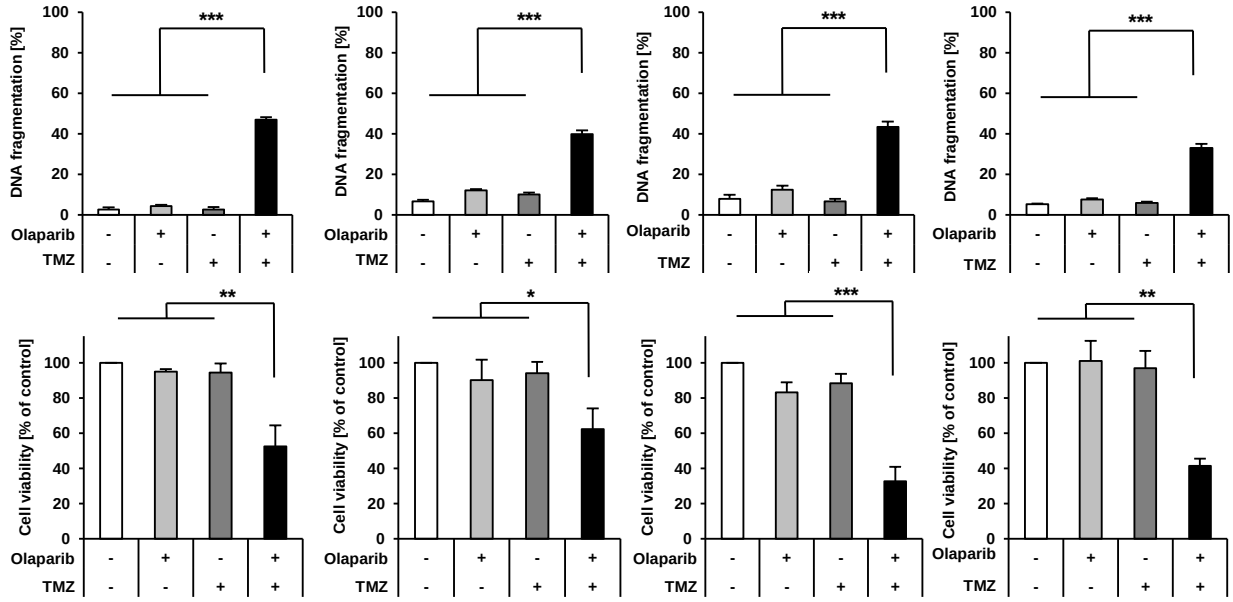

Figure 13: Olaparib synergized with TMZ to induce cell death in ES cells.

A4573 (left), SK-ES-1 (left middle), TC-32 (right middle) and TC-71 (right) cells were treated for 48 hours, respectively TC-32 and TC-71 for 72 hours, with 0.3 µM olaparib and/or 50 µM TMZ. Apoptosis was determined by analysis of DNA fragmentation of PI-stained nuclei using flow cytometry. Cell viability was measured by MTT assay and is shown as percentage of untreated control. Data are shown as mean +/- SD of three independent experiments performed in triplicate; *, $P < 0.05$; **, $P < 0.01$; ***, $P < 0.001$.

fragmentation and reduction of cell viability in ES cell lines A4573 and SK-ES-1 (Figure 14). To explore the effects of olaparib/TMZ and olaparib/SN-38 combination treatments on long-term survival of ES cells, we performed colony assays of A4573 and SK-ES-1 cells. We observed that olaparib in combination with TMZ or SN-38 significantly reduced colony formation of ES cells compared to solvent control or either treatment alone (Figure 15).

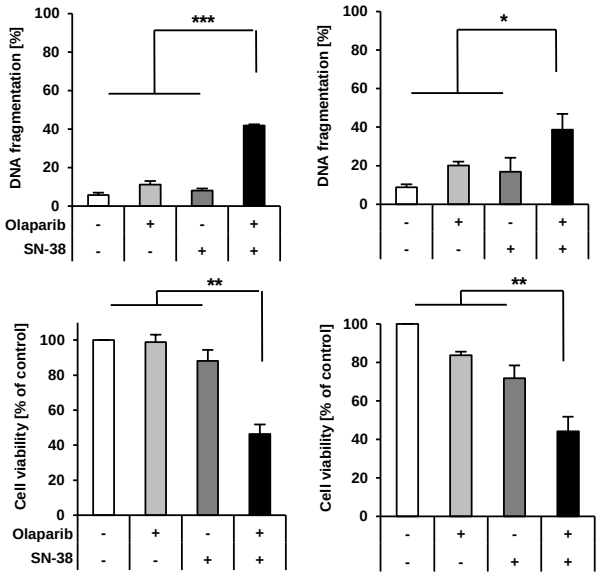

Figure 14: Olaparib synergized with SN-38 to induce cell death in ES cells.

A4573 (left), SK-ES-1 (right) cells were treated for 48 hours with 0.3 µM olaparib and/or 0.6 nM SN-38. Apoptosis was determined by analysis of DNA fragmentation of PI-stained nuclei using flow cytometry (upper panel). Cell viability was measured by MTT assay and is expressed as percentage of untreated control (lower panel)). Data are shown as mean +/- SD of three independent experiments performed in triplicate; *, P < 0.05; **, P < 0.01; ***, P < 0.001.

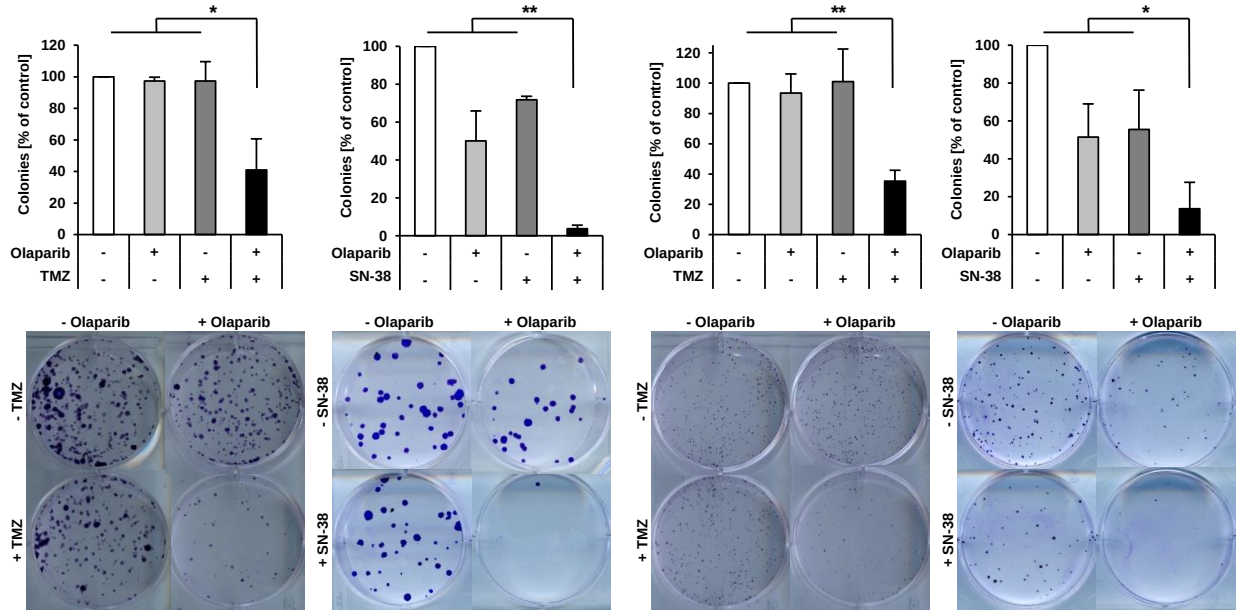

Figure 15: Olaparib together with TMZ or SN-38 suppressed colony formation of ES cells.

A4573 (left panels) and SK-ES-1 (right panels) cells were treated with 0.3 µM olaparib and/or 50 µM TMZ and/or 0.6 nM SN-38 for 24 hours, living cells were counted and subsequently 100 cells/well were re-seeded in drug-free medium in a six-well plate for additional 12 days. Colony formation was assessed by crystal violet staining and colonies were counted macroscopically. The number of colonies is expressed as percentage of untreated control (upper panels) and representative images are shown (lower panels). Data are shown as mean +/- SD of three independent experiments performed in triplicate; *, P < 0.05; **, P < 0.01.

As TMZ together with SN-38 has been administered together in clinical protocols for second-line treatment of Ewing's sarcoma (113), we additionally tested a triple-therapy approach of olaparib, TMZ and SN-38 in two different ES cell lines, to analyze whether addition of SN-38 can further enhance the efficacy of olaparib/TMZ combination treatment. Indeed, we showed that triple therapy of olaparib, TMZ and SN-38 was significantly more effective to reduce cell viability of ES cell lines in comparison to the single treatments or the different combinations (Figure 16).

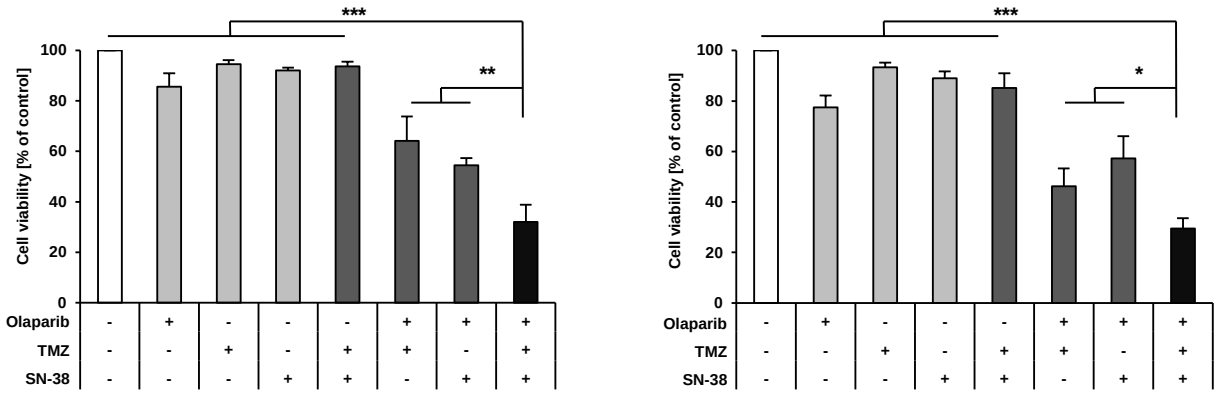

Figure 16: Triple therapy of olaparib, TMZ and SN-38 significantly reduced viability in ES cell lines.

A4573 (left) and SK-ES-1 (right) cells were treated for 72 hours with 0.3 µM olaparib and/or 10 µM TMZ and/or 0.2 nM SN-38. Cell viability was measured by crystal violet staining and is expressed as percentage of untreated control. Data are shown as mean +/- SD of three independent experiments performed in triplicate; *, $P < 0.05$; **, $P < 0.01$; ***, $P < 0.001$.

To this end, these experiments demonstrated that combination of olaparib together with TMZ or SN-38 induced cell death, reduced cell viability and suppressed clonogenic growth in ES cells. Furthermore, triple therapy of ES cell lines with olaparib, TMZ and SN-38 additionally potentiated the anti-tumor effect. For mechanistic studies we focused on the combination of olaparib and TMZ, as this combination induced the most pronounced and uniform synergistic response throughout our previous experiments.

III.1.3 Olaparib/TMZ cotreatment caused G2-cell cycle arrest prior to cell death

For determination of the onset of cell death, we performed a time-dependent analysis of cell death induction in A4573 and SK-ES-1 cells. Therefore, DNA fragmentation upon treatment with olaparib/TMZ was measured over time. It was demonstrated, that Olaparib cooperated with TMZ to trigger cell death in a time-dependent manner. We defined the onset of cell death after 18 hours, as this was the first time point, where we detected a significant increase in cell death in A4573 upon combination treatment compared to solvent treated or single drug treated cells (Figure 17). SK-ES-1 demonstrated a tendency for the increase in DNA fragmentation after 18 hours.

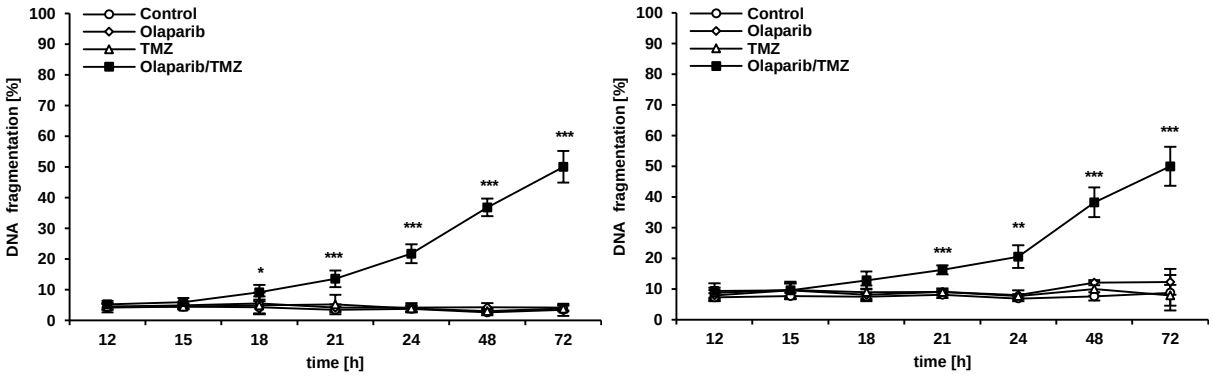

Figure 17: Cell death kinetic of A4573 (left) and SK-ES-1 (right) ES cell lines upon combination treatment of olaparib and TMZ.

A4573 and SK-ES-1 cells were treated with 0.3 µM olaparib and/or 50 µM TMZ for indicated time. Apoptosis was determined by quantification of DNA fragmentation of PI-stained nuclei using flow cytometry. Data are shown as mean +/- SD of three independent experiments performed in triplicate; **, P < 0.01; ***, P < 0.001.

As it has been previously shown that olaparib/TMZ combination treatment induced DNA damage, we checked for DNA damage response (DDR) (80,81). Therefore, we investigated phosphorylation of checkpoint kinases 1 and 2 (Chk1 and Chk2) as typical markers for DNA damage (114). It was shown that treatment of A4573 and SK-ES-1 cells, with a combination of olaparib and TMZ, resulted in phosphorylation of Chk1 and Chk2, pointing to an early activation of DDR pathways (Figure 18). Next, cell cycle analysis using flow cytometry and FlowJo™ software was performed.

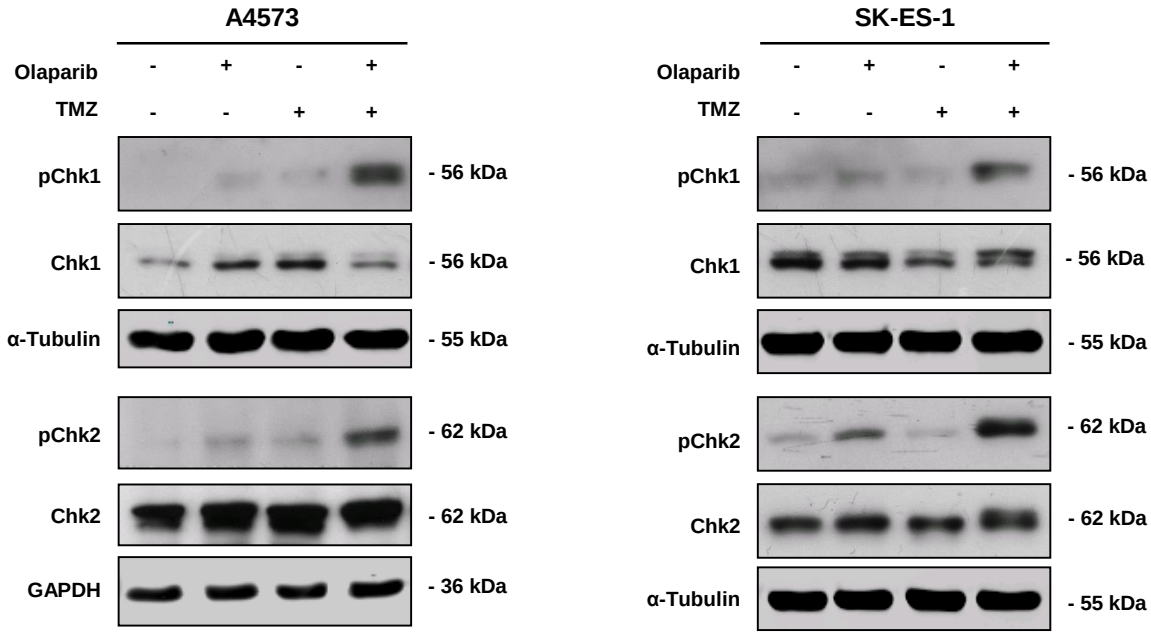

Figure 18: Cotreatment of olaparib/TMZ activated checkpoint kinases Chk1 and Chk2.

A4573 and SK-ES-1 cells were treated with 0.3 µM olaparib and/or 50 µM TMZ for 18 hours. Phosphorylation of checkpoint kinases was assessed by Western blotting. Expression of GAPDH or α-Tubulin served as loading controls. Representative blots of two independent experiments are shown.

Besides activation of checkpoint kinases it was recognized by FACS analysis that cells suffered under cell cycle arrest, depending on cotreatment of olaparib/TMZ. Our analysis revealed a cell cycle arrest in G_2-/M-phase upon combination treatment with olaparib/TMZ compared to single treatment or untreated

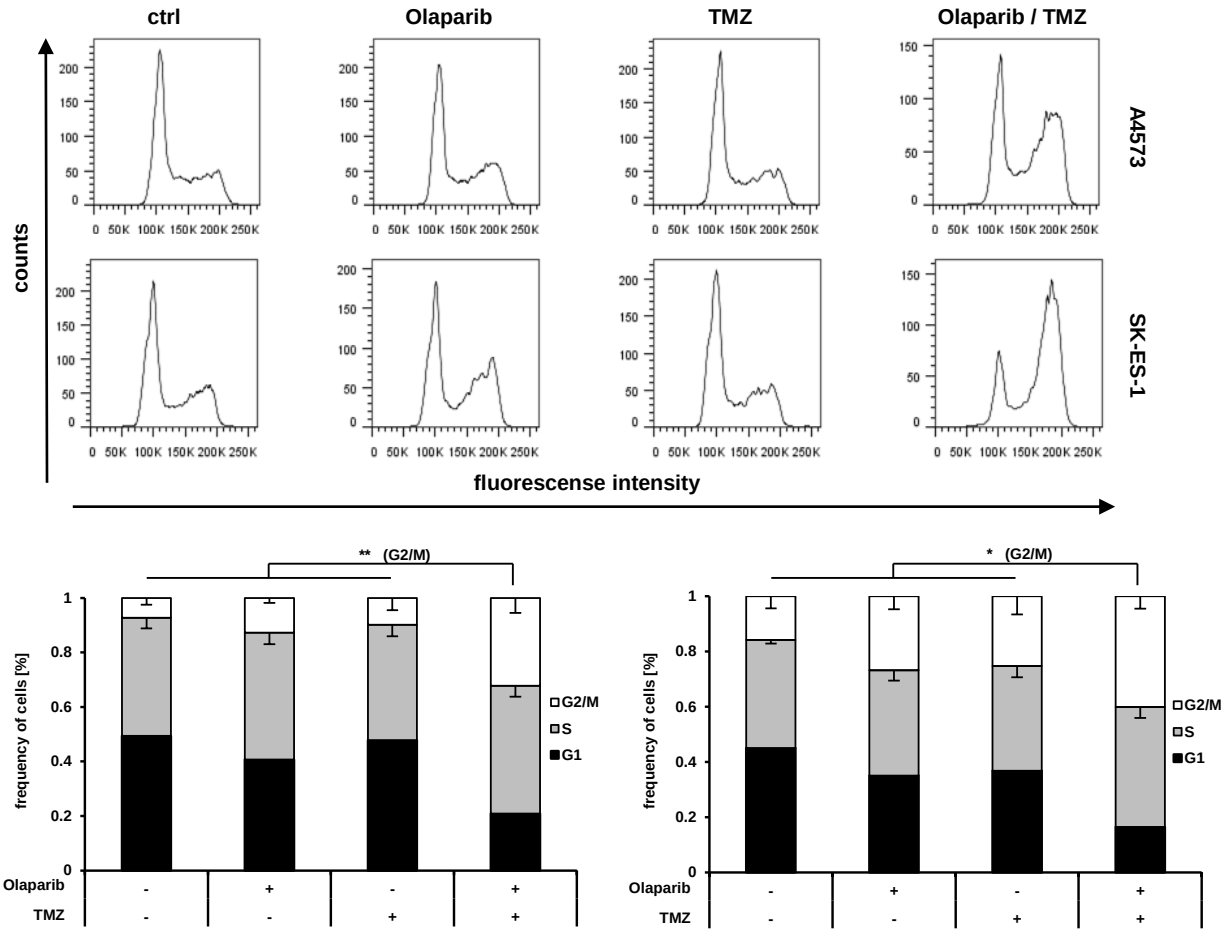

Figure 19: Checkpoint kinase-mediated G2-M arrest was determined prior to cell death induction.

For cell cycle analysis, ES cells were treated for 18 hours with 0.3 µM Olaparib and/or 50 µM TMZ. DNA was stained with PI and cell cycle analysis was performed using FlowJo™ software. Representative histograms for control and treated samples are shown. Data for A4573 (left) and SK-ES-1 (right) are shown as mean +/- SD of three independent experiments performed in triplicate; *, $P < 0.05$; **, $P < 0.01$ comparing olaparib/TMZ cotreated to single treated or untreated cells in G2/M phase.

cells (Figure 19). To distinguish between G_2- and M-phase arrest, phosphorylation of histone H3, as typical marker for M-phase arrest, was analyzed (115). Of note, cotreatment of olaparib/TMZ did not cause phosphorylation of histone H3, whereas the microtubule interfering drug vincristine, used as a positive control, clearly induced phosphorylation pointing to induction of M-phase arrest in those cells (Figure 20). Together, this set of experiments demonstrated that the combination of olaparib and TMZ induced cell cycle arrest in the G_2-phase of the cell cycle prior to cell death induction in A4573 and SK-ES-1 ES cell lines.

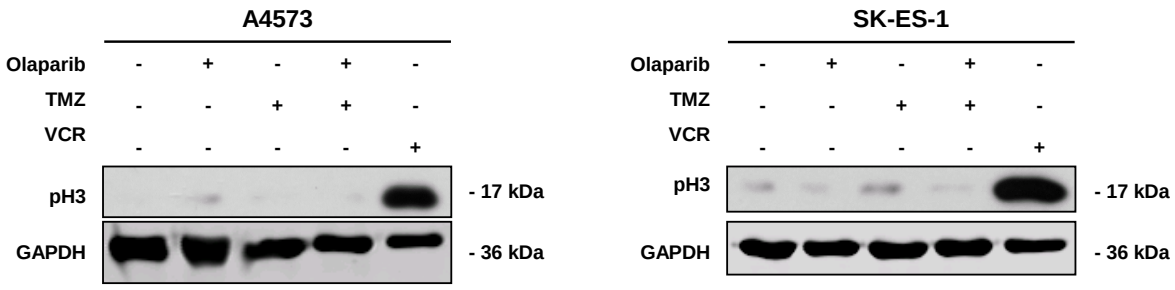

Figure 20: Olaparib/TMZ-cotreatment did not lead to M-phase dependent phosphorylation of histone H3.

ES cells were treated with 0.3 µM olaparib and/or 50 µM TMZ or 2.5 nM vincristine for 18 hours. Expression of mitotic marker pH3 was analyzed by Western blotting. Expression of GAPDH served as loading control. Representative blots of two independent experiments are shown.

III.1.4 Olaparib/TMZ-induced cell death was executed via caspase-dependent effector pathways

To investigate whether caspases were involved in olaparib/TMZ-induced cell death the broad-range caspase inhibitor zVAD.fmk was used. The addition of zVAD.fmk led to a significant reduction of cell death upon treatment with olaparib/TMZ, indicating that caspases were involved in cell death induction (Figure 21). For verification of the involvement and activation of caspases in olaparib/TMZ-mediated cell death, Western blots of caspase-9, caspase-8, caspase-3 and PARP were performed. As positive control for caspase activation we used SK-ES-1 cells treated with the tumor necrosis factor-related apoptosis-inducing ligand (TRAIL) receptor 2 antagonist antibody lexatumumab. It was demonstrated that olaparib/TMZ cotreatment induced cleavage of caspase-9 into p37/p35, caspase-3 into p17/p12 and PARP into p89 fragments (Figure 22). Of note, cleavage of caspase-8 was not detected, pointing to the fact that we predominantly observed intrinsic apoptosis, mediated by the mitochondria. In contrast to SK-ES-1 cells, the A4573 have been reported to express very low levels of caspase-8, demonstrating the fact that caspase-8 is often epigenetically silenced in ES (116,117). These experiments showed that the combination of olaparib/TMZ triggered caspase activation and caspase-dependent intrinsic apoptosis in ES cells.

To strengthen our hypothesis that olaparib/TMZ-induced cell death is mediated via the mitochondria, we further analyzed mitochondrial outer membrane potential (MOMP) by measuring loss of mitochondrial membrane potential (LMMP) in a time-dependent manner. Notably, Olaparib and TMZ cooperated to trigger LMMP over time, subsequent to the onset of apoptosis at 21 hours (Figure 23).

Furthermore, we assessed the expression levels of BCL-2 family proteins via Western blot, as they are the key regulators of the mitochondrial pathway (60). Determination of expression levels of different BCl-2 family proteins showed a downregulation of MCL-1 and NOXA expression upon olaparib/TMZ treatment.

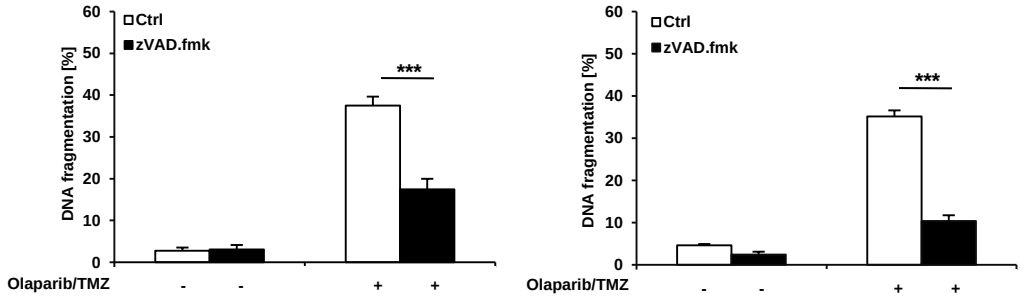

Figure 21: Addition of zVAD.fmk significantly reduced cell death induction upon treatment with olaparib/TMZ.

A4573 (left) and SK-ES-1 (right) cells were treated for 48 hours with 0.3 µM olaparib and/or 50 µM TMZ in the presence or absence of 50 µM zVAD.fmk. Apoptosis was determined by quantification of DNA fragmentation of PI-stained nuclei using flow cytometry. Data are shown as mean +/- SD of three independent experiments performed in triplicate; ***, P < 0.001

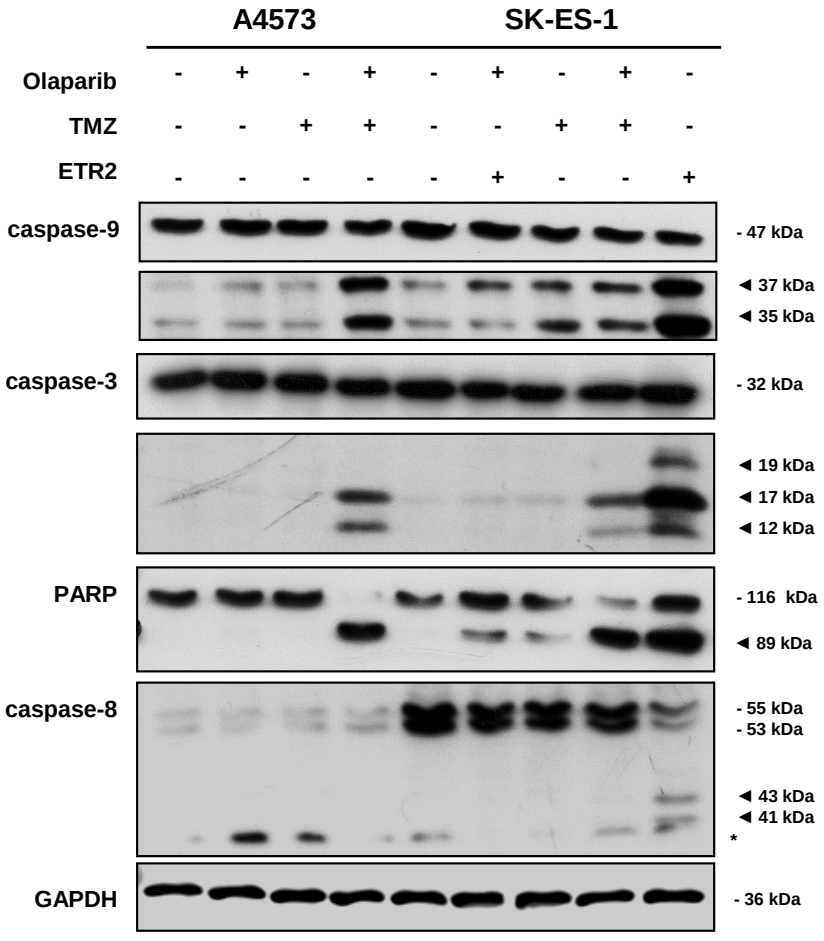

Figure 22: Olaparib/TMZ cotreatment induced cleavage of caspase-9, caspase-3 and PARP.

A4573 and SK-ES-1 cells were treated with 0.3 µM olaparib and/or 50 µM TMZ for 24 hours. Cleavage of caspase-9, caspase-3, caspase-8 and PARP was analyzed by Western blotting. Arrowheads indicate active cleavage fragments, expression of GAPDH served as loading control; asterisk denotes unspecified protein bands. SK-ES-1 cells treated for two hours with 2 µg/ml lexatumumab (ETR-2) served as positive control for caspase activation. Representative blots of two independent experiments are shown.

The expression levels of other important antiapoptotic BCL-2 family proteins, e.g. BCL-2 and BCL-X_L, remained unchanged as well as the expression levels of the proapoptotic BH3-only proteins, BIM, BMF or PUMA (Figure 24).

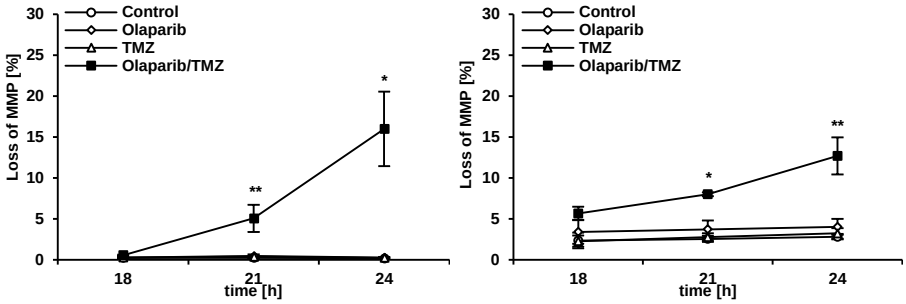

Figure 23: Kinetic of loss of mitochondrial membrane potential in A4573 (left) and SK-ES-1 (right) ES cells.

A4573 and SK-ES-1 cells were treated with 0.3 µM olaparib and/or 50 µM TMZ for indicated times and loss of MMP in the living cell population was determined by flow cytometry using TMRM fluorescent dye. Data are shown as mean +/- SD of three independent experiments performed in triplicate; *, P < 0.05; **, P < 0.01

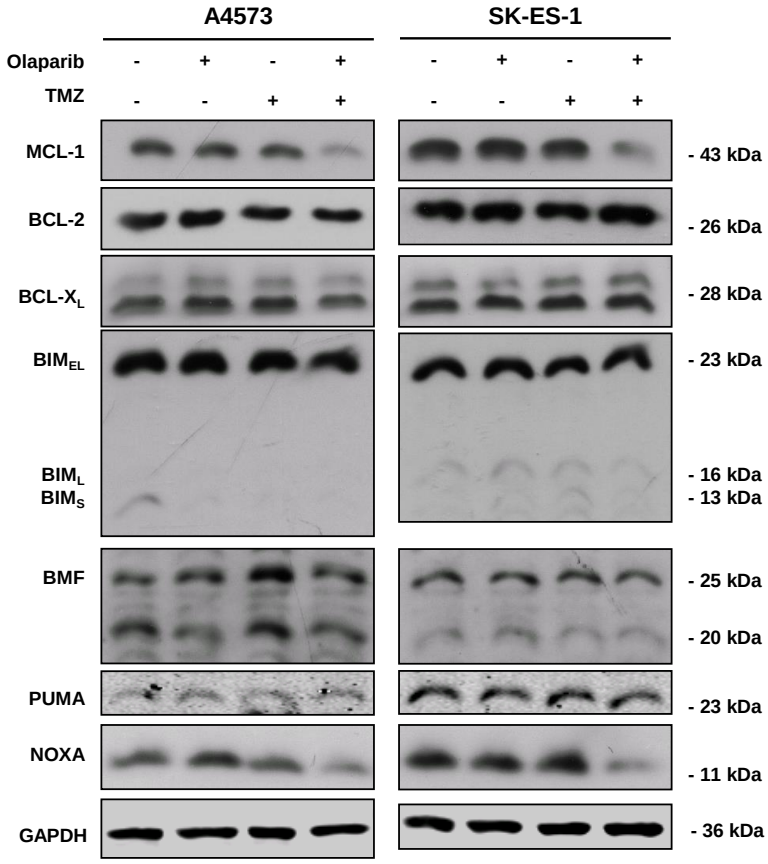

Figure 24: Expression of BCL-2 family proteins in A4573 and SK-ES-1 cells upon treatment with olaparib/TMZ.

A4573 and SK-ES-1 cells were treated with 0.3 µM olaparib and/or 50 µM TMZ for 18 hours. Expression of BCL-2 family proteins was analyzed by Western blot, expression of GAPDH served as loading control. Representative blots of two independent experiments are shown.

III.1.5 Olaparib/TMZ cotreatment promoted proteasomal degradation of MCL-1

As shown, we detected downregulation of MCL-1 expression levels in A4573 and SK-ES-1 cells upon combined treatment with olaparib and TMZ. To test whether downregulation of MCL-1 resulted from its proteasomal degradation and/or by caspase-mediated cleavage of MCL-1, we treated ES cells additionally with the proteasome inhibitor Bortezomib, the caspase inhibitor zVAD.fmk or both. Notably, addition of bortezomib, but not zVAD.fmk, to olaparib/TMZ treated A4573 and SK-ES-1 ES cells significantly restored MCL-1 expression levels. Neither the addition of zVAD.fmk to olaparib/TMZ treated cells, nor the addition of zVAD.fmk to olaparib/TMZ/bortezomib treated cells increased MCL-1 expression levels, as graphically evaluated by Western blot densitometry with ImageJ™ software (Figure 25). This clearly demonstrated that MCL-1 became degraded via the proteasome upon treatment with olaparib/TMZ.

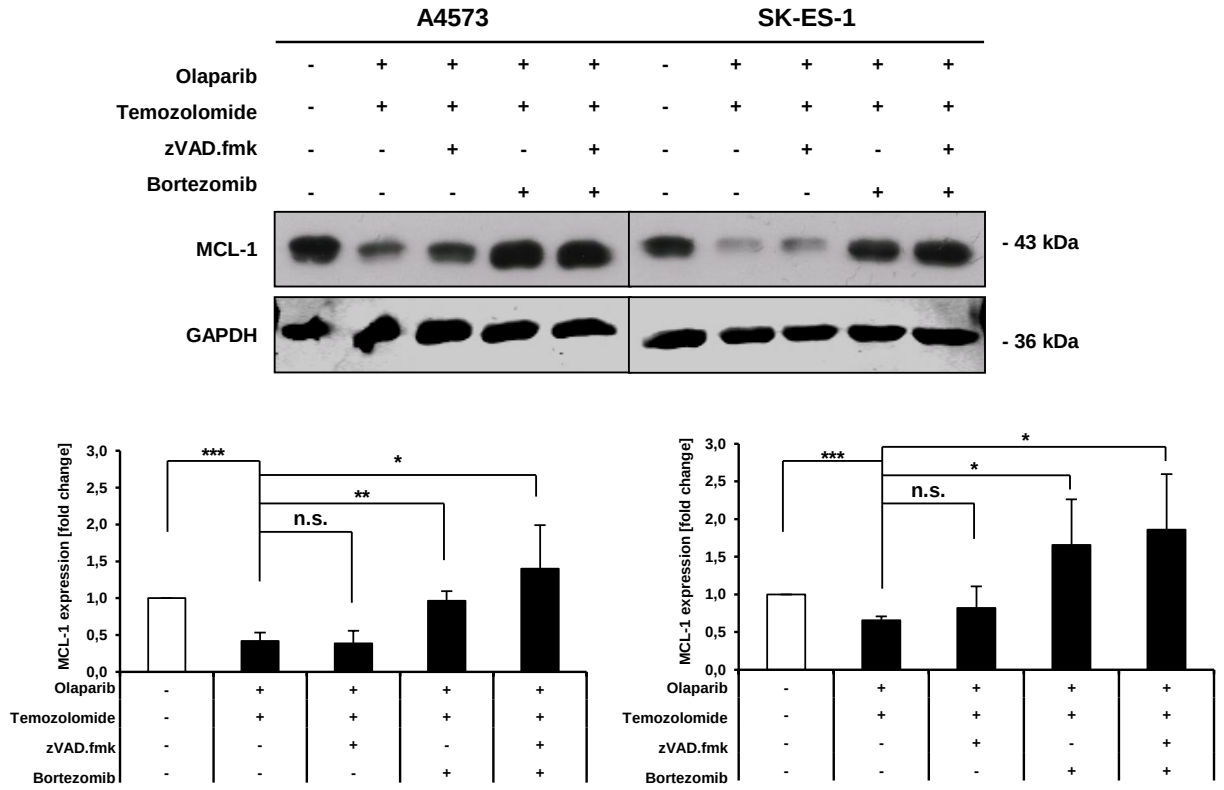

Figure 25: MCL-1 was degraded by the proteasome in A4573 and SK-ES-1 cells upon olaparib/TMZ cotreatment.

A4573 (left) and SK-ES-1 (right) cells were treated for 18 hours with 0.3 µM olaparib and/or 50 µM TMZ and/or 50 µM zVAD.fmk and/or 5 ng/ml bortezomib. Expression of MCL-1 was analyzed by Western blotting, expression of GAPDH served as loading control. For further evaluation Western blots were quantified using ImageJ™ software and changes in MCL-1 protein levels are given as fold change in comparison to untreated control. Data are shown as mean +/- SD of three independent Western blots; *, $P < 0.05$; **, $P < 0.01$.

To further analyze the importance of MCL-1 for olaparib/TMZ-mediated cell death, we generated ES cells expressing a phosphomutant of MCL-1 (MCL-1 4A). Due to the lack of phosphorylation sites in its phospho-degron, MCL-1 4A was not degradable by the proteasome (Figure 26) (118). Remarkably, ectopic expression of MCL-1 4A significantly reduced olaparib/TMZ-induced apoptosis in ES cells (Figure 26).

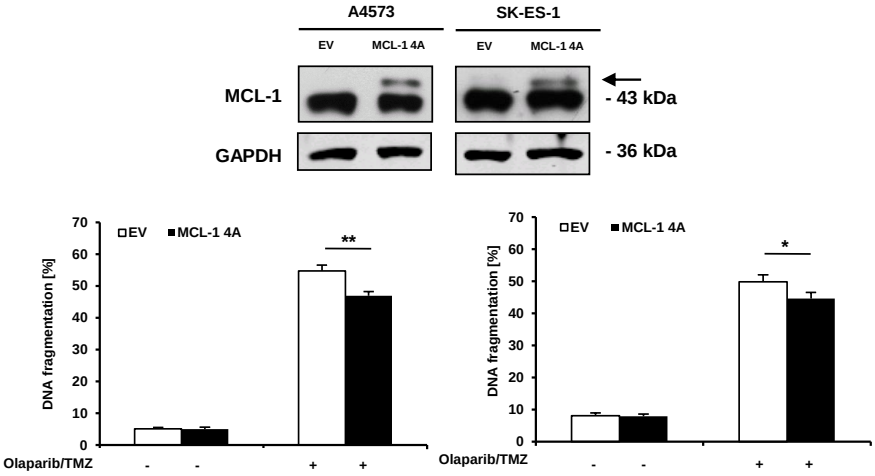

Figure 26: Overexpression of phosphomutant MCL-1 4A reduced cell death upon olaparib/TMZ combination treatment.
A4573 (left) and SK-ES-1 (right) cells were transfected with non-degradable phospho-defective mutant of MCL-1 (MCL-1 4A) or empty vector (EV). Expression of MCL-1 was analyzed by Western blotting, expression of GAPDH served as loading control, arrow indicates exogenously expressed MCL-1 and representative blots of two independent experiments are shown. Cells were treated for 48 hours with 0.3 µM olaparib and 50 µM TMZ and apoptosis was determined by quantification of DNA fragmentation of PI-stained nuclei using flow cytometry. Data are shown as mean +/- SD of three independent experiments performed in triplicate; *, P < 0.05; **, P < 0.01.

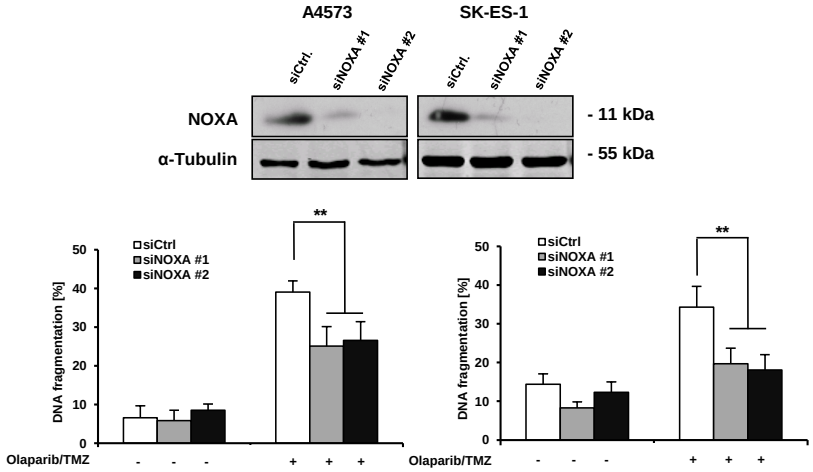

Figure 27: Silencing of NOXA by genetic silencing significantly reduced cell death upon olaparib/TMZ cotreatment.
A4573 (left) and SK-ES-1 (right) cells were transiently transfected with 10 nM non-silencing siRNA or two different constructs targeting NOXA. Expression of NOXA was analyzed by Western blotting, α-Tubulin served as loading control, representative blots of two independent experiments are shown. Transiently transfected ES cells were treated for 24 hours with 0.3 µM olaparib and 50 µM TMZ and apoptosis was determined by quantification of DNA fragmentation of PI-stained nuclei using flow cytometry. Data are shown as mean +/- SD of three independent experiments performed in triplicate; **, P < 0.01.

The BH3-only protein NOXA has been shown as key binding partner of MCL-1 (119), antagonizing its antiapoptotic function (120). Because a decrease in NOXA expression levels in A4573 and SK-ES-1 cells was noted upon olaparib/TMZ cotreatment (Figure 24), we aimed to analyze the role of NOXA in olaparib/TMZ-induced cell death. Therefore, we silenced NOXA by transfection with siRNA. Silencing of NOXA significantly reduced induction of cell death upon treatment with olaparib and TMZ in A4573 and SK-ES-1 cells, highlighting that NOXA plays an important role for cell death induction by the combination of olaparib and TMZ in ES cells (Figure 27).

III.1.6 Olaparib/TMZ cotreatment promoted BAK/BAX activation and MOMP

To confirm that olaparib/TMZ-induced cell death in A4573 and SK-ES-1 cells is conveyed by MOMP, we performed immunoprecipitation of BAK and BAX, two multi-domain proapoptotic pore forming proteins being responsible for LMMP upon cell death stimuli (65). As activation of BAK and BAX was accompanied by a conformational change, we detected activation of BAK and BAX by the use of conformation-specific antibodies. Of note, activation of BAK and BAX in A4573 and SK-ES-1 cells upon combination treatment with olaparib and TMZ was observed (Figure 28).

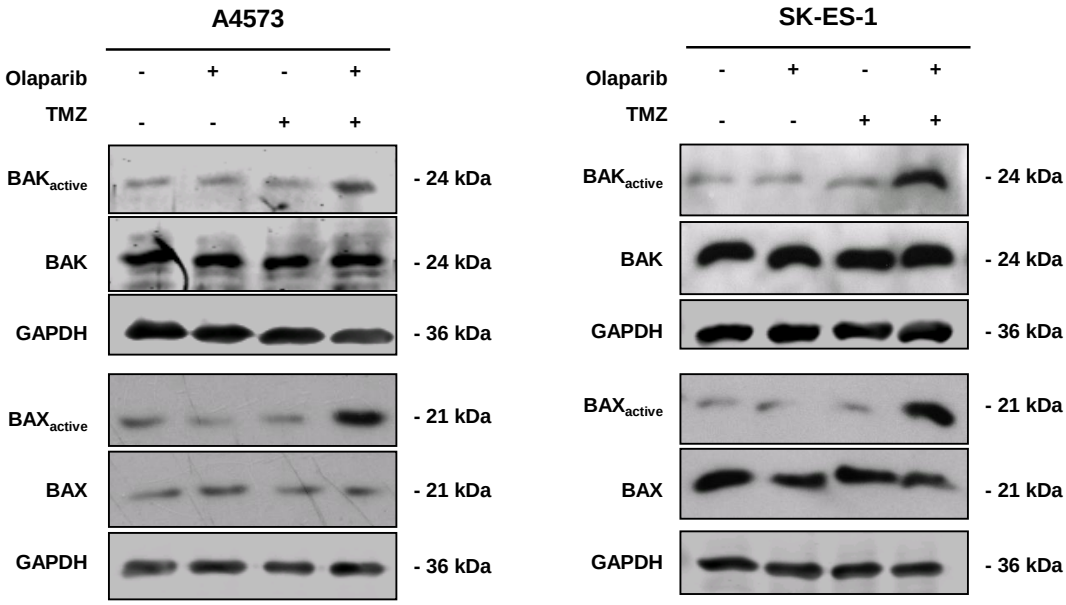

Figure 28: Olaparib/TMZ combination treatment triggered activation of BAK and BAX.

A4573 and SK-ES-1 cells were treated with 0.3 µM olaparib and/or 50 µM TMZ for 21 hours. Active conformations of BAK or BAX were immunoprecipitated using active conformation-specific antibodies and were analyzed by Western blotting. Expression of total BAK or BAX and GAPDH served as loading controls. Representative blots of two independent experiments are shown.

To investigate the functional relevance of concomitant knockdown of BAK and BAX upon combined treatment with olaparib/TMZ in A4573 and SK-ES-1 cells, a combined knockdown of BAK and BAX by transfection with siRNA was performed. We observed that olaparib/TMZ-induced apoptosis in both cell lines was significantly reduced upon combined knockdown of BAK and BAX in all siRNA construct combinations, highlighting the importance of BAK and BAX for cell death induction (Figure 29).

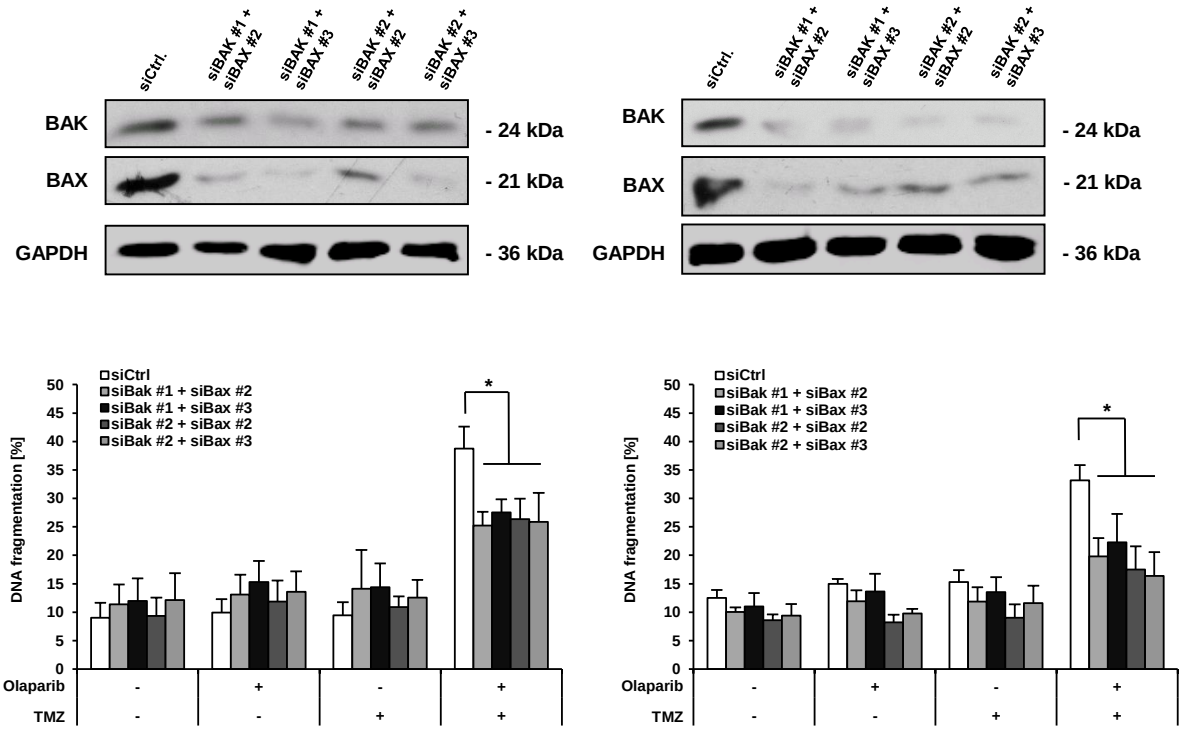

Figure 29: Combined knockdown of BAK/BAX significantly reduced cell death induced upon treatment with olaparib/TMZ.
A4573 (left) and SK-ES-1 (right) cells were transiently transfected with 10 nM non-silencing siRNA or 5 nM each of different combinations of constructs targeting BAK or BAX and expression of BAK and BAX was analyzed by Western blotting. GAPDH served as loading control. Representative blots of two independent experiments are shown. Transiently transfected ES cells were treated for 24 hours with 0.3 µM olaparib and/or 50 µM TMZ and apoptosis was determined by quantification of DNA fragmentation of PI-stained nuclei using flow cytometry. Data are shown as mean +/- SD of three independent experiments performed in triplicate; *, $P < 0.05$

III.1.7 Overexpression of BCL-2 protected ES cells towards olaparib/TMZ-induced apoptosis

To further examine the requirement of the mitochondrial pathway upon olaparib/TMZ-induced apoptosis we generated ES cells ectopically expressing a murine variant of the antiapoptotic protein BCL-2. As BCL-2 mainly sequesters proapoptotic BH3-only proteins (e.g. BID, BIM and PUMA) as well as BAK and BAX, it has been well known to prevent mitochondrial apoptosis (60,67,121). BCL-2 overexpression protected from

olaparib/TMZ-induced apoptosis in A4573 and SK-ES-1 cells, underscoring that induction of apoptosis is interceded by the mitochondrial pathway (Figure 30).

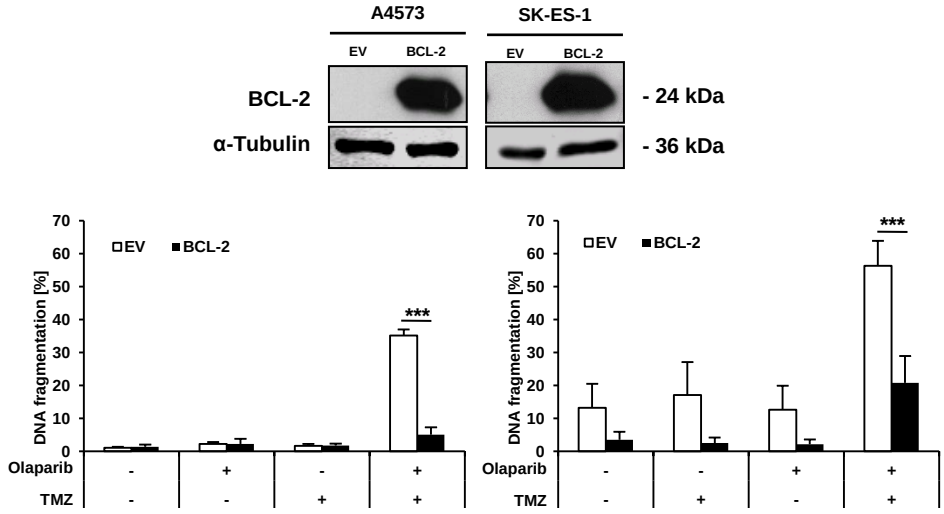

Figure 30: Olaparib/TMZ-induced apoptosis is completely inhibited upon BCL-2 overexpression.

A4573 (left) and SK-ES-1 (right) cells were transfected with a murine BCL-2 construct or empty vector and BCL-2 expression was analyzed by Western blotting. Expression of α-Tubulin served as loading controls. Representative blots of two independent experiments are shown. BCL-2-overexpressing ES cells were treated for 48 hours with 0.3 µM olaparib and 50 µM TMZ and apoptosis was determined by quantification of DNA fragmentation of PI-stained nuclei using flow cytometry. Data are shown as mean +/- SD of three independent experiments performed in triplicate; ***, $P < 0.001$.

Taking together, we conclusively demonstrated the sensitivity of ES towards PARP inhibitors. In our screening we detected talazoparib to oppose the highest cytotoxicity in ES with accompanied lowest IC_{50} values, whereas on the other hand we demonstrated TMZ to be the most favorable drug to interact together with PARP inhibitors and exhibited the lowest CI values together with olaparib. The investigation of molecular mechanisms of PCD in ES cells were described by the activation of checkpoint kinases upon combination treatment of olaparib and TMZ, followed by G_2-phase cell cycle arrest and increased cell death. Of note, the combination of olaparib/TMZ was very potent in suppressing long-term clonogenic growth of both ES cell lines. The type of cell death was determined as intrinsic apoptosis, as combination of olaparib/TMZ triggered BCL-2 family protein alterations, BAK/BAX activation, LMMP and finally activation of caspases.

III.2 Treatment of osteosarcoma with PARP inhibitors

III.2.1 Talazoparib triggered differential sensitivity of osteosarcoma cell lines

In previous experiments we investigated the vulnerability of ES towards PARP inhibition. In a screening approach we tested four different PARP inhibitors, trying to elucidate the best synergistic combinatorial setting, with talazoparib showing the highest cytotoxicity *in vitro* (92). This has been similarly demonstrated by Murai *et al.* (79,80). Additionally, in recent studies talazoparib has been thoroughly investigated *in vitro* and *in vivo* demonstrating its potency as PARP inhibitor (122,123). Therefore in ensuing studies of treatment of osteosarcoma (OS) cell lines, the focus was set on talazoparib monotherapy as prototypical PARP inhibitor. The aim was to determine the sensitivity of OS towards PARP inhibition with or without the addition of chemotherapeutics.

We recently showed that the genetic background of OS primary samples in 80% exhibited combinations of single cell substitutions, loss of heterozygosity (LOH) or large scale genomic instability leading to features of BRCA deficiency (46). In preliminary testing the osteosarcoma cell lines MG63, SaOS-2 and MNNG-HOS were found to be sensitive against talazoparib. Additionally, PARP inhibition potentiated chemosensitization of the genotoxic drugs TMZ and SN-38 in OS. To endorse these findings, studies of five different cell lines (MG63, ZK-58, SaOS-2, MNNG-HOS and U2OS) with varying genetic background (see Table 1) were performed. We acquired the IC_{50} value of talazoparib in OS cell lines by analyzing cell viability upon treatment with talazoparib monotherapy. Interestingly, three different classes of sensitivity were detected, with MG63 and ZK-58 cells showing the lowest IC_{50} values in the nanomolar concentration range of talazoparib (MG63 = 448.06 nM and ZK-58 = 115.98 nM). Intermediate

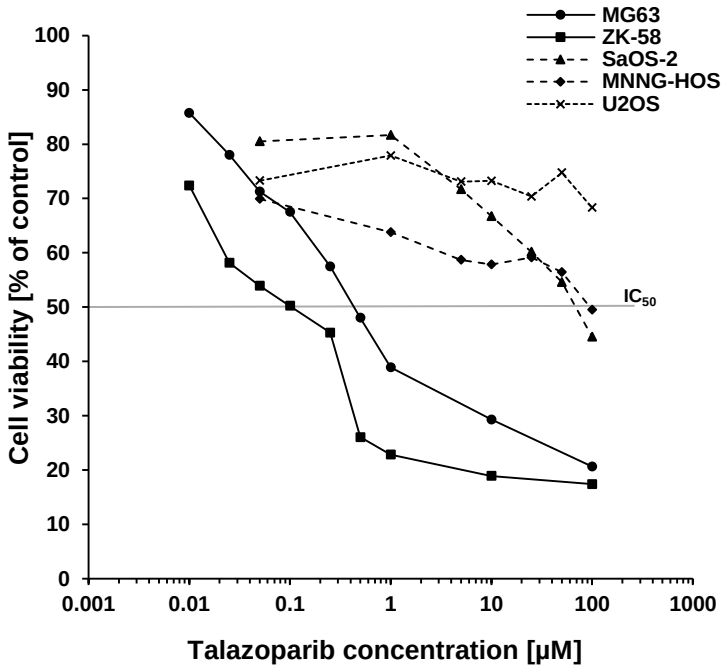

Figure 31: Talazoparib reduced cell viability of OS cells with genetic signatures of BRCAness.

OS cells were treated for 72 hours with indicated concentrations of talazoparib. Cell viability was assessed by MTT assay and is shown as percentage of untreated control. IC_{50} values were calculated using SigmaPlot™.

sensitivity to talazoparib was observed for SaOS-2 and MNNG-HOS cells, which exhibited IC_{50} values in the micromolar concentration range (SaOS-2 = 33.57 µM and MNNG-HOS = 87.56 µM). U2OS, as third class, remained largely resistant towards PARP inhibition, with still opposing ~ 70% viability upon treatment with 100 µM talazoparib (Figure 31).

Table 4: Determination of IC_{50} toxicity of talazoparib in osteosarcoma.

Osteosarcoma cell line	IC_{50} value of talazoparib
MG63	0.448 µM
ZK-58	0.115 µM
SaOS-2	33.57 µM
MNNG-HOS	87.56 µM
U2OS	> 100 µM

IC_{50} toxicity for osteosarcoma cell lines was generated graphically using SigmaPlot™ software. Raw data given by cell viability, displayed in Figure 31, were used for quantification.

Remarkably, the observed response to PARP inhibition broadly correlated with the different genetic background of the cell lines (Table 1). Thus, all responding cell lines harbored defects in homologous recombination (HR) pathway genes, so called BRCAness, which resulted in vulnerability against PARP inhibition. Precisely, e.g. MG63 cells exhibited losses in *BAP1*, *FANCA* and *FANCD2*, whereas ZK-58 cells carried a disruptive gain in *FANCD2* and loss of *BARD1*. Additionally, both cell lines scored positive in the homologous recombination deficiency (HRD)-loss of heterozygosity (LOH) score, a DNA-based degree of genomic instability, which has been indicated as a maker for BRCAness (51). SaOS-2 cells harbored losses in *CHEK2* and *TP53*, whereas MNNG-HOS cells had disruptive gains in *PTEN* and *FANCD2* as well as loss of *ATM.* The prior two cell lines scored as borderline, respectively positive in HRD-LOH and were hardly analyzable due to their triploidy, but still own a substantial load of rearrangements and allele imbalances (46). In contrast, U2OS, cells which were talazoparib resistant, carried solely a heterozygous *BRCA2* mutation and according to our findings most likely one intact *BRCA2* allele was left compensating for the inhibition of PARP. This is in compliance with their negative score in the HRD-LOH, which supposed them to not harbor features of BRCAness (46). Summarizing, it was revealed that there were different classes of sensitivity towards PARP inhibition by talazoparib among our five tested OS cell lines, largely depending on the genetic background and degree of BRCAness of these cells.

III.2.2 Screening for synergistic drug interactions of talazoparib and chemotherapeutic drugs

Parallel to our previous study we aimed to investigate the question whether PARP inhibitors modulate chemosensitivity of OS cells towards classical chemotherapeutic drugs. Therefore, we tested the effects on cell viability of talazoparib together with several anticancer drugs clinically used for osteosarcoma (cisplatin (Cis), doxorubicin (Doxo), methotrexate (MTX) and the combination of etoposide/carboplatin (etop/carbo) as this is given in relapse (37). Furthermore, temozolomide (TMZ) and SN-38 were included to our testing regimen as those drugs were most often, very potently reinforced by PARP inhibitors (92) and already demonstrated a good synergism in combination with PARP inhibitors. To distinguish among synergistic, additive or antagonistic drug interactions combination indices (CI) and fraction affected (Fa) values were calculated based on our screening results of talazoparib and chemotherapeutics (Figure 32, Table 5). For comparability reasons CI over Fa plots were created, with concentrations in which each drug combination, consisting of talazoparib plus chemotherapeutic, resulted in best synergism (Figure 33, Table 5). Best synergism in this matter was indicated by lowest CI value accompanied by highest fraction affected of one concentration of chemotherapeutic in combination with three different talazoparib concentrations. Remarkably, two groups of cell lines were identified according to drug interactions, responder and non-responder. Whereas MG63, ZK-58, SaOS-2 and MNNG-HOS cells altogether showed an increase in inhibition of cell viability with increasing drug concentrations (responder), the U2OS cell line did not show a dose-dependency in high concentration ranges and no consistent synergistic interactions (non-responder) (Figure 32). This was supported by the notion that CI values for U2OS cells mostly showed no synergism (CI > 0.9) and/or Fa values were below 0.3 (Figure 33).

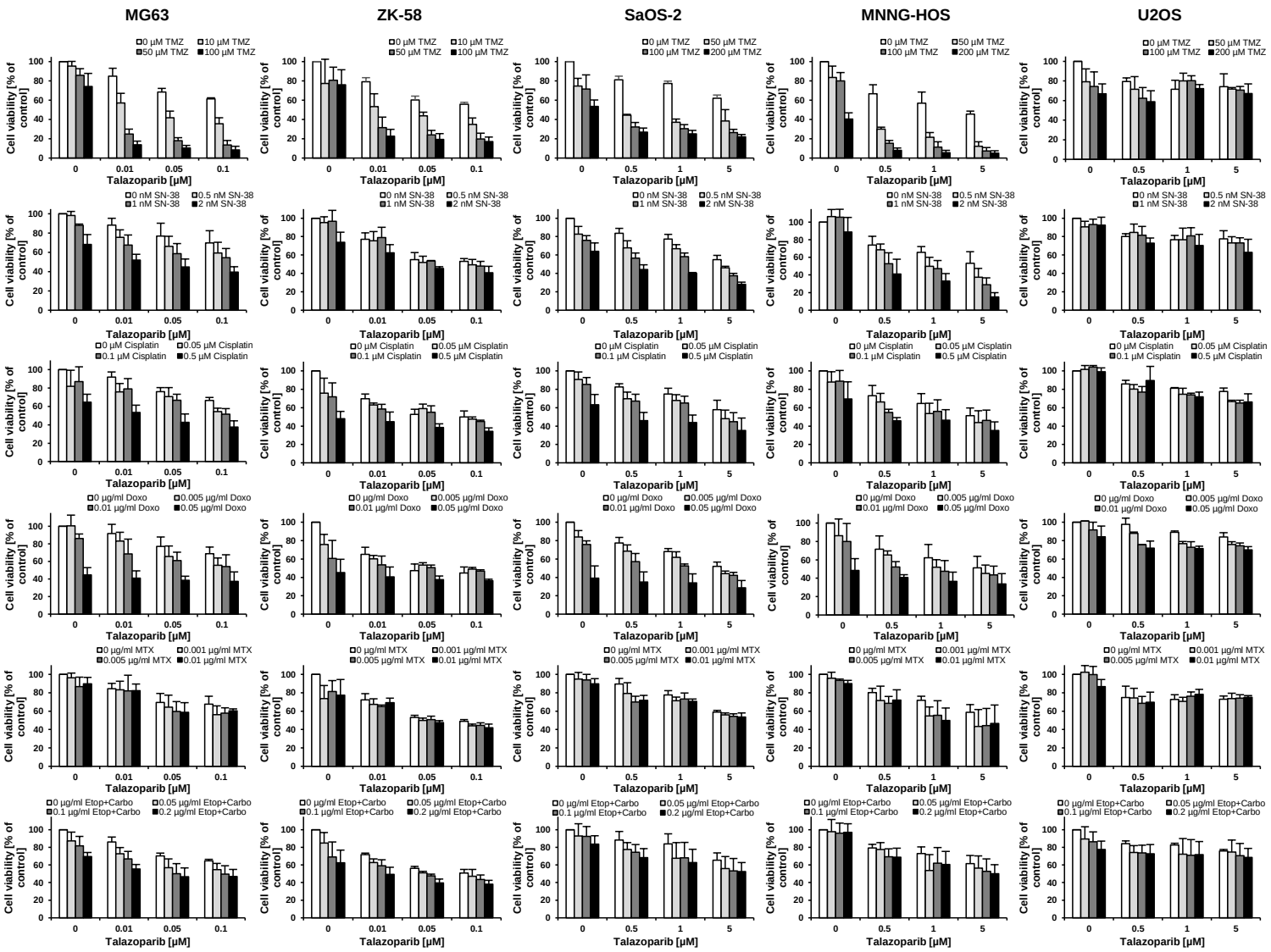

Figure 32: Screening for drug interactions of talazoparib and chemotherapeutic drugs in OS cells.

MG63, ZK-58, SaOS-2, MNNG-HOS and U2OS cells were treated for 72 hours with indicated concentrations of talazoparib in combination with indicated concentrations of anticancer drugs (*i.e*. TMZ, SN-38, cisplatin, doxorubicin, methotrexate and a combination of etoposide/carboplatin). Cell viability was assessed by MTT assay and is expressed as percentage of untreated cells. Data are shown as mean +/- SD of three independent experiments performed in triplicate.

Table 5: CI and Fa values of cell viability in OS by combination treatment of talazoparib and chemotherapeutics.

MG63			
Tala [nM]	TMZ [µM]	Fa	CI
10	10	0.429	0.113
10	50	0.75	0.042
10	**100**	**0.862**	**0.031**
50	10	0.582	0.145
50	50	0.821	0.036
50	**100**	**0.896**	**0.025**
100	10	0.644	0.172
100	50	0.865	0.031
100	**100**	**0.916**	**0.022**

MG63			
Tala [nM]	SN-38 [nM]	Fa	CI
10	0.5	0.244	0.485
10	1	0.324	0.607
10	**2**	**0.479**	**0.826**
50	0.5	0.338	0.615
50	1	0.413	0.64
50	**2**	**0.552**	**0.776**
100	0.5	0.407	0.629
100	1	0.456	0.69
100	**2**	**0.604**	**0.737**

MG63			
Tala [nM]	Cis [µM]	Fa	CI
10	0.05	0.243	0.425
10	0.1	0.209	0.965
10	**0.5**	**0.466**	**0.331**
50	0.05	0.292	0.812
50	0.1	0.331	0.719
50	**0.5**	**0.572**	**0.258**
100	0.05	0.455	0.568
100	0.1	0.485	0.507
100	**0.5**	**0.624**	**0.291**

MG63			
Tala [nM]	Doxo [µg/ml]	Fa	CI
10	0.005	0.168	0.588
10	**0.01**	**0.314**	**0.467**
10	0.05	0.59	1.124
50	0.005	0.344	0.593
50	**0.01**	**0.39**	**0.633**
50	0.05	0.614	1.143
100	0.005	0.444	0.607
100	**0.01**	**0.458**	**0.707**
100	0.05	0.626	1.195

MG63			
Tala [nM]	MTX [µg/ml]	Fa	CI
10	**0.001**	**0.168**	**0.965**
10	0.005	0.18	1.002
10	0.01	0.176	1.33
50	**0.001**	**0.357**	**0.45**
50	0.005	0.403	0.314
50	0.01	0.413	0.317
100	**0.001**	**0.438**	**0.409**
100	0.005	0.421	0.503
100	0.01	0.396	0.671

MG63			
Tala [nM]	Carbo/Etop [µg/ml]	Fa	CI
10	0.05	0.271	0.513
10	0.1	0.331	0.54
10	**0.2**	**0.444**	**0.504**
50	0.05	0.432	0.421
50	0.1	0.499	0.355
50	**0.2**	**0.532**	**0.434**
100	0.05	0.453	0.624
100	0.1	0.504	0.522
100	**0.2**	**0.531**	**0.583**

ZK-58			
Tala [nM]	TMZ [µM]	Fa	CI
10	10	0.466	0.094
10	50	0.684	0.015
10	**100**	**0.773**	**0.006**
50	10	0.563	0.212
50	50	0.759	0.035
50	**100**	**0.807**	**0.019**
100	10	0.651	0.2
100	50	0.802	0.042
100	**100**	**0.828**	**0.029**

ZK-58			
Tala [nM]	SN-38 [nM]	Fa	CI
10	0.5	0.246	1.127
10	1	0.21	1.858
10	**2**	**0.377**	**0.77**
50	0.5	0.48	0.668
50	1	0.465	0.843
50	**2**	**0.546**	**0.646**
100	0.5	0.506	1.019
100	1	0.52	0.999
100	**2**	**0.593**	**0.729**

ZK-58			
Tala [nM]	Cis [µM]	Fa	CI
10	0.05	0.369	1.548
10	0.1	0.415	1.581
10	**0.5**	**0.551**	**1.641**
50	0.05	0.41	2
50	0.1	0.448	1.944
50	**0.5**	**0.616**	**0.961**
100	0.05	0.525	1.121
100	0.1	0.551	1.008
100	**0.5**	**0.658**	**0.707**

ZK-58			
Tala [nM]	Doxo [µg/ml]	Fa	CI
10	0.005	0.398	0.958
10	0.01	0.463	0.722
10	**0.05**	**0.594**	**0.865**
50	0.005	0.465	1.701
50	0.01	0.493	1.444
50	**0.05**	**0.624**	**0.895**
100	0.005	0.509	2
100	0.01	0.53	1.753
100	**0.05**	**0.636**	**1.038**

ZK-58			
Tala [nM]	MTX [µg/ml]	Fa	CI
10	0.001	0.327	2
10	0.005	0.35	2
10	**0.01**	**0.309**	**2**
50	0.001	0.5	2
50	0.005	0.493	2
50	**0.01**	**0.523**	**2**
100	0.001	0.56	2
100	0.005	0.554	2
100	**0.01**	**0.58**	**2**

ZK-58			
Tala [nM]	Carbo/Etop [µg/ml]	Fa	CI
10	0.05	0.371	0.659
10	0.1	0.41	0.721
10	**0.2**	**0.506**	**0.702**
50	0.05	0.49	0.709
50	0.1	0.524	0.667
50	**0.2**	**0.604**	**0.556**
100	0.05	0.529	0.873
100	0.1	0.564	0.748
100	**0.2**	**0.619**	**0.649**

SaOS-2			
Tala [nM]	TMZ [µM]	Fa	CI
0.5	50	0.556	0.142
0.5	**100**	**0.678**	**0.12**
0.5	200	0.731	0.16
1	50	0.628	0.097
1	**100**	**0.695**	**0.11**
1	200	0.749	0.141
5	50	0.615	0.186
5	**100**	**0.736**	**0.102**
5	200	0.626	0.411

SaOS-2			
Tala [nM]	SN-38 [nM]	Fa	CI
0.5	0.5	0.323	0.542
0.5	1	0.435	0.422
0.5	**2**	**0.559**	**0.359**
1	0.5	0.333	0.728
1	1	0.417	0.594
1	**2**	**0.601**	**0.318**
5	0.5	0.54	0.651
5	1	0.625	0.428
5	**2**	**0.719**	**0.278**

SaOS-2			
Tala [nM]	Cis [µM]	Fa	CI
0.5	0.05	0.403	0.321
0.5	0.1	0.327	0.747
0.5	**0.5**	**0.541**	**0.559**
1	0.05	0.322	0.731
1	0.1	0.349	0.854
1	**0.5**	**0.562**	**0.554**
5	0.05	0.52	0.624
5	0.1	0.553	0.627
5	**0.5**	**0.648**	**0.541**

SaOS-2			
Tala [nM]	Doxo [µg/ml]	Fa	CI
0.5	0.005	0.315	0.803
0.5	0.01	0.429	0.587
0.5	**0.05**	**0.651**	**0.82**
1	0.005	0.383	0.738
1	0.01	0.475	0.568
1	**0.05**	**0.658**	**0.816**
5	0.005	0.558	0.676
5	0.01	0.577	0.697
5	**0.05**	**0.713**	**0.721**

SaOS-2			
Tala [nM]	MTX [µg/ml]	Fa	CI
0.5	0.001	0.207	0.421
0.5	0.005	0.3	0.216
0.5	**0.01**	**0.282**	**0.246**
1	0.001	0.286	0.468
1	0.005	0.267	0.536
1	**0.01**	**0.294**	**0.448**
5	0.001	0.44	0.939
5	0.005	0.457	0.855
5	**0.01**	**0.463**	**0.828**

SaOS-2			
Tala [nM]	Carbo/Etop [µg/ml]	Fa	CI
0.5	0.05	0.225	0.383
0.5	0.1	0.256	0.387
0.5	**0.2**	**0.316**	**0.369**
1	0.05	0.324	0.289
1	0.1	0.32	0.358
1	**0.2**	**0.372**	**0.335**
5	0.05	0.441	0.534
5	0.1	0.467	0.474
5	**0.2**	**0.475**	**0.497**

MNNG-HOS			
Tala [nM]	TMZ [µM]	Fa	CI
0.5	50	0.7	0.17
0.5	**100**	**0.846**	**0.172**
0.5	200	0.921	0.204
1	50	0.784	0.123
1	**100**	**0.888**	**0.134**
1	200	0.944	0.158
5	50	0.878	0.078
5	**100**	**0.928**	**0.097**
5	200	0.95	0.146

MNNG-HOS			
Tala [nM]	SN-38 [nM]	Fa	CI
0.5	0.5	0.314	0.718
0.5	1	0.473	0.326
0.5	**2**	**0.589**	**0.425**
1	0.5	0.501	0.258
1	1	0.528	0.324
1	**2**	**0.669**	**0.382**
5	0.5	0.625	0.291
5	1	0.712	0.239
5	**2**	**0.849**	**0.275**

MNNG-HOS			
Tala [nM]	Cis [µM]	Fa	CI
0.5	0.05	0.337	0.576
0.5	0.1	0.452	0.205
0.5	**0.5**	**0.544**	**0.199**
1	0.05	0.463	0.294
1	0.1	0.44	0.399
1	**0.5**	**0.535**	**0.279**
5	0.05	0.562	0.504
5	0.1	0.537	0.664
5	**0.5**	**0.647**	**0.264**

MNNG-HOS			
Tala [nM]	Doxo [µg/ml]	Fa	CI
0.5	0.005	0.348	0.762
0.5	0.01	0.477	0.355
0.5	**0.05**	**0.593**	**0.701**
1	0.005	0.481	0.345
1	0.01	0.526	0.325
1	**0.05**	**0.634**	**0.584**
5	0.005	0.549	0.621
5	0.01	0.565	0.602
5	**0.05**	**0.661**	**0.616**

MNNG-HOS			
Tala [nM]	MTX [µg/ml]	Fa	CI
0.5	0.001	0.285	0.393
0.5	**0.005**	**0.315**	**0.29**
0.5	0.01	0.28	0.441
1	0.001	0.452	0.147
1	**0.005**	**0.445**	**0.158**
1	0.01	0.501	0.095
5	0.001	0.566	0.255
5	**0.005**	**0.558**	**0.275**
5	0.01	0.533	0.348

MNNG-HOS			
Tala [nM]	Carbo/Etop [µg/ml]	Fa	CI
0.5	0.05	0.224	0.836
0.5	0.1	0.305	0.271
0.5	**0.2**	**0.312**	**0.248**
1	0.05	0.462	0.089
1	0.1	0.38	0.22
1	**0.2**	**0.395**	**0.186**
5	0.05	0.435	0.596
5	0.1	0.471	0.403
5	**0.2**	**0.499**	**0.298**

U2OS			
Tala [nM]	TMZ [µM]	Fa	CI
0.5	50	0.286	0.425
0.5	**100**	**0.377**	**0.307**
0.5	200	0.412	0.442
1	50	0.2	2
1	**100**	**0.196**	**2**
1	200	0.279	1.781
5	50	0.282	0.919
5	**100**	**0.293**	**0.993**
5	200	0.328	1.032

U2OS			
Tala [nM]	SN-38 [nM]	Fa	CI
0.5	0.5	0.154	2
0.5	1	0.185	2
0.5	**2**	**0.27**	**2**
1	0.5	0.235	2
1	1	0.192	2
1	**2**	**0.297**	**2**
5	0.5	0.269	2
5	1	0.27	2
5	**2**	**0.372**	**2**

U2OS			
Tala [nM]	Cis [µM]	Fa	CI
0.5	0.05	0.198	0.233
0.5	**0.1**	**0.229**	**0.107**
0.5	0.5	0.104	2
1	0.05	0.254	0.112
1	**0.1**	**0.262**	**0.096**
1	0.5	0.281	0.088
5	0.05	0.334	0.098
5	**0.1**	**0.35**	**0.074**
5	0.5	0.337	0.113

U2OS			
Tala [nM]	Doxo [µg/ml]	Fa	CI
0.5	0.005	0.121	0.347
0.5	**0.01**	**0.244**	**0.267**
0.5	0.05	0.281	0.962
1	0.005	0.233	0.246
1	**0.01**	**0.271**	**0.297**
1	0.05	0.287	0.997
5	0.005	0.241	0.773
5	**0.01**	**0.255**	**0.806**
5	0.05	0.299	1.334

U2OS			
Tala [nM]	MTX [µg/ml]	Fa	CI
0.5	0.001	0.257	1.267
0.5	**0.005**	**0.316**	**0.103**
0.5	0.01	0.303	0.215
1	0.001	0.294	0.03
1	**0.005**	**0.238**	**2**
1	0.01	0.218	2
5	0.001	0.263	2
5	**0.005**	**0.259**	**2**
5	0.01	0.25	2

U2OS			
Tala [nM]	Carbo/Etop [µg/ml]	Fa	CI
0.5	0.05	0.259	0.234
0.5	**0.1**	**0.263**	**0.391**
0.5	0.2	0.271	0.677
1	0.05	0.277	0.232
1	**0.1**	**0.289**	**0.338**
1	0.2	0.283	0.647
5	0.05	0.253	0.879
5	**0.1**	**0.295**	**0.542**
5	0.2	0.315	0.641

Combination indices (CI) and fraction affected (FA) were calculated as described in materials and methods for cell viability induced by combined treatment for 72 hours with indicated concentrations of talazoparib and chemotherapeutics. Bold concentrations indicate their usage for creation of Figure 33. Cut-off for antagonistic CI values was 2.

To further characterize the four responsive OS cell lines, three different classes of synergy were appointed. Highly synergistic chemotherapeutic interactions together with talazoparib were defined with CI < 0.2 and Fa > 0.5. Intermediate synergistic interactions were defined with CI > 0.2 < 0.9 and Fa > 0.5 and weak synergistic interactions were defined with CI > 0.2 < 0.9 and Fa >0.3 < 0.5 (Figure 33). Screening genotoxic drugs for synergism in combination with talazoparib we observed the best synergism for TMZ together with talazoparib. This combination resulted in a highly synergistic reduction of cell viability of all responding OS cell lines (Figure 32, Figure 33). For SN-38, intermediate synergy with strong variations in the cell lines was observed. SaOS-2 and MNNG-HOS exhibited a better synergy in the cotreatment of SN-38 with talazoparib (CI < 0.4 and Fa > 0.5) compared to MG63 and ZK-58 (CI ˜ 0.8 and Fa > 0.5) (Figure 32, Figure 33). Moreover, intermediate synergy for the combinations of cisplatin or doxorubicin together with talazoparib was observed (Figure 32, Figure 33). Though, we observed a heterogeneous response pattern for doxorubicin with two cell lines displaying intermediate synergism, MG63 cells presenting a weak synergism and ZK-58 cells presenting a high synergism (Figure 32, Figure 33). Methotrexate together with talazoparib predominantly yielded in weak synergy, as only few combinations in ZK-58 and MNNG-HOS cells were found to affect more than 50 % of the cell population (Figure 32, Figure 33). Furthermore, we tested a triple treatment consisting of talazoparib, etoposide and carboplatin. In this regimen a heterogeneous pattern of weak to intermediate synergy, depending on the cell line was observed (Figure 32, Figure 33).

Thus, sensitization with TMZ, which strongly acted in concert together with talazoparib to reduce cell viability in a highly synergistic manner in MG63, ZK-58, SaOS-2 and MNNG-HOS cell lines was demonstrated. While SN-38, cisplatin and doxorubicin yielded in an intermediate synergism, still resulting in a combinatorial effect for some drug concentrations and cell lines, the combination of MTX or the triple-therapy of etoposide/carboplatin together with talazoparib seemed not favorable.

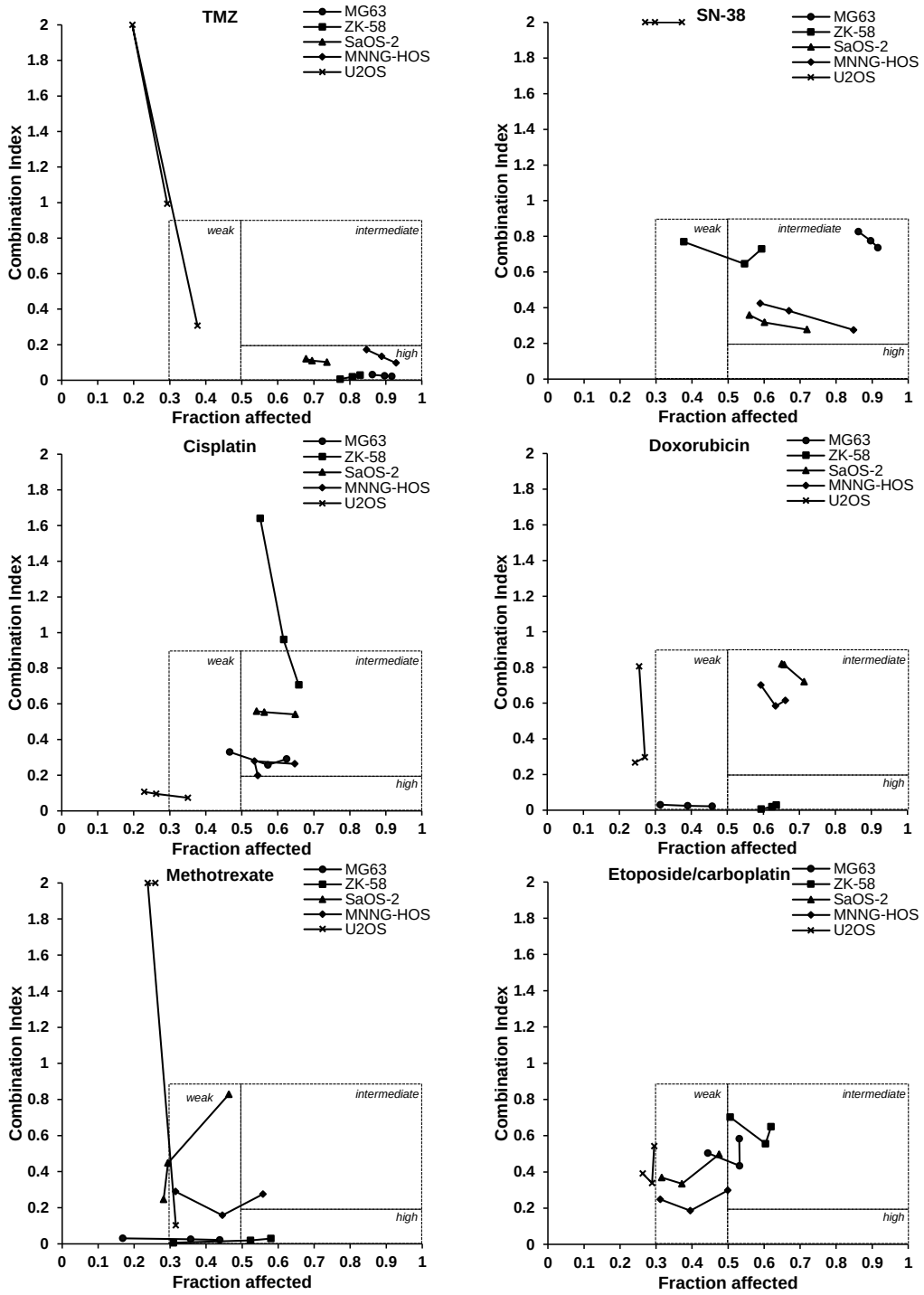

Figure 33: Talazoparib synergized with several chemotherapeutic drugs, in particular TMZ, in OS cells.

CI/Fa plots were created according to the materials and methods based on data shown in Figure 32 for combinations of talazoparib and chemotherapeutic drugs. CI/Fa values are shown for talazoparib concentrations ranging from 10 nM to 5 µM depending on the cell line (MG63, ZK-58: 10, 50, 100 nM; SaOS-2, MNNG-HOS, U2OS: 0.5, 1, 5 µM) in combination with the following concentrations of chemotherapeutics: 100 µM TMZ, 2 nM SN-38, 0.5 µM cis for MG63, ZK-58, SaOS-2 and MNNG-HOS and 0.1 µM cis for U2OS, 0.01 µg/ml doxo for MG63 and U2OS and 0.05 µg/ml doxo for ZK-58, SaOS-2 and MNNG-HOS, 0.001 µg/ml MTX for MG63, 0.005 µg/ml for MNNG-HOS and U2OS and 0.01 µg/ml for ZK-58 and SaOS-2, 0.1 µg/ml of both etop/carbo for U2OS and 0.02 µg/ml of both etop/carbo for MG63, ZK-58, SaOS-2 and MNNG-HOS.

III.2.3 TMZ was most effective in combination with talazoparib to induce cell death in OS cells

We concentrated on the two most sensitive OS cell lines MG63 and ZK-58, since they exhibited the most pronounced effect to talazoparib monotherapy and talazoparib/TMZ combination therapy. We aimed to investigate the antitumor activity of selected drug combinations in additional assays. Therefore, DNA fragmentation, as a marker of apoptotic cell death, in the combinations of TMZ, cisplatin or doxorubicin together with talazoparib was determined. We selected cisplatin and doxorubicin preferable to SN-38, as they are generally used in the standard therapy of OS (37). Of note, talazoparib cooperated with TMZ to significantly increase DNA fragmentation in both OS cell lines (Figure 34). While a weakened increase, nonetheless significant, of talazoparib in combination with cisplatin and doxorubicin in ZK-58 cells was demonstrated, these drugs did not combine to significantly induce cell death in MG63 cells. Additionally,

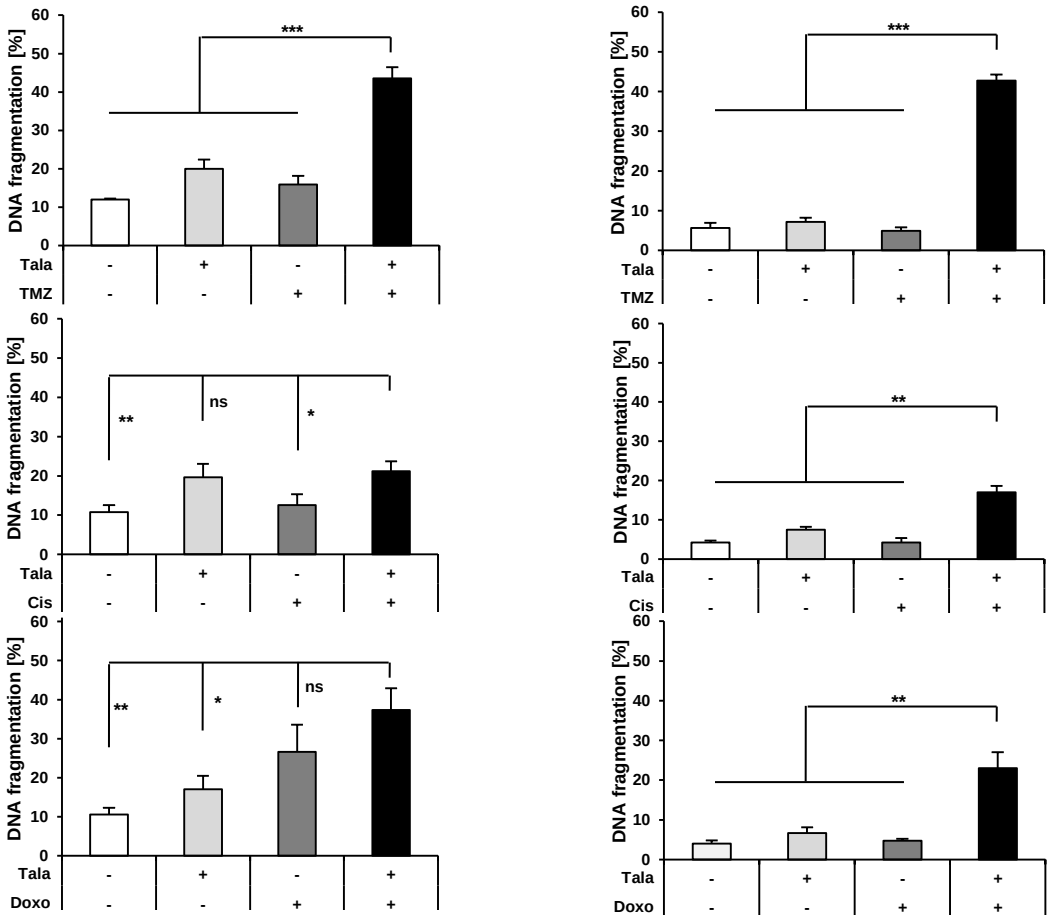

Figure 34: Talazoparib/TMZ cotreatment was superior to cisplatin or doxorubicin to trigger cell death.

MG63 (left) and ZK-58 (right) cells were treated for 72 hours with 10 nM talazoparib and/or 100 µM TMZ, 50 nM cisplatin or 10 ng/ml doxorubicin as indicated. Apoptosis was determined by quantification of DNA fragmentation of PI-stained nuclei using flow cytometry. Data are shown as mean +/- SD of three independent experiments performed in triplicate; *, $P < 0.05$; **, $P < 0.01$; ***, $P < 0.001$; ns, not significant.

combinations of cisplatin or doxorubicin together with talazoparib resulted in overall less DNA fragmentation in MG63 and ZK-58 cells in comparison to the combination of TMZ together with talazoparib (Figure 34).

III.2.4 TMZ was most effective in combination with talazoparib to suppress clonogenic growth of OS cells

As additional read-out for assessing chosen drug combination in MG63 and ZK-58 colony formation, as parameter of long-term clonogenic growth was selected. Together, talazoparib/TMZ significantly decreased and nearly abrogated clonogenic growth of MG63 and ZK-58 OS cell lines (Figure 35). In contrast, cisplatin and doxorubicin failed to inhibit clonogenic growth of OS cell lines MG63 and ZK-58 upon cotreatment with talazoparib (Figure 35). In summary, these results highlighted that the combination

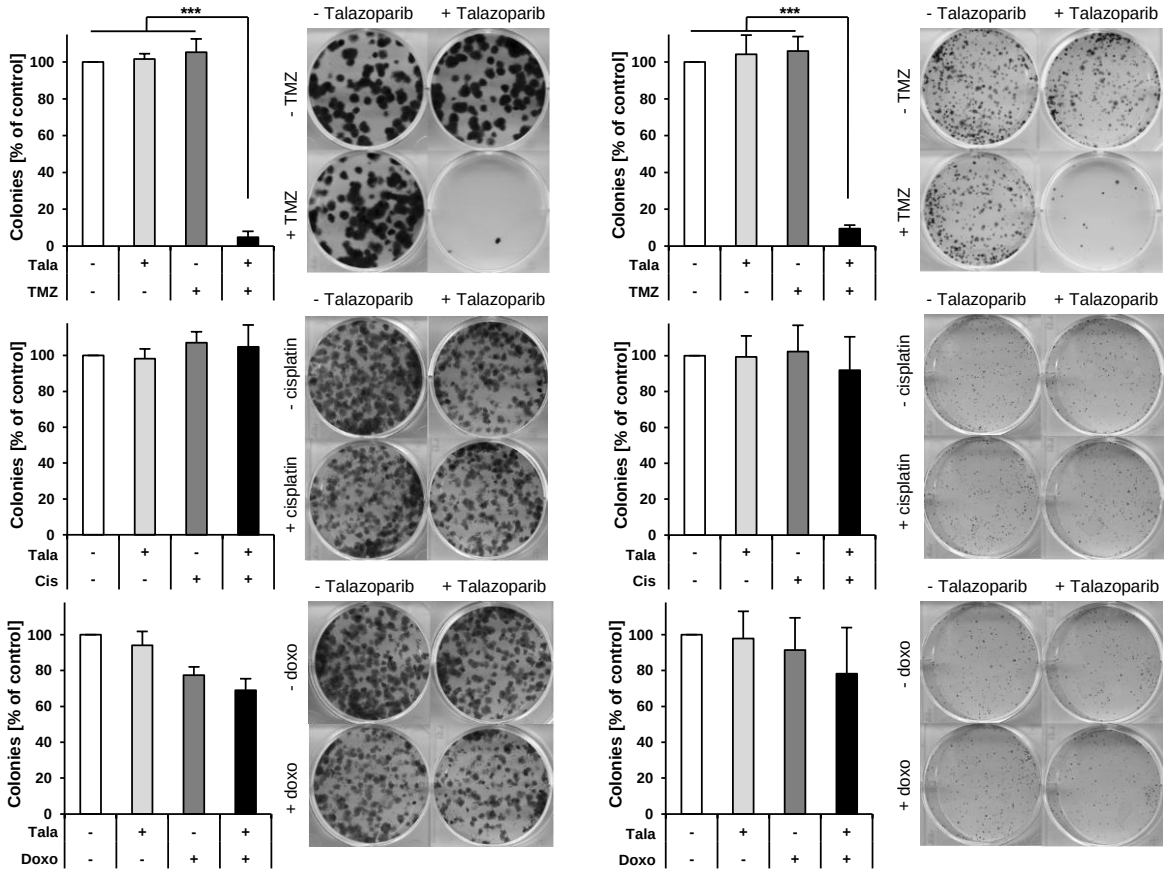

Figure 35: Talazoparib/TMZ cotreatment was superior to cisplatin or doxorubicin to suppress clonogenic growth.

MG63 (left) and ZK-58 (right) cells were treated with 10 nM talazoparib and/or 100 µM TMZ, 50 nM cisplatin or 10 ng/ml doxorubicin for 24 hours, living cells were counted and subsequently 100 cells/well were re-seeded in drug-free medium in a six-well plate. Colony formation was assessed after 12 days for talazoparib/TMZ and after 10 days for talazoparib/cisplatin or talazoparib/doxorubicin by crystal violet staining and colonies were counted macroscopically. The number of colonies is expressed as percentage of untreated control and representative images are shown. Data are shown as mean +/- SD of three independent experiments performed in triplicate; ***, $P < 0.001$.

of talazoparib/TMZ was more effective than the combinations of talazoparib/cisplatin or talazoparib/doxorubicin to trigger cell death or suppressing clonogenic growth in MG63 and ZK-58 cells. As proof of principle for combination treatment tolerability we tested talazoparib as monotherapy or in combination with TMZ. PARP inhibitors are widely well tolerated with sparsely demonstrating dose-limiting haematological adverse events in few clinical studies (112). For both drugs, concentrations that significantly reduced cell viability in OS were utilized. No adverse effects of the tested combination were observed on peripheral blood lymphocytes (PBL's) as indicated by PI staining (Figure 36). Hence, in mechanistic studies we focused on the combination treatment of talazoparib and TMZ for OS cells.

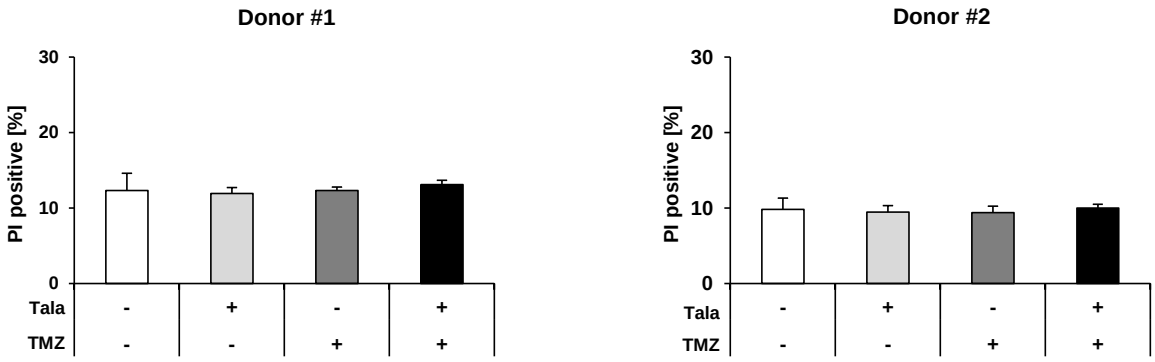

Figure 36: Determination of talazoparib- and TMZ-toxicity in PBL's.

PBL's isolated from two independent donors were treated with 10 nM talazoparib and/or 100 µM TMZ for 48 hours and cell death was assessed by measuring the membrane integrity indicated by PI staining using flow cytometry. Data are shown as mean +/- SD of one experiment performed in triplicate.

III.2.5 Talazoparib/TMZ cotreatment induced caspase-dependent cell death

In our prior experiments the best combination treatment for BRCAness positive OS cell lines, consisting of a combination of talazoparib and TMZ, was revealed. Next, we aimed to investigate the underlying mechanisms of cell death induction for this combination in OS cells. As demonstrated before that the combination of olaparib and TMZ induced intrinsic apoptosis in ES cells, we subsequently focused on key experiments in OS. Therefore, monitoring cell death in a time-dependent manner in MG63 and ZK-58 cells upon talazoparib/TMZ treatment was our first approach. A significant increase in DNA fragmentation was observed upon talazoparib/TMZ cotreatment in comparison to solvent treated or single drug treated MG63 cells after 48 hours and in ZK-58 cells after 24 hours (Figure 37). To further determine the type of cell death, activation of caspases was investigated. We performed caspase-3/-7 activity assay employing the ImageXpress Micro LS system. Treatment of talazoparib/TMZ significantly increased caspase-3/-7 activity in MG63 and ZK-58 cells (Figure 38).

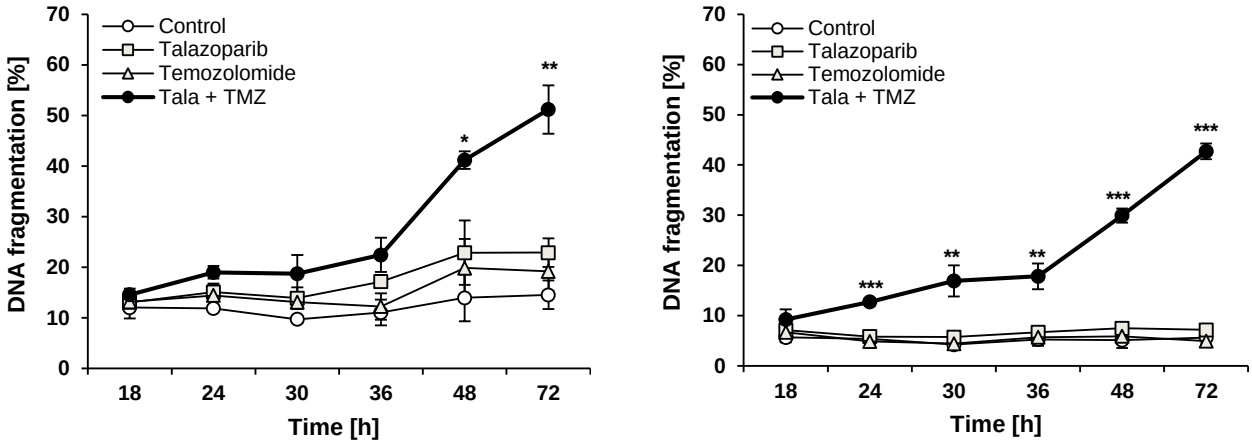

Figure 37: Talazoparib/TMZ-induced cell death in OS cells was significantly increased over time.

MG63 (left) and ZK-58 (right) cells were treated with 10 nM talazoparib and/or 100 µM TMZ for indicated times. Apoptosis was determined by quantification of DNA fragmentation of PI-stained nuclei using flow cytometry. Data are shown as mean +/- SD of three independent experiments performed in triplicate; *, P < 0.05; **, P < 0.01; ***, P < 0.001.

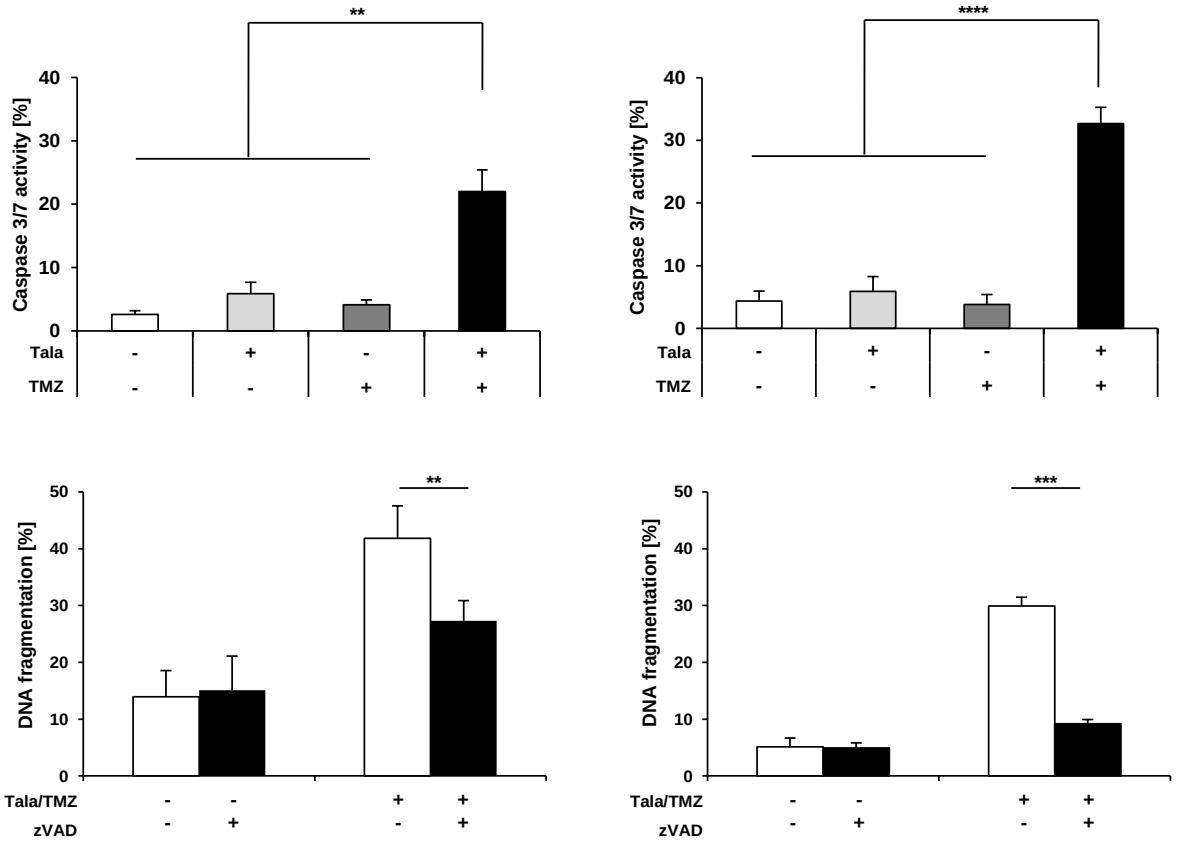

Figure 38: Talazoparib/TMZ-induced cell death was caspase-dependent.

MG63 (left) and ZK-58 (right) cells were treated with 10 nM talazoparib and/or 100 µM TMZ for 48 hours in the presence or absence of 50 µM zVAD.fmk. Cell nuclei were stained with Hoechst 33342 and caspase activity was measured using caspase-3/7 cell reagent and microscopy. Apoptosis was determined by quantification of DNA fragmentation of PI-stained nuclei using flow cytometry. Data are shown as mean +/- SD of three independent experiments performed in triplicate; **, P < 0.01; ***, P

Addition of zVAD.fmk significantly reduced talazoparib/TMZ-induced cell death in MG63 and ZK-58 cells (Figure 38). This set of experiments jointly demonstrated that the combination of talazoparib/TMZ induced caspase-dependent cell death in MG63 and ZK-58 cells (Figure 38).

III.2.6 Talazoparib/TMZ cotreatment triggered BAK/BAX activation and MOMP

Demonstrating that activation of caspases was involved in talazoparib/TMZ-mediated cell death, we next aimed to investigate the involvement of the mitochondrial pathway of apoptosis. We addressed this question by assessing whether BAK and BAX are activated by the cotreatment of talazoparib/TMZ in MG63 and ZK-58 cells. Therefore, immunoprecipitation of active BAK and BAX proteins was performed, using conformation-specific antibodies (II.10). Notably, marked activation of BAK and BAX was observed upon combination treatment of talazoparib/TMZ in MG63 and ZK-58 cells (Figure 39). Consistent with previous results (Figure 37), BAK/BAX activation in ZK-58 cells was observed after 24 hours, compared to an activation of BAK/BAX after 36 hours in MMNG-HOS cells (Figure 39). As BAK/BAX activation have been reported to be directly involved in pore formation and LMMP, we next investigated mitochondrial perturbations by JC-1 staining (121). Of Note, talazoparib acted in concert with TMZ to trigger LMMP in MG63 and ZK-58 cells. The onset of LMMP in MG63 cells was observed to a later time point (36 hours) than in ZK-58 cells (24 hours) (Figure 40), which was consistent with previous observations, demonstrating a decelerated induction of cell death in MG63 cells (Figure 40).

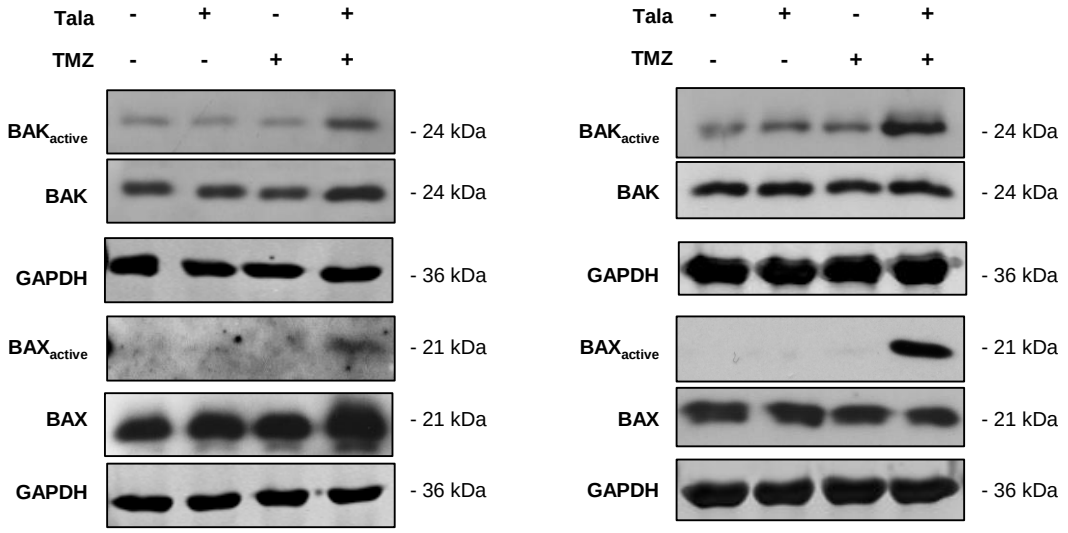

Figure 39: The combination of talazoparib and TMZ triggered BAK/BAX activation in OS cells.

MG63 (left) and ZK-58 (right) cells were treated with 10 nM talazoparib and/or 100 µM TMZ for 36 hours (MG63) or 24 hours (ZK-58). Active conformations of BAK or BAX were immunoprecipitated using active conformation-specific antibodies and were analyzed by Western blotting. Expression of total BAK or BAX and GAPDH served as loading controls. Representative blots of two independent experiments are shown.

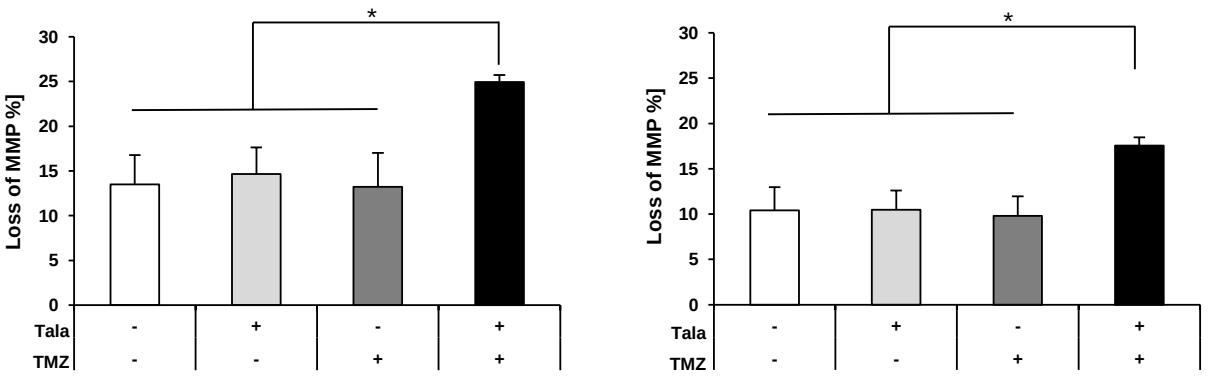

Figure 40: Talazoparib/TMZ-mediated cell death was accompanied by LMMP.

MG63 (left) and ZK-58 (right) cells were treated with 10 nM talazoparib and/or 100 µM TMZ for 36 hours (MG63) or 24 hours (ZK-58). Loss of MMP in the living cell population was determined by flow cytometry using JC-1 fluorescent dye. Data are shown as mean +/- SD of three independent experiments performed in triplicate; *, $P < 0.05$.

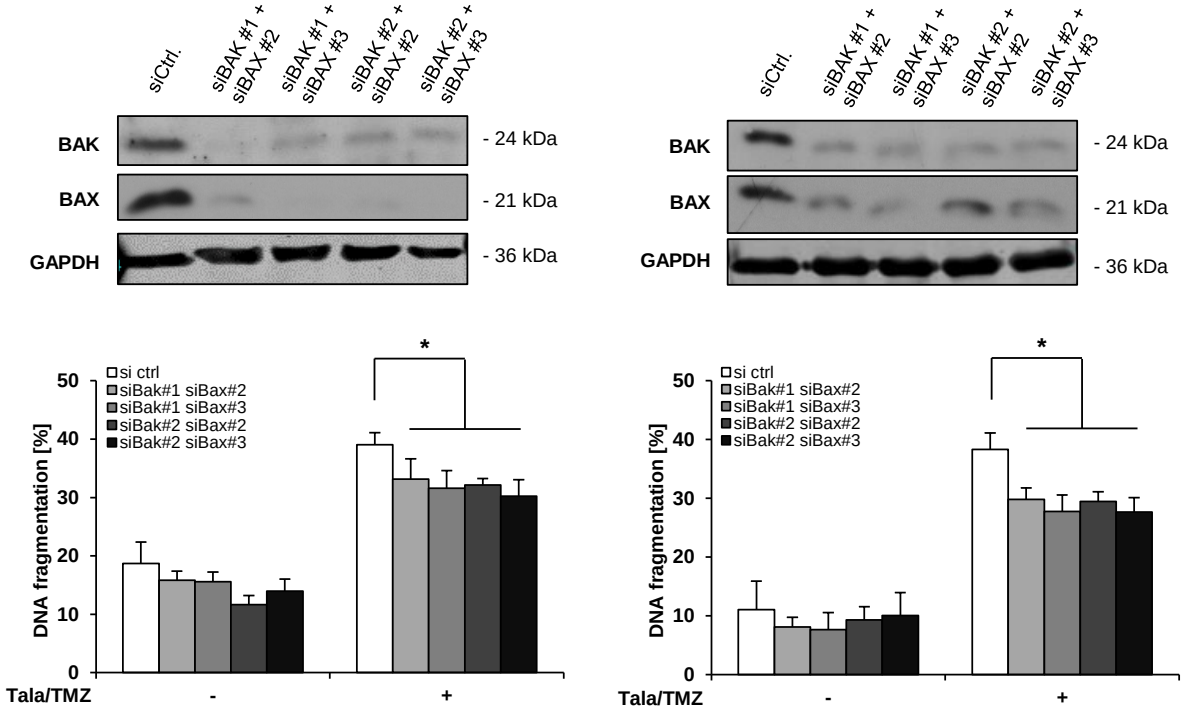

Figure 41: Combined siRNA knockdown of BAK and BAX significantly reduced talazoparib/TMZ-induced apoptosis.

MG63 (left) and ZK-58 (right) cells were transiently transfected with 10 nM non-silencing siRNA or 5 nM each of different combinations of constructs targeting BAK or BAX and expression of BAK and BAX was analyzed by Western blotting, GAPDH served as loading control. Representative blots of two independent experiments are shown. Transiently transfected OS cells were treated for 48 hours with 10 nM talazoparib and 100 µM TMZ and apoptosis was determined by quantification of DNA fragmentation of PI-stained nuclei using flow cytometry. Data are shown as mean +/- SD of three independent experiments performed in triplicate; *, $P < 0.05$.

Further, the importance of BAK/BAX for talazoparib/TMZ-induced apoptosis was assessed by combined silencing of BAK and BAX with siRNA in MG63 and ZK-58 cells. This combinatory knockdown of BAK and BAX significantly reduced cell death upon treatment with talazoparib/TMZ in MG63 and ZK-58 cells, emphasizing their role in apoptosis induction upon these conditions (Figure 41).

In conclusion, it was demonstrated how BRCAness in OS cell lines determined sensitivity to talazoparib, depending on their different genetic background. Additionally, we revealed that talazoparib/TMZ combination treatment was the most effective combination regimen for cell death induction in OS cells and inhibited long-term clonogenic growth of MG63 and ZK-58 cells. Furthermore, in selected key experiments, the assumption that talazoparib/TMZ-induced cell death exhibited key hallmarks of intrinsic apoptosis was confirmed. Moreover, this was demonstrated by BAK/BAX activation, LMMP and caspase activation. To this end, all experiments showed the similar mode of cell death in OS, which we previously identified and characterized for the combination treatment of olaparib and TMZ in ES.

III.2.7 HDAC inhibition was able to sensitize PARP inhibitor resistant U2OS cells

In a preliminary trial to overcome PARP inhibitor-resistance we tested U2OS cells, previously described as being resistant towards 100 µM talazoparib and not to respond to combination treatment with talazoparib/TMZ (see Figure 42, left panel). Remarkably, triple therapy of talazoparib, TMZ and the HDAC inhibitor JNJ-26481585 significantly decreased cell viability of PARP inhibitor-resistant U2OS cells (Figure 42, right panel) opening new therapeutic possibilities.

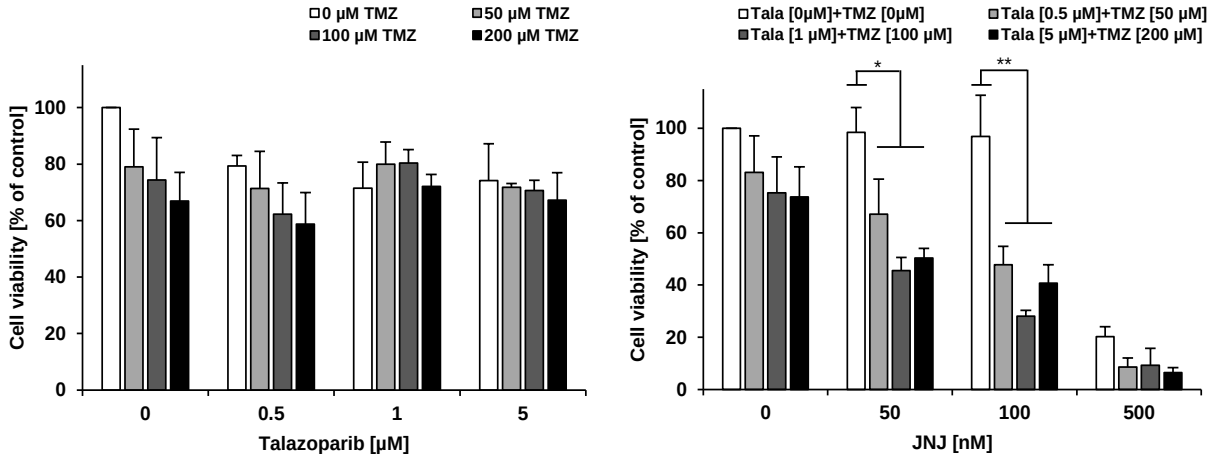

Figure 42: Triple therapy of talazoparib, TMZ and JNJ significantly decreased cell viability in U2OS cells.

U2OS cells were treated for 72 hours with indicated concentrations of talazoparib (Tala), TMZ or the HDAC inhibitor JNJ-26481585 (JNJ). Cell viability was measured by MTT assay and is expressed as percentage of untreated control. Data are shown as mean +/- SD of three independent experiments performed in triplicate; *, $P < 0.05$; **, $P < 0.01$.

IV Discussion

Since the 1980's, PARP inhibitors have been employed as therapy option against different tumor entities (72). Currently, over 170 clinical trials are listed with the five most prominent PARP inhibitors (olaparib, talazoparib, niraparib, rucaparib and veliparib), accounting for nearly all of the active clinical trials (57 out of 61 open clinical trials) (85). Initially, PARP inhibitors have been noted for their activity in *BRCA1* and *BRCA2* negative cancers, in which they showed very promising results in killing *BRCA1/2* deficient tumors (74–76). This fostered the development of more potent and sophisticated PARP inhibitors (82) and on the other hand, PARP inhibitors and their possibilities to specifically kill tumors drew the academic society's attention (83,112). Recently, two major findings opened new avenues for PARP inhibitor based therapies. First, in 2012, it was discovered that PARP inhibitors displayed a very high efficacy in killing Ewing's sarcoma cells (31,32). Second, it was revealed that PARP inhibitors were not only efficient in killing cells with *BRCA1* and *BRCA2* mutations, but were effective in killing cells with loss-of-function mutations in the homologous recombination pathway (termed BRCAness) (47,124–127). Interestingly, in a screening of 123 primary OS we detected many samples that harbor mutation signatures being reminiscent of BRCAness in OS (46). Therefore, we aimed to investigate the optimal treatment options for PARP inhibitors combined with frequently applied chemotherapeutics and examined the underlying type of cell death in ES and OS.

IV.1 PARP inhibitor sensitivity in Ewing's sarcoma and osteosarcoma

In the first part of this study toxicity of different PARP inhibitors in ES cells was assessed. Therefore, two different ES cell lines, A4573 and SK-ES-1, both bearing the *EWS-FLI1* fusion gene responsible for tumorigenesis (27,128,129), were treated with four different PARP inhibitors (olaparib, talazoparib, niraparib and veliparib, see Figure 7). Marked differences in single-agent toxicities among the four PARP inhibitors were observed, with decreasing potency in following order: talazoparib (IC_{50} ~ 10 nM) > niraparib (IC_{50} ~ 300 nM) > olaparib (IC_{50} ~ 1 000 nM) > veliparib (IC_{50} ~ 10 000 nM). These results were confirmed by complementary studies similarly indicating the different levels of cytotoxicity (80,81,88), however all inhibitors target PARP catalytic activity with the same order of magnitude (IC_{50} in low nanomolar range) (70). Differences in cytotoxicity cannot be explained by differential off-target effects of PARP inhibitors, since olaparib, veliparib and talazoparib (differing from 10-fold to 1 000-fold cytotoxicity) showed the same selectivity profile against 13 out of 17 human PARP family members *in vitro* with PARP inhibitors selectively binding PARP1-4 (70,73). But, these differences can be potentially explained by PARP trapping (79–81,130,131). PARP trapping describes the ability of PARP inhibitors to allosterically disturb the conformational flexibility and dynamics of PARP proteins, thereby strongly enhancing its affinity for the

single-strand break repair intermediate leading to accumulation of inactivated, trapped PARP at the site of DNA lesions (70). Pommier *et al.* investigated five PARP inhibitors, among those veliparib, primarily a catalytic inhibitor, exerted the lowest trapping activity. Olaparib, niraparib and rucaparib were more active and showed a higher PARP trapping activity than veliparib (~ 100-fold). To date, talazoparib is the most potent, trapping agent (~ 100-fold higher PARP trapping activity than olaparib, niraparib and rucaparib) (70,80,81). These studies propose an inverse correlation of enzymatic PARP inhibition and anticancer cytotoxicity, which was confirmed by our finding that the cytotoxicity of PARP inhibitors correlate with trapping activity of the different inhibitors (80,92). This is in agreement with the observations that trapped PARP-DNA complexes are much more responsible for PARP inhibitor-mediated cytotoxicity than unrepaired DNA single-strand breaks caused by catalytic inhibition of PARP (70,79–81,92).

As we and others could already demonstrate that talazoparib is the most potent PARP inhibitor (80,92), which is additionally evaluated in various studies, including the pediatric preclinical testing program (PPTP) (122,123), we focused on talazoparib as prototypical PARP inhibitor in OS. In contrast to ES, in which about 85% of the cases tumors bear the *EWS-FLI1* fusion gene responsible for tumorigenesis (27), OS is a highly heterogeneous type of tumor (39,42). Therefore, in this study the focus was on the efficacy of talazoparib monotherapy to induce vulnerability in OS. Susceptibility of OS to PARP inhibitors was implicated recently, as we identified mutation signatures characteristic for *BRCA* deficiency utilizing exome sequencing (46). It was demonstrated that the response to talazoparib monotherapy can be associated to their mutational background defining BRCAness (Figure 31). Four out of five different OS cell lines tested, responded to talazoparib treatment (MG63, ZK-58, SaOS-2 and MNNG-HOS). Of note, those four cell lines harbor genetic alterations in genes, functionally analogous to *BRCA1/2* mutations (46). These alterations include disruptions in *PTEN* and *FANCD2* as well as loss of function in *BAP1*, *ATM*, *BARD1, FANCA* and *CHEK2*. While none of the tested cell lines showed a bi-allelic *BRCA1/2* mutation (46), U2OS cells carry a heterozygous *BRCA2* mutation with most likely one intact allele left compensating for BRCAness. This was further indicated by our *in vitro* data demonstrating no response of U2OS cells up to 100 µM talazoparib (see Figure 31) (46). Among responsive cell lines, MG63 and ZK-58 were detected to be more sensitive to talazoparib monotherapy, with an IC_{50} in the nanomolar range compared to SaOS-2 and MNNG-HOS displaying an IC_{50} in the micromolar range. This might be explained by differences in HRD-LOH score and their mutational profile (Table 1). Homologous recombination deficiency (HRD)-loss of heterozygosity (LOH) is a DNA-based measure of genomic instability (51,132), which was positive for MG63 and ZK-58. Additionally, MG63 showed a positive Popova signature, another signature descriptive for BRCAness (133). Two other cell lines responding to talazoparib monotherapy, yet in an attenuated manner, SaOS-2 and

MNNG-HOS, did score borderline, respectively positive for HRD-LOH, displaying many genomic rearrangements and allelic imbalances (46). These cells are triploid and thus difficult to analyze. Moreover, differences in vulnerability to talazoparib monotherapy might stem from individual mutational patterns in genes involved in the HR pathway that might further impact the DNA repair response of those OS cells. Indeed, the genes mutated in the OS cell lines *BAP1*, *FANCA*, *PTEN*, *ATM*, *BARD1*, *CHEK2* and *FANCD2* are all functionally relevant for HR repair (47). In detail, it has been described previously that loss of *PTEN* can cause genomic instability (134), and *PTEN*-deficient cells exerted higher vulnerability towards olaparib (125). Additionally, *ATM*-deficient lymphoid tumor cells showed sensitivity against olaparib *in vitro* as well as *in vivo* (126). BARD1 and BRCA1 heterodimerize at DNA damage sites and facilitate their repair (135). Furthermore, phosphorylation of BRCA1 by Chk2 at S988 has been demonstrated to regulate DNA damage repair by the HR pathway (136). In addition, ubiquitination of FANCD2 is pivotal for the clearance of DNA interstrand cross-links (137). Moreover, it has been described that *FANCD2* defiency, as part of the Fanconi anemia pathway, as well as deficiency of *ATM* or *CHEK2* can lead to non-functional homologous recombination and vulnerability to PARP inhibition (138). Because of those findings in OS talazoparib monotherapy, we conclude that a high genomic instability as well as deficiency/loss of function in homologous recombination (HR) pathway genes can cause BRCAness (47), resulting in an increased vulnerability to PARP inhibitors, especially talazoparib, depending on individual mutation profiles and the homologous repair capability.

IV.2 Combination of PARP inhibitors and chemotherapeutic drugs

In section IV.1 we demonstrated and discussed the promising *in vitro* activity of PARP inhibitors in ES (high PARP levels due to *EWS-FLI1*) and OS (BRCAness). However, these encouraging *in vitro* data were not easily transferable to an *in vivo* model. In a recent study, five ES xenograft models did only show minimal growth delay upon talazoparib monotherapy (123). Additionally, in a phase 2 clinical trial, olaparib monotherapy failed to show significant activity in ES patients (139). Therefore, as PARP inhibitors largely failed in *in vivo* studies to show convincing responses in tumor surveillance of ES, we screened PARP inhibitors in combination with a broad range of chemotherapeutic drugs, with each set of chemotherapeutics comprising the first-line therapy regimens for ES and OS, respectively. The two independent screening methodologies showed an overlap in the activity of chemotherapeutics used, as TMZ and SN-38 are highly suggested to synergize with PARP inhibitors. Therefore, we included them for both screening modules (80,88,91). Treatment of TMZ in combination with PARP inhibitors (olaparib or talazoparib) resulted in the best synergism observed for both tumor entities (see Figure 12 and Figure 33). TMZ, as alkylating agent,

provokes the PARP trapping ability of PARP inhibitors. It merely induces two different types of DNA lesions. First, it induces O^6-methylguanine adducts, which cause DNA double-strand breaks, followed by futile cycles of mismatch repair culminating in apoptosis. Second and more relevant for cotreatment with PARP inhibitors, TMZ induces N^3-methyladenine and N^7-methylguanine DNA adducts, which are responsible for over 90% of all methylation events generated by TMZ. Notably, those methylations are nonlethal in most normal and tumor cells as they are rapidly repaired by base excision repair (BER) (140,141). Repair of those methyl adducts by BER requires PARP to detect and sequester 5'-deoxyribose phosphate (91,142,143) and it has been demonstrated that 5'-deoxyribose is a preferred substrate for PARP trapping (79,122). This implies that DNA damage induced by TMZ is switched from nonlethal into cytotoxic lesions by PARP trapping due to the addition of PARP inhibitors. The extend of TMZ cytotoxicity among the PARP inhibitors is variable, but fits with the trapping capacity of these inhibitors (79,92). This observation was further strengthened, since PARP depletion in olaparib/TMZ or veliparib/TMZ-treated cells induced the same, weak potentiation of TMZ (79). In summary, this implicates that a combination of talazoparib, as potent PARP trapper, with TMZ is more favorable than a combination of veliparib, as weak PARP trapper, with TMZ. It further implicates that TMZ is responsible for the cytotoxicity observed upon TMZ/PARP inhibition, by creating N^3 and N^7 methyl adducts, rather than a PARP inhibition sensitizing for TMZ-induced cytotoxicity (70). In our studies, we used this phenomenon to reduce the PARP inhibitors and TMZ concentrations, to a sublethal and well tolerable dose. Haematological toxicities are described as dose limiting factor for the widely well tolerable PARP inhibitor therapy (112,144). In our approach, the applied concentrations of talazoparib and TMZ, sufficient for killing ES and OS tumor cells, did not affect PBL's (Figure 36), thereby permitting a therapeutic window for therapy. For talazoparib, plasma concentrations up to 66 nM are observed to be clinically relevant (145,146), and for TMZ, plasma concentrations up to 100 µM are clinically applicable (147–149). Indeed, the combination of PARP inhibition/TMZ has not only preclinically been tested in our studies (92), but is currently evaluated in phase I/II studies in clinical settings (exemplary see NCT02116777 and NCT02049593) (85).

In our investigations, the topoisomerase I inhibitor SN-38 exhibited the second most pronounced effect when combined with PARP inhibitors. In ES, PARP inhibition/SN-38 was potent as olaparib/TMZ, indicated by DNA fragmentation, cell viability and colony formation studies (see Figure 13 and Figure 14). In OS, it showed synergism comparable to other tested combinations, yet far less potent than the combination with TMZ (see Figure 33). Because doxorubicin and cisplatin are clinically more relevant in OS treatment, we focused on these drugs in our comparative combination studies. It was implicated that the synergistic activity of topoisomerase I inhibitors and PARP inhibitors rely on the inhibition of catalytic functions rather

than PARP trapping (79). Both, olaparib and veliparib (olaparib ~ 100-fold higher trapping activity compared to veliparib) sensitize tumor cells to CPT in the same order (79). During repair of topoisomerase I inhibitor induced DNA lesions, PARP cooperates with tyrosyl-DNA phosphodiesterase 1 (TDP1) and X-ray repair cross-complementing protein 1 (XRCC1) for resolving DNA damage (150,151). Therefore, synergism of combination of topoisomerase I and PARP inhibitors originate from blocking PARP catalytic function. Several phase 1 clinical trials are currently investigating PARP inhibitors in combination with topoisomerase I inhibitors(NCT02049593, NCT02392793 and NCT00576654) (85).

Calculation of CI values according to Chou-Talalay (110) demonstrated weak to intermediate synergism for a broad range of genotoxic drugs in both tumor entities . Whether those drugs act synergistically (in a weak to moderate manner) or additively cannot be concluded unambiguously by calculation of CI or Fa because some drugs exhibited low CI values, but did weakly attenuate cell viability of OS cells. For this reason, assessment of DNA fragmentation and investigation of colony formation was additionally performed for the talazoparib/doxorubicin and talazoparib/cisplatin combinations in OS (see Figure 34 and Figure 35). Of note, combination of doxorubicin or cisplatin and PARP inhibitors solitary slightly increased cell death as indicated by DNA fragmentation, but did not affect long-term survival indicated by non-altered clonogenic growth of OS cells. This can be explained by another mechanism of PARP inhibitors in combination with chemotherapeutics. Besides inducing PARP trapping (TMZ) or influencing PARP catalytic activity (SN-38), a large group of genotoxic drugs show a mutually independent or additive mechanism in combination to PARP inhibition. Although demonstrating some synergistic effects for combining these agents with PARP inhibitors, topoisomerase II inhibitors etoposide and doxorubicin, the platinum-based cross-linking agent's cisplatin or carboplatin and the alkylating agent ifosfamide do not induce PARP-DNA trapping or PARP catalytic inhibition (79,92,152). Moreover, in cases for etoposide and cisplatin, it was demonstrated that repair of DNA lesions generated by those drugs does not include PARP-mediated pathways (98,153,154). In conclusion, for PARP inhibitors in combination with those drugs, two independent cell death mechanisms act in parallel, one depending on the mode of action of the chemotherapeutic agents and the other one by PARP inhibitors, killing the cells by acting on DNA lesions, randomly occurring during cell proliferation. Combinations with additive effects or even antagonism, as observed for VCR, AMD and MTX combined with olaparib or talazoparib are also caused by the above mentioned distinct cell killing pathways. However, cell death in those combination of both drugs did not exceed the cumulative cell death of the monotherapies, representing even more unsatisfactory combinatorial approaches.

IV.3 Cell death mediated by PARP inhibitors (olaparib, talazoparib) in combination with TMZ

Our molecular studies of PARP inhibitors and TMZ in OS and in particular in ES revealed that intrinsic apoptosis plays a major role in the synergy. Up till now, the downstream molecular signaling pathways underlying this synergism have largely remained elusive (92). In previous studies it was described how TMZ generates DNA lesions, which are preferentially bound by PARP, leading to subsequently trapping onto the DNA (79). This trapping ultimately results in replication fork stalling and collapse of the replication fork (155). It was shown how DNA damage is mediated and induced concomitant cell cycle arrest in ES cells (see Figure 18, Figure 19 and Figure 20). Cooperative treatment of PARP inhibitors and TMZ most likely activates ATM and ATR, which are kinases well described for phosphorylating and activating Chk1 and Chk2 (114). Checkpoint kinases are responsible for the G_2/M-phase checkpoint control (114). Consistently, G_2-cell cycle arrest prior to cell death induction by olaparib and TMZ was observed (see Figure 19 and Figure 20). In addition, screening for alterations in expression BCL-2 family of proteins upon combination treatment, a significant decrease in expression levels of MCL-1 and NOXA was detected (Figure 24). Binding of NOXA to MCL-1 has been reported to facilitate degradation of the complex by the proteasome (119,156). NOXA is important in olaparib/TMZ-mediated apoptosis as knockdown of *NOXA* by genetic silencing significantly reduced cell death (Figure 27). Consistently, when treated with Bortezomib, a proteasome inhibitor (157), we were able to significantly rescue cells from olaparib/TMZ-induced downregulation of MCL-1 (Figure 25). Stability of MCL-1, a key antiapoptotic protein, is tightly regulated at multiple levels and MCL-1 ubiquitination targets the proteins for proteasomal degradation after ubiquitination (158). Currently, four different E3 ubiquitin-ligases (Mule, SCF/β-TrCP, SCF/Fbw7 and Trim17) are reported for MCL-1 ubiquitination (158). Constitutive degradation of MCL-1 is maintained by Mule (159), whereas phosphorylation of the phospho-degron by several kinases (e.g. JNK or GSK-3) targets for ubiquitination of MCL-1 by SCF/β-TrCP, SCF/Fbw7 and Trim17 in interphase or post mitotic cells (158,160). Therefore, expression of a phospho-defective mutant variant of MCL-1 significantly reduced olaparib/TMZ-induced apoptosis (Figure 26). Changes in expression levels of BCL-2 family proteins, as the observed decrease in MCL-1 levels, are reported to lead to activation of BAK and BAX (65,160), thus changing their conformation and promoting the assembly of a pore in the outer mitochondrial membrane finally leading to LMMP (65). Therefore, we investigated mitochondrial perturbations by immunoprecipitation of active BAK and BAX (Figure 28), measuring LMMP (see Figure 23) and combined knockdown of BAK/BAX (Figure 29). As observed olaparib/TMZ cotreatment induced pore formation at the mitochondria, being regarded as end point in the apoptotic cascade (161). Upon LMMP, numerous

apoptotic factors are released in to the cytoplasm, including cytochrome c and SMAC, that activate downstream effector-caspases (52). Therefore, activation of caspases was investigated, as central effector proteins for death induction, by Western blotting (Figure 22) as well as caspases dependency using the pan-caspase inhibitor zVAD.fmk (Figure 21). Indeed, olaparib/TMZ-mediated cell death demonstrated caspase involvement and upon overexpression of BCL-2, which blocks mitochondrial depolarization (162), olaparib/TMZ-mediated apoptosis (Figure 30) was completely abolished. Together these observations underscored the importance of the mitochondrial pathway in the mechanism of this combination regimen.

Like for the PARP inhibitor/TMZ-induced cell death mechanism in ES, in OS we focused on key experiments to unravel the mechanisms leading to cell death. Of note, we likewise demonstrated the importance of caspases in talazoparib/TMZ-mediated cell death in OS using a microscope-based assay for caspase-3/-7 activation or the addition of zVAD.fmk (Figure 37 and Figure 38). Correspondingly, talazoparib/TMZ experiments in OS clearly highlighted the importance of BAK and BAX, also by combined knockdown experiments, in talazoparib/TMZ-mediated apoptosis (Figure 39, Figure 40 and Figure 41). Together with the evidence gained from our preceding studies in ES, it was confirmed that talazoparib/TMZ-induced cell death in OS is mediated via the intrinsic apoptotic pathway.

IV.4 Mechanisms of PARP inhibitor-mediated resistance

Cancer cells that acquire resistance to chemotherapeutic drugs are a critical hurdle in antitumor therapy. Acquired drug resistance results from the constant selection pressure in the presence of chemotherapeutic agents, a classic example of Darwinian evolution. In the case of TMZ, classical resistance mechanisms are attributed to, e.g. a decrease in cellular drug uptake, increased drug efflux by membrane pumps or enhanced repair of drug-induced DNA damage (141). Likewise, for PARP inhibitors, several mechanisms of resistance are described, which are discussed in more detail below (155,163). First, in combination with TMZ, resistance against PARP inhibition can be caused by overexpression of *MDR1*, encoding the P-glycoprotein (P-gp) (multidrug-resistance-protein 1, MDR1) that induces efflux of PARP inhibitor molecules and thereby a reduction intracellular PARP inhibitor levels. This process has been reported for various drugs, including olaparib (164,165). Second, loss of 53BP1 expression, a protein which is generally responsible for preventing HR and promoting non-homologous end-joining (NHEJ) (166), seems to specifically restore the HR-function in *BRCA1*-deficient cells (165,167,168). These studies demonstrate how 53BP1-loss restores HR activity in HR-compromised *BRCA1*-deficient cells. Furthermore, restoring HR seems to be sufficient to repair topotecan-induced DNA lesions, but not DNA lesions generated by the crosslinking agent cisplatin (167,168). The third described mechanism of resistance to

PARP inhibitors does mainly concern cells harboring elevated PARP levels and hence oppose vulnerability to PARP inhibition, such as ES. Different groups demonstrated that acquired resistance to PARP inhibitors in those tumors did result from reduced PARP protein levels (169,170). An additional described mechanism to oppose resistance to PARP inhibitors, primarily accounting to *BRCA1* and *BRCA2* deficient cancers, includes restauration of BRCA2 function (171–174). Translation of functional BRCA2 protein results in the restauration of the ability to repair DNA damage, induced by PARP inhibitors (155). *BRCA2*-mutant cells, being vulnerable to PARP inhibitors or platinum salts, acquired resistance by expression of functional BRCA2 (171,172). Furthermore, PARP inhibitor resistance by secondary mutations in *BRCA2* was proven to present clinical relevance. Two out of six patients, suffering from carboplatin-resistant ovarian cancer that carried *BRCA* mutations and who were treated with olaparib, exhibited resistance to this drug. Notably, both patients presented secondary mutations restoring the open reading frame of BRCA2 (175). Summarizing, we described the most frequent mechanisms of PARP inhibitor resistance, implicating the need of strategies to overcome such resistance mechanisms.

IV.5 Overcoming the resistance mechanisms

Resistance of tumor cells against pharmacological drugs is a major issue in the treatment of many forms of cancers, due to recurrence of mostly cross-resistant tumors. Therefore, strategies that overcome resistance mechanisms are of high demand in cancer therapy (155). In many cases, recurrent cancers display cross resistances towards a broad range of drugs, making them more difficult to treat than the primary tumor. In this situation, application of chemotherapeutics or pharmacological inhibitors, such as PARP inhibitors in platinum salt-resistant tumors, often displays limitations due to cross-resistance (175). Overexpression of *MDR1*, accompanied by an enhanced efflux of many drugs often limits efficient treatment. Pharmacological inhibition of P-gp by treatment with, for instance verapamil could restore the intracellular levels of both chemotherapeutics and pharmacological inhibitors and thereby induce cytotoxicity (176). Another mechanism of resistance is the reestablishment of genetic pathways, which were disabled beforehand. Like the secondary mutations in *BRCA2* that partially restored HR. Histone deacetylase inhibitors (HDACi) counteract histone deacetylation and are altering gene expression by silencing the chromatin (177,178). Indeed, several studies demonstrated that HDACi lead to genetic alterations in HR pathway genes and protein levels, resulting in non-functional HR (179–182). Remarkably, we correspondingly demonstrated, that addition of JNJ to our previous combination regimen resulted in a significant loss of U2OS cell viability (Figure 42, right). This might offers new treatment options for patients with tumors not being vulnerable to PARP inhibitors, as well as for patients with PARP inhibitor resistant tumors, as this “pharmacological BRCAness” might sensitize tumors once again to synthetic lethality.

IV.6 Graphical synopsis

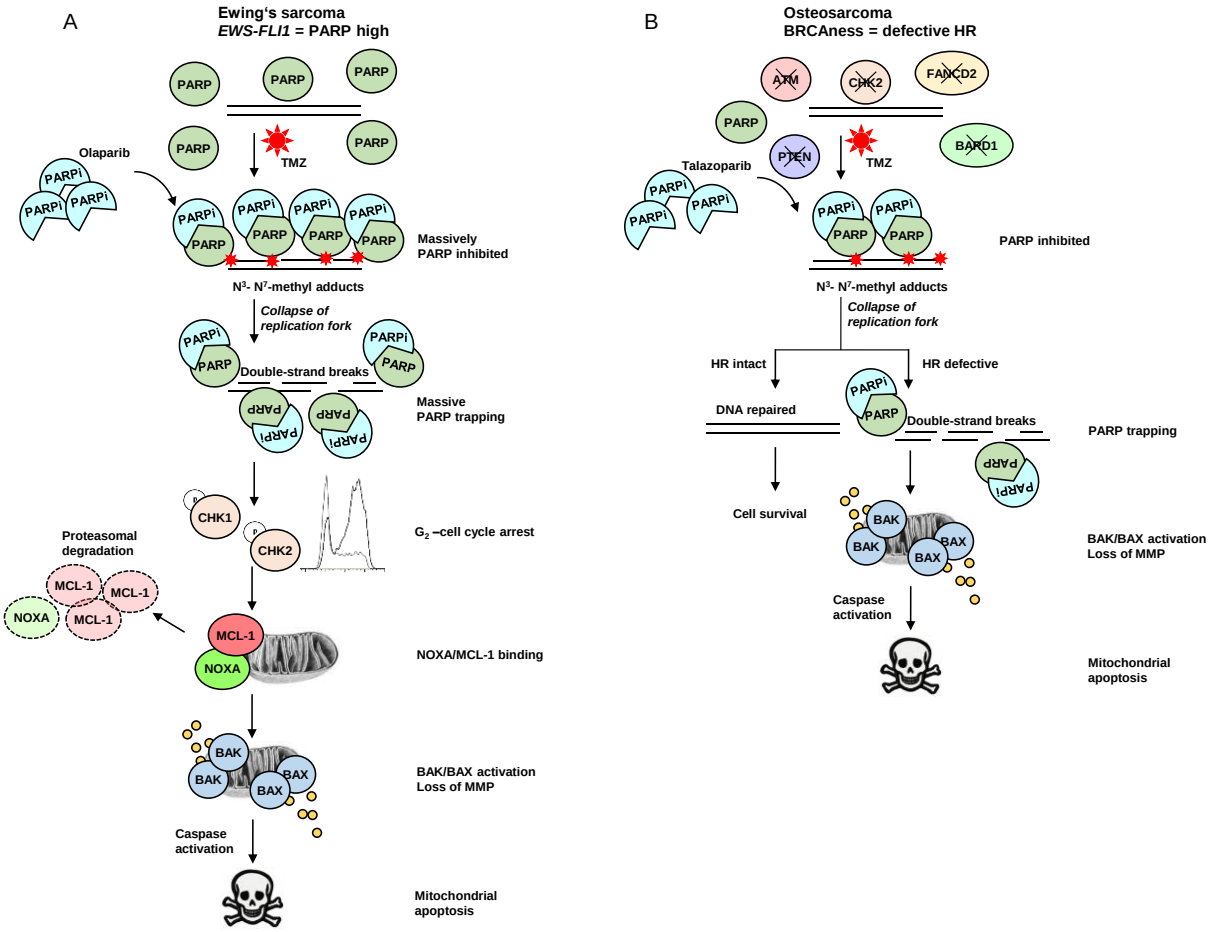

Figure 43: Despite different genetic background in ES and OS PARP inhibitor/TMZ cotreatment induces intrinsic apoptosis.

Molecular cell death signaling of olaparib/TMZ **(A)** and talazoparib/TMZ **(B)-**mediated apoptosis. Combination of PARP inhibitors and TMZ synergistically induces cell-cycle arrest, alterations in expression of BCL-2 family proteins, mitochondrial perturbations and caspase activation culminating in apoptosis. TMZ mediated N^3-N^7-methyl adducts potentiate cytotoxicity of PARP trapping, then triggering the mitochondrial cell death cascade in both combination regimens independent of the underlying genetic background.

V Outlook

In the last decades, since the initial discovery, PARP inhibitors have come a long way to 2014, in which the first PARP inhibitor, olaparib, was FDA-approval for treatment of *BRCA* deficient ovarian cancer. Since then, a further milestone was reached in 2015 as olaparib indications were expanded by FDA-designated breakthrough therapy status in castration resistant prostate cancer (CRPC). The recently described progress facilitated PARP inhibitor treatment strategies from bench to bedside in the past 10 years. However, further clinical studies to investigate PARP inhibitor monotherapy, short- and long-term safety effects, combined approaches of PARP inhibitors with chemotherapeutics as well as investigation of resistance mechanisms have to be performed. Nevertheless, PARP inhibitors seem to be an attractive and promising treatment option hitting the Achilles heel of ES, which express high levels of PARP protein due to the presence of the fusion gene. Furthermore, PARP inhibitors are exceptional examples of how synthetic lethal therapeutic strategies can be employed for tumors harboring BRCAness, as newly implicated in OS.

Regarding ES, many preclinical studies provided evidence concerning the efficacy of PARP inhibitors in combination with chemotherapeutics. Now, these findings have to be confirmed in clinical trials and trials investigating niraparib or talazoparib with or without TMZ in ES have already started (NCT02392793, NCT02044120). Concerning the mechanisms of interaction of PARP inhibitors and chemotherapeutics, mechanistic studies showing DNA interference were performed by Murai *et al.* (79,81), whereas we investigated and elucidated the molecular mechanism underlying PARP inhibitor/TMZ-mediated cell death. But some questions still remained elusive, for instance whether a proposed triple therapy of olaparib, SN-38 and TMZ (Figure 16) would result in a beneficial tumor surveillance or if increased host toxicity due to the triple therapy does not permit a therapeutic window.

In regard of the use of PARP inhibitors for OS treatment, we were the first to demonstrate vulnerability to talazoparib. As previously a large percentage of OS primary samples was defined to harbor features of BRCAness, the discovery of a biomarker for BRCAness and PARP inhibitor sensitivity would offer great opportunities. Yet, no clinical studies involving PARP inhibition in OS have been started, however many applicable knowledge has already been gained by multiple studies in ovarian cancer, CRPC and triple negative breast cancer, all displaying features of BRCAness. Investigations of the addition of HDACi together with PARP inhibitor therapy are in preliminary studies. This might set the basis for restoring vulnerability of resistant cells and might be an important option for overcoming acquired PARP inhibitor resistance mechanisms.

VI References

1. Hanahan D, Weinberg RA. Hallmarks of cancer: the next generation. Cell. Elsevier; 2011 Mar 4;144(5):646–74.
2. Cheng N, Chytil A, Shyr Y, Joly A, Moses HL. Transforming growth factor-beta signaling-deficient fibroblasts enhance hepatocyte growth factor signaling in mammary carcinoma cells to promote scattering and invasion. Mol Cancer Res. 2008 Oct 1;6(10):1521–33.
3. Bhowmick NA, Neilson EG, Moses HL. Stromal fibroblasts in cancer initiation and progression. Nature. 2004 Nov 18;432(7015):332–7.
4. Burkhart DL, Sage J. Cellular mechanisms of tumour suppression by the retinoblastoma gene. Nat Rev Cancer. Nature Publishing Group; 2008 Jul 24;8(9):671–82.
5. Ghebranious N, Donehower LA. Mouse models in tumor suppression. Oncogene. Nature Publishing Group; 1998 Dec 24;17(25):3385–400.
6. Lakin ND, Jackson SP. Regulation of p53 in response to DNA damage. Oncogene. 1999 Dec 13;18(53):7644–55.
7. Yang L, Pang Y, Moses HL. TGF-beta and immune cells: an important regulatory axis in the tumor microenvironment and progression. Trends Immunol. 2010 Jun;31(6):220–7.
8. Dvorak HF. Tumors: wounds that do not heal. Similarities between tumor stroma generation and wound healing. N Engl J Med. 1986 Dec 25;315(26):1650–9.
9. Galluzzi L, Kroemer G. Necroptosis: a specialized pathway of programmed necrosis. Cell. Elsevier; 2008 Dec 26;135(7):1161–3.
10. Klymkowsky MW, Savagner P. Epithelial-mesenchymal transition: a cancer researcher's conceptual friend and foe. Am J Pathol. Elsevier; 2009 May 1;174(5):1588–93.
11. Polyak K, Weinberg RA. Transitions between epithelial and mesenchymal states: acquisition of malignant and stem cell traits. Nat Rev Cancer. Nature Publishing Group; 2009 Apr;9(4):265–73.
12. HANAHAN D, FOLKMAN J. Patterns and Emerging Mechanisms of the Angiogenic Switch during Tumorigenesis. Cell. 1996 Aug 9;86(3):353–64.
13. Blasco MA. Telomeres and human disease: ageing, cancer and beyond. Nat Rev Genet. 2005 Aug;6(8):611–22.
14. Ince TA, Richardson AL, Bell GW, Saitoh M, Godar S, Karnoub AE, et al. Transformation of different human breast epithelial cell types leads to distinct tumor phenotypes. Cancer Cell. 2007 Aug;12(2):160–70.
15. Kawai T, Hiroi S, Nakanishi K, Meeker AK. Telomere length and telomerase expression in atypical adenomatous hyperplasia and small bronchioloalveolar carcinoma of the lung. Am J Clin Pathol. The Oxford University Press; 2007 Feb 1;127(2):254–62.
16. Negrini S, Gorgoulis VG, Halazonetis TD. Genomic instability--an evolving hallmark of cancer. Nat Rev Mol Cell Biol. Nature Publishing Group; 2010 Mar;11(3):220–8.
17. Korkola J, Gray JW. Breast cancer genomes--form and function. Curr Opin Genet Dev. 2010 Feb;20(1):4–14.
18. Adams JM, Cory S. The Bcl-2 apoptotic switch in cancer development and therapy. Oncogene. 2007 Feb 26;26(9):1324–37.
19. Warburg O. The metabolism of tumours. Investigations from the Kaiser-Wilhelm Institute for Biology, Berlin-Dahlem. Edited by Otto Warburg, Kaiser-Wilhelm Institute for Biology, Berlin-Dahlem. Translated from the German edition, with accounts of additional recent res. Br J Surg. 1931 Jul;19(73):168–168.
20. Ewing J. Diffuse Endothelioma of Bone. Proc NY Pathol So. 1921 Mar 1;22(2):95–8.

21. Riggi N, Cironi L, Provero P, Suvà M-L, Kaloulis K, Garcia-Echeverria C, et al. Development of Ewing's sarcoma from primary bone marrow-derived mesenchymal progenitor cells. Cancer Res. 2005 Dec 15;65(24):11459–68.

22. Balamuth NJ, Womer RB. Ewing's sarcoma. Lancet Oncol. Elsevier; 2010 Feb 2;11(2):184–92.

23. Zhu L, McManus MM, Hughes DPM. Understanding the Biology of Bone Sarcoma from Early Initiating Events through Late Events in Metastasis and Disease Progression. Front Oncol. 2013 Jan;3(September):230.

24. Juergens C, Weston C, Lewis I, Whelan J, Paulussen M, Oberlin O, et al. Safety assessment of intensive induction with vincristine, ifosfamide, doxorubicin, and etoposide (VIDE) in the treatment of Ewing tumors in the EURO-E.W.I.N.G. 99 clinical trial. Pediatr Blood Cancer. 2006 Jul;47(1):22–9.

25. Smith M a, Seibel NL, Altekruse SF, Ries L a G, Melbert DL, O'Leary M, et al. Outcomes for children and adolescents with cancer: challenges for the twenty-first century. J Clin Oncol. 2010 May 20;28(15):2625–34.

26. Delattre O, Zucman J, Melot T, Garau X, Zucker J, Lenoir G, et al. The Ewing Family Of Tumors - A Subgroup Of Small-Round-Cell Tumors Defined By Specific Chimeric Transcripts. N Engl J Med. 1994;331:294–9.

27. Delattre O, Zucman J, Plougastel B, Desmaze C, Melot T, Peter M, et al. Gene fusion with an ETS DNA-binding domain caused by chromosome translocation in human tumours. Nature. 1992;

28. Kovar H. Context matters: the hen or egg problem in Ewing's sarcoma. Semin Cancer Biol. 2005 Jun;15(3):189–96.

29. Erkizan HH V, Uversky VVN, Toretsky JJ a. Oncogenic partnerships: EWS-FLI1 protein interactions initiate key pathways of Ewing's sarcoma. Clin Cancer Res. 2010 Aug 15;16(16):4077–83.

30. Toomey EC, Schiffman JD, Lessnick SL. Recent advances in the molecular pathogenesis of Ewing's sarcoma. Oncogene. Nature Publishing Group; 2010 Aug 12;29(32):4504–16.

31. Garnett MJ, Edelman EJ, Heidorn SJ, Greenman CD, Dastur A, Lau KW, et al. Systematic identification of genomic markers of drug sensitivity in cancer cells. Nature. 2012 Mar 29;483(7391):570–5.

32. Brenner JC, Feng FY, Han S, Patel S, Goyal S V, Bou-Maroun LM, et al. PARP-1 inhibition as a targeted strategy to treat Ewing's sarcoma. Cancer Res. 2012 Apr 1;72(7):1608–13.

33. Wellcome Trust Sanger Institute. Home page - Genomics of Drug Sensitivity in Cancer [Internet]. [cited 2016 Feb 23]. Available from: http://www.cancerrxgene.org/

34. Bloom ET. Further Definition by Cytotoxicity Tests of Cell Surface Antigens of Human Sarcomas in Culture Further Definition by Cytotoxicity Tests of Cell Surface Antigens of Human Sarcomas in Culture1. 1972;32(May):960–7.

35. Zhang J, Hu S, Schofield DE, Sorensen PHB, Triche TJ. Selective Usage of D-Type Cyclins by Ewing ' s Tumors and Rhabdomyosarcomas. 2004;6026–34.

36. Sankar S, Theisen ER, Bearss J, Mulvihill T, Hoffman LM, Sorna V, et al. Reversible LSD1 inhibition interferes with global EWS/ETS transcriptional activity and impedes Ewing sarcoma tumor growth. Clin Cancer Res. 2014 Sep 1;20(17):4584–97.

37. Luetke A, Meyers PA, Lewis I, Juergens H. Osteosarcoma treatment - where do we stand? A state of the art review. Cancer Treat Rev. 2014 May;40(4):523–32.

38. Cotterill SJ, Wright CM, Pearce MS, Craft AW. Stature of young people with malignant bone tumors. Pediatr Blood Cancer. 2004 Jan;42(1):59–63.

39. Geller DS, Gorlick R. Osteosarcoma: a review of diagnosis, management, and treatment strategies. Clin Adv Hematol Oncol. 2010 Oct;8(10):705–18.

40. Collins M, Wilhelm M, Conyers R, Herschtal A, Whelan J, Bielack S, et al. Benefits and adverse events in younger versus older patients receiving neoadjuvant chemotherapy for osteosarcoma: findings from a meta-analysis. J Clin Oncol. 2013 Jun 20;31(18):2303–12.

41. Carrle D, Bielack S. Osteosarcoma lung metastases detection and principles of multimodal therapy. Cancer Treat Res. 2009 Jan;152:165–84.

42. Toguchida J, Ishizaki K, Sasaki MS, Nakamura Y, Ikenaga M, Kato M, et al. Preferential mutation of paternally derived RB gene as the initial event in sporadic osteosarcoma. Nature. Nature Publishing Group; 1989 Mar 9;338(6211):156–8.

43. Wunder JS, Gokgoz N, Parkes R, Bull SB, Eskandarian S, Davis AM, et al. TP53 mutations and outcome in osteosarcoma: a prospective, multicenter study. J Clin Oncol. 2005 Mar 1;23(7):1483–90.

44. Chen X, Bahrami A, Pappo A, Easton J, Dalton J, Hedlund E, et al. Recurrent somatic structural variations contribute to tumorigenesis in pediatric osteosarcoma. Cell Rep. 2014 Apr 10;7(1):104–12.

45. Stephens PJ, Greenman CD, Fu B, Yang F, Bignell GR, Mudie LJ, et al. Massive genomic rearrangement acquired in a single catastrophic event during cancer development. Cell. 2011 Jan 7;144(1):27–40.

46. Kovac M, Blattmann C, Ribi S, Smida J, Mueller NS, Engert F, et al. Exome sequencing of osteosarcoma reveals mutation signatures reminiscent of BRCA deficiency. Nat Commun. Nature Publishing Group; 2015 Jan 3;6:8940.

47. Lord CJ, Ashworth A. BRCAness revisited. Nat Rev Cancer. Nature Publishing Group; 2016 Jan 18;16(2):110–20.

48. Siggelkow H, Niedhart C, Kurre W, Ihbe A, Schulz A, Atkinson MJ, et al. In vitro differentiation potential of a new human osteosarcoma cell line (HOS 58). Differentiation. 1998 Jun;63(2):81–91.

49. Ottaviano L, Schaefer K-L, Gajewski M, Huckenbeck W, Baldus S, Rogel U, et al. Molecular characterization of commonly used cell lines for bone tumor research: a trans-European EuroBoNet effort. Genes Chromosomes Cancer. 2010 Jan;49(1):40–51.

50. Ozaki T, Neumann T, Wai D, Schäfer K-L, van Valen F, Lindner N, et al. Chromosomal alterations in osteosarcoma cell lines revealed by comparative genomic hybridization and multicolor karyotyping. Cancer Genet Cytogenet. 2003 Jan;140(2):145–52.

51. Abkevich V, Timms KM, Hennessy BT, Potter J, Carey MS, Meyer LA, et al. Patterns of genomic loss of heterozygosity predict homologous recombination repair defects in epithelial ovarian cancer. Br J Cancer. 2012 Nov 6;107(10):1776–82.

52. Fuchs Y, Steller H. Live to die another way: modes of programmed cell death and the signals emanating from dying cells. Nat Rev Mol Cell Biol. Nature Publishing Group; 2015 May 20;16(6):329–44.

53. Kerr JF, Wyllie AH, Currie AR. Apoptosis: a basic biological phenomenon with wide-ranging implications in tissue kinetics. Br J Cancer. Nature Publishing Group; 1972 Aug 1;26(4):239–57.

54. Mariño G, Niso-Santano M, Baehrecke EH, Kroemer G. Self-consumption: the interplay of autophagy and apoptosis. Nat Rev Mol Cell Biol. Nature Publishing Group; 2014 Feb 8;15(2):81–94.

55. Vanden Berghe T, Linkermann A, Jouan-Lanhouet S, Walczak H, Vandenabeele P. Regulated necrosis: the expanding network of non-apoptotic cell death pathways. Nat Rev Mol Cell Biol. Nature Publishing Group; 2014 Feb 23;15(2):135–47.

56. Aredia F, Scovassi AI. Poly(ADP-ribose): a signaling molecule in different paradigms of cell death. Biochem Pharmacol. Elsevier Inc.; 2014 Nov 1;92(1):157–63.

57. Xie Y, Hou W, Song X, Yu Y, Huang J, Sun X, et al. Ferroptosis: process and function. Cell Death Differ. Macmillan Publishers Limited; 2016 Jan 22;23(3):369–79.

58. Hengartner MO. The biochemistry of apoptosis. Nature. Nature Publishing Group; 2000 Oct 12;407(6805):770–6.

59. Thornberry NA. Caspases: Enemies Within. Science (80-). American Association for the Advancement of Science; 1998 Aug 28;281(5381):1312–6.

60. Czabotar PE, Lessene G, Strasser A, Adams JM. Control of apoptosis by the BCL-2 protein family: implications for physiology and therapy. Nat Rev Mol Cell Biol. Nature Publishing Group; 2014 Jan 20;15(1):49–63.

61. Deng J, Carlson N, Takeyama K, Dal Cin P, Shipp M, Letai A. BH3 profiling identifies three distinct classes of apoptotic blocks to predict response to ABT-737 and conventional chemotherapeutic agents. Cancer Cell. 2007 Aug;12(2):171–85.

62. Ni Chonghaile T, Sarosiek K a, Vo T-T, Ryan J a, Tammareddi A, Moore VDG, et al. Pretreatment mitochondrial priming correlates with clinical response to cytotoxic chemotherapy. Science. 2011 Nov 25;334(6059):1129–33.

63. Certo M, Del Gaizo Moore V, Nishino M, Wei G, Korsmeyer S, Armstrong S a, et al. Mitochondria primed by death signals determine cellular addiction to antiapoptotic BCL-2 family members. Cancer Cell. 2006 May;9(5):351–65.

64. Gross A, Mcdonnell JM, Korsmeyer SJ. BCL-2 family members and the mitochondria in apoptosis. 1999;1899–911.

65. Gillies L a, Kuwana T. Apoptosis regulation at the mitochondrial outer membrane. J Cell Biochem. 2014 Apr;115(4):632–40.

66. Montero J, Sarosiek KA, DeAngelo JD, Maertens O, Ryan J, Ercan D, et al. Drug-Induced Death Signaling Strategy Rapidly Predicts Cancer Response to Chemotherapy. Cell. 2015 Feb;160(5):977–89.

67. Chipuk JE, Moldoveanu T, Llambi F, Parsons MJ, Green DR. The BCL-2 family reunion. Mol Cell. Elsevier Inc.; 2010 Feb 12;37(3):299–310.

68. Sarosiek K a, Chi X, Bachman J a, Sims JJ, Montero J, Patel L, et al. BID preferentially activates BAK while BIM preferentially activates BAX, affecting chemotherapy response. Mol Cell. Elsevier Inc.; 2013 Sep 26;51(6):751–65.

69. Fulda S, Galluzzi L, Kroemer G. Targeting mitochondria for cancer therapy. Nat Rev Drug Discov. Nature Publishing Group; 2010 Jun;9(6):447–64.

70. Shen Y, Aoyagi-Scharber M, Wang B. Trapping Poly(ADP-Ribose) Polymerase. J Pharmacol Exp Ther. 2015 Apr 23;353(3):446–57.

71. Selleckchem. Selleckchem.com - Inhibitor Expert (Inhibitors, Compound Libraries) [Internet]. [cited 2016 Feb 23]. Available from: http://www.selleckchem.com/

72. Durkacz BW, Omidiji O, Gray DA, Shall S. (ADP-ribose)n participates in DNA excision repair. Nature. Nature Publishing Group; 1980 Feb 7;283(5747):593–6.

73. Wahlberg E, Karlberg T, Kouznetsova E, Markova N, Macchiarulo A, Thorsell A-G, et al. Family-wide chemical profiling and structural analysis of PARP and tankyrase inhibitors. Nat Biotechnol. Nature Publishing Group, a division of Macmillan Publishers Limited. All Rights Reserved.; 2012 Feb 19;30(3):283–8.

74. Bryant HE, Schultz N, Thomas HD, Parker KM, Flower D, Lopez E, et al. Specific killing of BRCA2-deficient tumours with inhibitors of poly(ADP-ribose) polymerase. Nature. Nature Publishing Group; 2005 Apr 14;434(7035):913–7.

75. Farmer H, McCabe N, Lord CJ, Tutt ANJ, Johnson DA, Richardson TB, et al. Targeting the DNA repair defect in BRCA mutant cells as a therapeutic strategy. Nature. Nature Publishing Group; 2005 Apr 14;434(7035):917–21.

76. Fong PC, Boss DS, Yap TA, Tutt A, Wu P, Mergui-Roelvink M, et al. Inhibition of Poly(ADP-Ribose) Polymerase in Tumors from BRCA Mutation Carriers. N Engl J Med. 2009 Jul 9;361(2):123–34.

77. Saleh-Gohari N, Bryant HE, Schultz N, Parker KM, Cassel TN, Helleday T. Spontaneous homologous recombination is induced by collapsed replication forks that are caused by endogenous DNA single-strand breaks. Mol Cell Biol. 2005 Aug 15;25(16):7158–69.

78. Masson M, Niedergang C, Schreiber V, Muller S, Menissier-de Murcia J, de Murcia G. XRCC1 is specifically associated with poly(ADP-ribose) polymerase and negatively regulates its activity following DNA damage. Mol Cell Biol. 1998 Jun;18(6):3563–71.

79. Murai J, Zhang Y, Morris J, Ji J, Takeda S, Doroshow JH, et al. Rationale for poly(ADP-ribose) polymerase (PARP) inhibitors in combination therapy with camptothecins or temozolomide based on PARP trapping versus catalytic inhibition. J Pharmacol Exp Ther. 2014 Jun;349(3):408–16.

80. Murai J, Huang S-YN, Renaud A, Zhang Y, Ji J, Takeda S, et al. Stereospecific PARP trapping by BMN 673 and comparison with olaparib and rucaparib. Mol Cancer Ther. 2014 Feb;13(2):433–43.

81. Murai J, Huang SN, Das BB, Renaud A, Zhang Y, Doroshow JH, et al. Trapping of PARP1 and PARP2 by Clinical PARP Inhibitors. Cancer Res. 2012 Nov 1;72(21):5588–99.

82. Zaremba T, Curtin NJ. PARP inhibitor development for systemic cancer targeting. Anticancer Agents Med Chem. 2007 Sep;7(5):515–23.

83. Rouleau M, Patel A, Hendzel MJ, Kaufmann SH, Poirier GG. PARP inhibition: PARP1 and beyond. Nat Rev Cancer. Nature Publishing Group; 2010 Apr;10(4):293–301.

84. O'Connor MJ. Targeting the DNA Damage Response in Cancer. Mol Cell. 2015 Nov;60(4):547–60.

85. U.S. National Institutes of Health. Home - ClinicalTrials.gov [Internet]. [cited 2016 Feb 23]. Available from: https://clinicaltrials.gov/ct2/home

86. Deeks ED. Olaparib: first global approval. Drugs. 2015 Feb;75(2):231–40.

87. Helleday T. PARP inhibitor recognised as FDA breakthrough therapy in castration resistant prostate cancer: beyond germline BRCA mutations. Ann Oncol. 2016 Feb 9;mdw048.

88. Stewart E, Goshorn R, Bradley C, Griffiths LM, Benavente C, Twarog NR, et al. Targeting the DNA repair pathway in Ewing sarcoma. Cell Rep. 2014 Nov 6;9(3):829–41.

89. American Cancer Society. Types of chemotherapy drugs | American Cancer Society [Internet]. [cited 2016 Feb 29]. Available from: http://www.cancer.org/treatment/treatmentsandsideeffects/treatmenttypes/chemotherapy/chemotherapyprinciplesanin-depthdiscussionofthetechniquesanditsroleintreatment/chemotherapy-principles-types-of-chemo-drugs

90. Clark AS, Deans B, Stevens MFG, Tisdale MJ, Wheelhouse RT, Denny BJ, et al. Antitumor Imidazotetrazines. 32.1 Synthesis of Novel Imidazotetrazinones and Related Bicyclic Heterocycles To Probe the Mode of Action of the Antitumor Drug Temozolomide. J Med Chem. American Chemical Society; 1995 Apr 1;38(9):1493–504.

91. Horton JK, Wilson SH. Predicting enhanced cell killing through PARP inhibition. Mol Cancer Res. 2013 Jan;11(1):13–8.

92. Engert F, Schneider C, Weiβ LM, Probst M, Fulda S. PARP Inhibitors Sensitize Ewing Sarcoma Cells to Temozolomide-Induced Apoptosis via the Mitochondrial Pathway. Mol Cancer Ther. 2015 Dec 1;14(12):2818–30.

93. Hurley LH. DNA and its associated processes as targets for cancer therapy. Nat Rev Cancer. Nature Publishing Group; 2002 Mar 1;2(3):188–200.

94. Jung Y, Lippard SJ. Direct cellular responses to platinum-induced DNA damage. Chem Rev. American Chemical Society; 2007 May;107(5):1387–407.

95. Grier HE, Krailo MD, Tarbell NJ, Link MP, Fryer CJ, Pritchard DJ, et al. Addition of ifosfamide and etoposide to standard chemotherapy for Ewing's sarcoma and primitive neuroectodermal tumor of bone. N Engl J Med. 2003;348(8):694–701.

96. U.S. National Library of Medicine. LIVERTOX® - Ifosfamide [Internet]. [cited 2016 Mar 1]. Available from: http://livertox.nih.gov/Ifosfamide.htm

97. Pommier Y, Leo E, Zhang H, Marchand C. DNA topoisomerases and their poisoning by anticancer and antibacterial drugs. Chem Biol. Elsevier; 2010 May 28;17(5):421–33.

98. Pommier Y. Drugging topoisomerases: lessons and challenges. ACS Chem Biol. 2013 Jan 18;8(1):82–95.

99. Pourquier P, Pommier Y. Topoisomerase I-mediated DNA damage. Adv Cancer Res. 2001;80:189–216.

100. Nitiss JL. Investigating the biological functions of DNA topoisomerases in eukaryotic cells. Biochim Biophys Acta - Gene Struct Expr. 1998 Oct;1400(1-3):63–81.

101. Minford J, Pommier Y, Filipski J, Kohn KW, Kerrigan D, Mattern M, et al. Isolation of intercalator-dependent protein-linked DNA strand cleavage activity from cell nuclei and identification as topoisomerase II. Biochemistry. American Chemical Society; 1986 Jan 1;25(1):9–16.

102. Tewey K, Rowe T, Yang L, Halligan B, Liu L. Adriamycin-induced DNA damage mediated by mammalian DNA topoisomerase II. Science (80-). American Association for the Advancement of Science; 1984 Oct 26;226(4673):466–8.

103. Moore A, Pinkerton R. Vincristine: Can its therapeutic index be enhanced? Pediatr Blood Cancer. 2009 Dec 15;53(7):1180–7.

104. Wertz IE, Kusam S, Lam C, Okamoto T, Sandoval W, Anderson DJ, et al. Sensitivity to antitubulin chemotherapeutics is regulated by MCL1 and FBW7. Nature. Nature Publishing Group; 2011 Mar 3;471(7336):110–4.

105. Müller W, Crothers DM. Studies of the binding of actinomycin and related compounds to DNA. J Mol Biol. 1968 Jan;35(2):251–90.

106. Sobell HM, Jain SC, Sakore TD, Nordman CE. Stereochemistry of actinomycin--DNA binding. Nat New Biol. 1971 Jun 16;231(24):200–5.

107. Rajagopalan PTR, Zhang Z, McCourt L, Dwyer M, Benkovic SJ, Hammes GG. Interaction of dihydrofolate reductase with methotrexate: ensemble and single-molecule kinetics. Proc Natl Acad Sci U S A. 2002 Oct 15;99(21):13481–6.

108. Weiss A, Gill J, Goldberg J, Lagmay J, Spraker-Perlman H, Venkatramani R, et al. Advances in therapy for pediatric sarcomas. Curr Oncol Rep. 2014 Jan;16(8):395.

109. Schulze-Koops H, Kalden JR. The balance of Th1/Th2 cytokines in rheumatoid arthritis. Best Pract Res Clin Rheumatol. 2001 Dec;15(5):677–91.

110. Chou T-C. Drug combination studies and their synergy quantification using the Chou-Talalay method. Cancer Res. 2010 Jan 15;70(2):440–6.

111. Brenner JC, Ateeq B, Li Y, Yocum AK, Cao Q, Asangani I a, et al. Mechanistic rationale for inhibition of poly(ADP-ribose) polymerase in ETS gene fusion-positive prostate cancer. Cancer Cell. 2011 May 17;19(5):664–78.

112. Sonnenblick A, de Azambuja E, Azim H a, Piccart M. An update on PARP inhibitors-moving to the adjuvant setting. Nat Rev Clin Oncol. Nature Publishing Group; 2014 Oct 7;1–15.

113. Vormoor B, Curtin NJ. Poly(ADP-ribose) polymerase inhibitors in Ewing sarcoma. Curr Opin Oncol. 2014 Jul;26(4):428–33.

114. Bartek J, Lukas J. Chk1 and Chk2 kinases in checkpoint control and cancer. 2003;(Figure 2):421–9.

115. Hans F, Dimitrov S. Histone H3 phosphorylation and cell division. Oncogene. Nature Publishing Group; 2001 May 28;20(24):3021–7.

116. Kontny HU, Hämmerle K, Klein R, Shayan P, Mackall CL, Niemeyer CM. Sensitivity of Ewing's sarcoma to TRAIL-induced apoptosis. Cell Death Differ. 2001 May;8(5):506–14.

117. Fulda S, Küfer MU, Meyer E, van Valen F, Dockhorn-Dworniczak B, Debatin KM. Sensitization for death receptor- or drug-induced apoptosis by re-expression of caspase-8 through demethylation or gene transfer.

Oncogene. 2001 Sep 13;20(41):5865–77.

118. Fujise K, Zhang D, Liu J, Yeh ET. Regulation of apoptosis and cell cycle progression by MCL1. Differential role of proliferating cell nuclear antigen. J Biol Chem. 2000 Dec 15;275(50):39458–65.

119. Nakajima W, Hicks M a, Tanaka N, Krystal GW, Harada H. Noxa determines localization and stability of MCL-1 and consequently ABT-737 sensitivity in small cell lung cancer. Cell Death Dis. Nature Publishing Group; 2014 Jan;5(2):e1052.

120. Gomez-Bougie P, Ménoret E, Juin P, Dousset C, Pellat-Deceunynck C, Amiot M. Noxa controls Mule-dependent Mcl-1 ubiquitination through the regulation of the Mcl-1/USP9X interaction. Biochem Biophys Res Commun. Elsevier Inc.; 2011 Sep 30;413(3):460–4.

121. Ryan J, Letai A. BH3 profiling in whole cells by fluorimeter or FACS. 2013;61:156–64.

122. Smith M a, Reynolds CP, Kang MH, Kolb EA, Gorlick R, Carol H, et al. Synergistic activity of PARP inhibition by talazoparib (BMN 673) with temozolomide in pediatric cancer models in the pediatric preclinical testing program. Clin Cancer Res. American Association for Cancer Research; 2015 Mar 15;21(4):819–32.

123. Smith MA, Hampton OA, Reynolds CP, Kang MH, Maris JM, Gorlick R, et al. Initial testing (stage 1) of the PARP inhibitor BMN 673 by the pediatric preclinical testing program: PALB2 mutation predicts exceptional in vivo response to BMN 673. Pediatr Blood Cancer. 2015 Jan;62(1):91–8.

124. Lord CJ, Ashworth A. The DNA damage response and cancer therapy. Nature. Nature Publishing Group; 2012 Jan 19;481(7381):287–94.

125. Mendes-Pereira AM, Martin SA, Brough R, McCarthy A, Taylor JR, Kim J-S, et al. Synthetic lethal targeting of PTEN mutant cells with PARP inhibitors. EMBO Mol Med. 2009 Sep;1(6-7):315–22.

126. Weston VJ, Oldreive CE, Skowronska A, Oscier DG, Pratt G, Dyer MJS, et al. The PARP inhibitor olaparib induces significant killing of ATM-deficient lymphoid tumor cells in vitro and in vivo. Blood. American Society of Hematology; 2010 Nov 25;116(22):4578–87.

127. Horton JK, Stefanick DF, Wilson SH. Involvement of poly(ADP-ribose) polymerase activity in regulating Chk1-dependent apoptotic cell death. DNA Repair (Amst). 2005 Sep 28;4(10):1111–20.

128. Mateo-Lozano S, Tirado OM, Notario V. Rapamycin induces the fusion-type independent downregulation of the EWS/FLI-1 proteins and inhibits Ewing's sarcoma cell proliferation. Oncogene. 2003 Dec 18;22(58):9282–7.

129. Deneen B, Welford SM, Ho T, Hernandez F, Kurland I, Denny CT. PIM3 Proto-Oncogene Kinase Is a Common Transcriptional Target of Divergent EWS/ETS Oncoproteins. Mol Cell Biol. 2003 Jun 1;23(11):3897–908.

130. Helleday T. The underlying mechanism for the PARP and BRCA synthetic lethality: clearing up the misunderstandings. Mol Oncol. Elsevier; 2011 Aug 1;5(4):387–93.

131. Kedar PS, Stefanick DF, Horton JK, Wilson SH. Increased PARP-1 Association with DNA in Alkylation Damaged, PARP-Inhibited Mouse Fibroblasts. Mol Cancer Res. 2012 Jan 13;10(3):360–8.

132. Telli ML, Timms KM, Reid JE, Hennessy B, Mills GB, Jensen KC, et al. Homologous Recombination Deficiency (HRD) Score Predicts Response to Platinum-Containing Neoadjuvant Chemotherapy in Patients with Triple Negative Breast Cancer. Clin Cancer Res. 2016 Mar 8;

133. Popova T, Manié E, Rieunier G, Caux-Moncoutier V, Tirapo C, Dubois T, et al. Ploidy and large-scale genomic instability consistently identify basal-like breast carcinomas with BRCA1/2 inactivation. Cancer Res. 2012 Nov 1;72(21):5454–62.

134. Shen WH, Balajee AS, Wang J, Wu H, Eng C, Pandolfi PP, et al. Essential role for nuclear PTEN in maintaining chromosomal integrity. Cell. 2007 Jan 12;128(1):157–70.

135. Li M, Yu X. Function of BRCA1 in the DNA Damage Response Is Mediated by ADP-Ribosylation. Cancer Cell. 2013 May;23(5):693–704.

136. Lee JS, Collins KM, Brown AL, Lee CH, Chung JH. hCds1-mediated phosphorylation of BRCA1 regulates the DNA damage response. Nature. Nature Publishing Group; 2000 Mar 9;404(6774):201–4.

137. Kim H, D'Andrea AD. Regulation of DNA cross-link repair by the Fanconi anemia/BRCA pathway. Genes Dev. 2012 Jul 1;26(13):1393–408.

138. McCabe N, Turner NC, Lord CJ, Kluzek K, Bialkowska A, Swift S, et al. Deficiency in the repair of DNA damage by homologous recombination and sensitivity to poly(ADP-ribose) polymerase inhibition. Cancer Res. 2006 Aug 15;66(16):8109–15.

139. Choy E, Butrynski JE, Harmon DC, Morgan JA, George S, Wagner AJ, et al. Phase II study of olaparib in patients with refractory Ewing sarcoma following failure of standard chemotherapy. BMC Cancer. BioMed Central; 2014 Jan 5;14(1):813.

140. Sarkaria JN, Kitange GJ, James CD, Plummer R, Calvert H, Weller M, et al. Mechanisms of chemoresistance to alkylating agents in malignant glioma. Clin Cancer Res. 2008 May 15;14(10):2900–8.

141. Zhang J, Stevens MFG, Bradshaw TD. Temozolomide: mechanisms of action, repair and resistance. Curr Mol Pharmacol. 2012 Jan;5(1):102–14.

142. Cistulli C, Lavrik OI, Prasad R, Hou E, Wilson SH. AP endonuclease and poly(ADP-ribose) polymerase-1 interact with the same base excision repair intermediate. DNA Repair (Amst). 2004 Jun 3;3(6):581–91.

143. Horton JK, Wilson SH. Strategic Combination of DNA-Damaging Agent and PARP Inhibitor Results in Enhanced Cytotoxicity. Front Oncol. 2013 Jan;3(September):257.

144. Wainberg ZA, de Bono JS, Mina L, Sachdev J, Byers LA, Chugh R, et al. Abstract C295: Update on first-in-man trial of novel oral PARP inhibitor BMN 673 in patients with solid tumors. Mol Cancer Ther. 2014;12(11_Supplement):C295–C295.

145. Hopkins TA, Shi Y, Rodriguez LE, Solomon LR, Donawho CK, DiGiammarino EL, et al. Mechanistic Dissection of PARP1 Trapping and the Impact on In Vivo Tolerability and Efficacy of PARP Inhibitors. Mol Cancer Res. 2015 Nov 1;13(11):1465–77.

146. Johann Sebastian De Bono. First-in-human trial of novel oral PARP inhibitor BMN 673 in patients with solid tumors. | 2013 ASCO Annual Meeting | Abstracts | Meeting Library. 2013.

147. Bobola MS, Silber JR, Ellenbogen RG, Geyer JR, Blank A, Goff RD. O6-methylguanine-DNA methyltransferase, O6-benzylguanine, and resistance to clinical alkylators in pediatric primary brain tumor cell lines. Clin Cancer Res. 2005 Apr 1;11(7):2747–55.

148. Newlands E, Blackledge G, Slack J, Rustin G, Smith D, Stuart N, et al. Phase I trial of temozolomide (CCRG 81045: M&B 39831: NSC 362856). Br J Cancer. Cancer Research Campaign; 1992 Feb;65(2):287–91.

149. Brada M, Judson I, Beale P, Moore S, Reidenberg P, Statkevich P, et al. Phase I dose-escalation and pharmacokinetic study of temozolomide (SCH 52365) for refractory or relapsing malignancies. Br J Cancer. Cancer Research Campaign; 1999 Nov;81(6):1022–30.

150. Das BB, Huang SN, Murai J, Rehman I, Amé J-C, Sengupta S, et al. PARP1-TDP1 coupling for the repair of topoisomerase I-induced DNA damage. Nucleic Acids Res. 2014 Apr 1;42(7):4435–49.

151. Pommier Y, Barcelo JM, Rao VA, Sordet O, Jobson AG, Thibaut L, et al. Repair of topoisomerase I-mediated DNA damage. Prog Nucleic Acid Res Mol Biol. 2006 Jan;81:179–229.

152. Norris RE, Adamson PC, Nguyen VT, Fox E. Preclinical evaluation of the PARP inhibitor, olaparib, in combination with cytotoxic chemotherapy in pediatric solid tumors. Pediatr Blood Cancer. 2014 Jan;61(1):145–50.

153. Bowman KJ, Newell DR, Calvert AH, Curtin NJ. Differential effects of the poly (ADP-ribose) polymerase (PARP) inhibitor NU1025 on topoisomerase I and II inhibitor cytotoxicity in L1210 cells in vitro. Br J Cancer. 2001 Jan 5;84(1):106–12.

154. Zhang Y-W, Regairaz M, Seiler JA, Agama KK, Doroshow JH, Pommier Y. Poly(ADP-ribose) polymerase and XPF-ERCC1 participate in distinct pathways for the repair of topoisomerase I-induced DNA damage in mammalian cells. Nucleic Acids Res. 2011 May 1;39(9):3607–20.

155. Lord CJ, Ashworth A. Mechanisms of resistance to therapies targeting BRCA-mutant cancers. Nat Med. Nature Publishing Group; 2013 Nov 7;19(11):1381–8.

156. Czabotar PE, Lee EF, Delft MF Van, Day CL, Smith BJ, Huang DCS, et al. Structural insights into the degradation of Mcl-1 induced by BH3 domains. 2007;104(15):6217–22.

157. Lu G, Punj V, Chaudhary PM. Proteasome inhibitor Bortezomib induces cell-cycle arrest and apoptosis in cell lines derived from Ewing's sarcoma family of tumors and synergizes with TRAIL. Cancer Biol Ther. 2008 Apr 27;7(4):603–8.

158. Mojsa B, Lassot I, Desagher S. Mcl-1 ubiquitination: unique regulation of an essential survival protein. Cells. 2014 Jan;3(2):418–37.

159. Zhong Q, Gao W, Du F, Wang X. Mule/ARF-BP1, a BH3-only E3 ubiquitin ligase, catalyzes the polyubiquitination of Mcl-1 and regulates apoptosis. Cell. 2005 Jul 1;121(7):1085–95.

160. Thomas LW, Lam C, Edwards SW. Mcl-1; the molecular regulation of protein function. FEBS Lett. Federation of European Biochemical Societies; 2010 Jul 16;584(14):2981–9.

161. Youle RJ, Strasser A. The BCL-2 protein family: opposing activities that mediate cell death. Nat Rev Mol Cell Biol. Nature Publishing Group; 2008 Jan 1;9(1):47–59.

162. Eichhorn JM, Alford SE, Sakurikar N, Chambers TC. Molecular analysis of functional redundancy among anti-apoptotic Bcl-2 proteins and its role in cancer cell survival. Exp Cell Res. Elsevier; 2014 Apr 1;322(2):415–24.

163. Fojo T, Bates S. Mechanisms of resistance to PARP inhibitors--three and counting. Cancer Discov. 2013 Jan;3(1):20–3.

164. Choi YH, Yu A-M. ABC transporters in multidrug resistance and pharmacokinetics, and strategies for drug development. Curr Pharm Des. 2014 Jan;20(5):793–807.

165. Jaspers JE, Kersbergen A, Boon U, Sol W, van Deemter L, Zander SA, et al. Loss of 53BP1 causes PARP inhibitor resistance in Brca1-mutated mouse mammary tumors. Cancer Discov. American Association for Cancer Research; 2013 Jan 1;3(1):68–81.

166. Bunting SF, Callén E, Wong N, Chen H-T, Polato F, Gunn A, et al. 53BP1 Inhibits Homologous Recombination in Brca1-Deficient Cells by Blocking Resection of DNA Breaks. Cell. 2010 Apr 16;141(2):243–54.

167. Bunting SF, Callén E, Kozak ML, Kim JM, Wong N, López-Contreras AJ, et al. BRCA1 functions independently of homologous recombination in DNA interstrand crosslink repair. Mol Cell. 2012 Apr 27;46(2):125–35.

168. Bouwman P, Aly A, Escandell JM, Pieterse M, Bartkova J, van der Gulden H, et al. 53BP1 loss rescues BRCA1 deficiency and is associated with triple-negative and BRCA-mutated breast cancers. Nat Struct Mol Biol. 2010 May 9;17(6):688–95.

169. Pettitt SJ, Rehman FL, Bajrami I, Brough R, Wallberg F, Kozarewa I, et al. A genetic screen using the PiggyBac transposon in haploid cells identifies Parp1 as a mediator of olaparib toxicity. PLoS One. 2013 Jan;8(4):e61520.

170. Liu X, Han EK, Anderson M, Shi Y, Semizarov D, Wang G, et al. Acquired resistance to combination treatment with temozolomide and ABT-888 is mediated by both base excision repair and homologous recombination DNA repair pathways. Mol Cancer Res. 2009 Oct;7(10):1686–92.

171. Edwards SL, Brough R, Lord CJ, Natrajan R, Vatcheva R, Levine DA, et al. Resistance to therapy caused by intragenic deletion in BRCA2. Nature. Nature Publishing Group; 2008 Feb 28;451(7182):1111–5.

172. Sakai W, Swisher EM, Karlan BY, Agarwal MK, Higgins J, Friedman C, et al. Secondary mutations as a mechanism of cisplatin resistance in BRCA2-mutated cancers. Nature. 2008 Feb 28;451(7182):1116–20.

173. Ikeda H, Matsushita M, Waisfisz Q, Kinoshita A, Oostra AB, Nieuwint AWM, et al. Genetic Reversion in an Acute Myelogenous Leukemia Cell Line from a Fanconi Anemia Patient with Biallelic Mutations in BRCA2. Cancer Res. 2003 May 15;63(10):2688–94.

174. Swisher EM, Sakai W, Karlan BY, Wurz K, Urban N, Taniguchi T. Secondary BRCA1 mutations in BRCA1-mutated ovarian carcinomas with platinum resistance. Cancer Res. 2008 Apr 15;68(8):2581–6.

175. Norquist B, Wurz KA, Pennil CC, Garcia R, Gross J, Sakai W, et al. Secondary Somatic Mutations Restoring BRCA1/2 Predict Chemotherapy Resistance in Hereditary Ovarian Carcinomas. J Clin Oncol. 2011 Jun 27;29(22):3008–15.

176. Karthikeyan S, Hoti SL. Development of Fourth Generation ABC Inhibitors from Natural Products: A Novel Approach to Overcome Cancer Multidrug Resistance. Anticancer Agents Med Chem. 2015 Jan;15(5):605–15.

177. Thiagalingam S, Cheng K-H, Lee HJ, Mineva N, Thiagalingam A, Ponte JF. Histone deacetylases: unique players in shaping the epigenetic histone code. Ann N Y Acad Sci. 2003 Mar;983:84–100.

178. Dokmanovic M, Clarke C, Marks PA. Histone deacetylase inhibitors: overview and perspectives. Mol Cancer Res. 2007 Oct 1;5(10):981–9.

179. Chao OS, Goodman OB. Synergistic loss of prostate cancer cell viability by coinhibition of HDAC and PARP. Mol Cancer Res. 2014 Dec 1;12(12):1755–66.

180. Krumm A, Barckhausen C, Kücük P, Tomaszowski K-H, Loquai C, Fahrer J, et al. Enhanced histone deacetylase activity in malignant melanoma provokes RAD51 and FANCD2 triggered drug resistance. Cancer Res. 2016 Mar 15;

181. Wiegmans AP, Yap P-Y, Ward A, Lim YC, Khanna KK. Differences in Expression of Key DNA Damage Repair Genes after Epigenetic-Induced BRCAness Dictate Synthetic Lethality with PARP1 Inhibition. Mol Cancer Ther. 2015 Oct 1;14(10):2321–31.

182. Konstantinopoulos PA, Wilson AJ, Saskowski J, Wass E, Khabele D. Suberoylanilide hydroxamic acid (SAHA) enhances olaparib activity by targeting homologous recombination DNA repair in ovarian cancer. Gynecol Oncol. 2014 Jun;133(3):599–606.

VII Abbreviations

Table 6: Abbreviations

AB	antibody
ATCC	American Type Culture Collection
BSA	bovine serum albumin
carbo	carboplatin
CHAPS	3-((3-cholamidopropyl) dimethylammonio)-1-propanesulfonate
Chk	Checkpoint kinase
CI	combination index/indices
Cis	cisplatin
CV	crystal violet
Dd	double distilled
DNA	desoxyribonuclease
Doxo	doxorubicin
EDTA	ethylenediaminetetraacetic acid
et al.	*et alii/aliae* (latin) and others
etop	etoposide
EV	empty vector
Fa	Fraction affected
FACS	fluorescence activated cell sorting
FCS	fetal calf serum
GAPDH	glyceraldehyde-3-phosphate dehydrogenase
HEPES	N-2-hydroxyethylpiperazine-N-2-ethane sulfonic acid
HRD-LOH	Homologous recombination deficiency-loss of heterozygosity
HRP	horseradish peroxidase
IC_{50}	inhibitory concentration
i.e.	*id est* (latin) that is
IP	immunoprecipitation
kD	kilo Dalton
MCL-1	induced myeloid leukemia cell differentiation protein Mcl-1
LMMP	Loss of mitochondrial membrane potential
mRNA	messenger RNA
MTT	methylthiazolyldiphenyl-tetrazolium bromide
MTX	methotrexate
NaCl	sodium chloride
Olap	olaparib
PARP	Poly(ADP)-ribose polymerase
PBS-T	phosphate buffered saline (tween-20)
pH	potential hydrogen
PI	propidium iodide
RNA	ribonucleic acid
RNAi	RNA interference
rpm	rounds per minute
RT	room temperature
SD	standard deviation
SDS	sodium dodecyl sulfate
siRNA	small interfering RNA
Tala	talazoparib
TMZ	temozolomide
WB	Western blot

VIII Materials

VIII.1 Cell lines

Table 7: Ewing's sarcoma cell lines

Cell line	p53	Fusion gene	Source
A4573	mutant	*EWS-FLI1*	AG Roessig
SK-ES-1	mutant	*EWS-FLI1*	AG Roessig
TC-32	mutant	*EWS-FLI1*	ATCC
TC-71	mutant	*EWS-FLI1*	ATCC

Table 8: Osteosarcoma cell lines

Cell line	p53	HRD-LOH	Mutational profile	Source
MG63	mutant	positive	*BAP1* ↓, *FANCA* ↓, *FANCD2* ↓	AG Nathrath
ZK-58	wt	positive	*BARD1* ↓, *FANCD2* ↑	AG Nathrath
SaOS-2	mutant	borderline	*CHEK2* ↓	AG Nathrath
MNNG-HOS	wt	borderline	*ATM* ↓, *PTEN* ↑, *FANCD2* ↑	AG Nathrath
U2OS	wt	negative	*BRCA2* ↓	AG Nathrath

Copy-number alterations (losses ↓, disruptive gains ↑)

Table 9: Packaging cell lines

Cell line	Subtype	Source
Phoenix (AMPHO)	2nd generation retrovirus-producing cell line	ATCC

VIII.2 Cell culture reagents

Table 10: Cell culture reagents

Reagent	Supplier
Blasticidine S hydrochloride	Carl Roth
Dulbecco's Modified Eagles Medium (DMEM) GlutaMAX-I	Life Technologies
Dulbecco's phosphate buffered saline (PBS)	Life Technologies
Fetal Calf Serum (FCS)	Life Technologies
Geneticin Disulfate salt (G418)	Sigma Aldrich
Penicillin/Streptomycin (10,000 U/ml)	Life Technologies
RPMI 1640 medium, GlutaMAX-I	Life Technologies
Sodium pyruvate (100 mM)	Life Technologies
Trypsin/EDTA (0.05%), phenol red	Life Technologies

VIII.3 Drugs & inhibitors

Table 11: Chemotherapeutic drugs

Drug	Mode of action	Supplier
Actinomycin D (AMD)	Anthracycline	Sigma Aldrich
Cisplatin (cis)	Alkylating agent	Medac
Carboplatin (carbo)	Alkylating agent	Medac
Doxorubicin (doxo)	Topoisomerase II inhibitor	Sigma Aldrich
Etoposide (etop)	Topoisomerase II inhibitor	Sigma Aldrich
Ifosfamide	Alkylating agent	Baxter
Methotrexate (MTX)	Antimetabolite	Medac
SN-38	Topoisomerase I inhibitor	Sigma Aldrich
Temozolomide (TMZ)	Alkylating agent	Sigma Aldrich
Vincristine (VCR)	Microtubule-inhibitor	Sigma Aldrich

Table 12: Small molecule inhibitors

Inhibitor	Mode of action	Supplier
Niraparib	PARP inhibitor	ChemieTek
Olaparib	PARP inhibitor	Selleckchem
Talazoparib	PARP inhibitor	Selleckchem
Veliparib	PARP inhibitor	Selleckchem
JNJ-26481585	HDAC inhibitor	Selleckchem

Table 13: Pharmacological inhibitors

Inhibitor	Mode of action	Supplier
Bortezomib	Proteasome inhibitor	Jansen-Cilag
ETR2	TRAIL receptor-2 antagonist	Human Genome Sciences
zVAD.fmk	Pan-caspase inhibition	Bachem

VIII.4 Antibodies

Table 14: Primary antibodies for Western blotting

Antibody	Working Dilution	Species	Supplier
anti-α-tubulin	1:5 000 in 2% BSA	mouse	Millipore
anti-BAK-	1:1 000 in 2% BSA	rabbit	BD Biosciences
anti-BAX-NT	1:1 000 in 2% BSA	rabbit	Millipore
anti-BCL-2	1:1 000 in 2% BSA	mouse	BD Biosciences
anti-BCL-X_L	1:1 000 in 2% BSA	rabbit	BD Biosciences
anti-BIM	1:1 000 in 2% BSA	rabbit	Cell Signaling
anti-BMF	1:1 000 in 2% BSA	rabbit	Novus Biologicals
anti-CHK1	1:1 000 in 2% BSA	mouse	Cell Signaling
anti-CHK2	1:1 000 in 2% BSA	mouse	Cell Signaling
anti-caspase-3	1:1 000 in 2% BSA	rabbit	Cell Signaling
anti-caspase-8	1:1 000 in 2% BSA	mouse	Enzo Life Science
anti-caspase-9	1:1 000 in 2% BSA	rabbit	Cell Signaling
anti-GAPDH	1:5 000 in 2% BSA	mouse	HyTest
anti-mBCL-2	1:1 000 in 2% BSA	mouse	Life Technologies
anti-MCL-1	1:1 000 in 2% BSA	rabbit	Enzo
anti-NOXA	1:1 000 in 2% BSA	mouse	Enzo Life Science
anti-PARP	1:1 000 in 2% BSA	mouse	Cell Signaling
anti-pCHK1	1:1 000 in 2% BSA	rabbit	Cell Signaling
anti-pCHK2	1:1 000 in 2% BSA	rabbit	Cell Signaling
anti-PUMA	1: 500 in 2% BSA	rabbit	Cell Signaling
anti-pH3	1:1 000 in 2% BSA	rabbit	Millipore

Table 15: Secondary antibodies for Western blotting

Antibody	Working Dilution	Species	Supplier
HRP-conjugated anti-mouse IgG	1:5 000 in 5% SMP in PBS-T	goat	Santa Cruz
HRP-conjugated anti-rabbit IgG	1:5 000 in 5% SMP in PBS-T	goat	Santa Cruz
IRDye800-conjugated anti-mouse IgG	1:5 000 in 5% SMP in PBS-T	donkey	LI-COR
IRDye680-conjugated anti-mouse IgG	1:5 000 in 5% SMP in PBS-T	donkey	LI-COR
IRDye800-conjugated anti-rabbit IgG	1:5 000 in 5% SMP in PBS-T	donkey	LI-COR
IRDye680-conjugated anti-rabbit IgG	1:5 000 in 5% SMP in PBS-T	donkey	LI-COR

Table 16: Primary antibodies for immunoprecipitation

Antibody	Amount	Species	Supplier
anti-BAK clone AB-1	4 µg/sample	mouse	Millipore
anti-BAX clone 6A7	4 µg/sample	mouse	Sigma

VIII.5 RNA interference (RNAi)

Table 17: Small interfering RNA (siRNA)

siRNA	Target	Cat. No.	Supplier
siControl	none	4390844	ThermoFisher
siBAK #1	BAK	s1880	ThermoFisher
siBAK #2	BAK	s1881	ThermoFisher
siBAX #1	BAX	S1889	ThermoFisher
siBAX #2	BAX	S1890	ThermoFisher
siNOXA #1	NOXA	s10708	ThermoFisher
siNOXA #2	NOXA	S10709	ThermoFisher

VIII.6 Plasmids

Table 18: BCL-2 overexpression

Plasmid	Plasmid backbone	Gene	Source
empty vector (EV)	pMSCV	none	C.A. Schmitt
BCL-2	pMSCV	mBCL-2	C.A. Schmitt

Table 19: MCL-1 phosphodegron-defective mutant

Name	Plasmid backbone	Gene	Source
empty vector (EV)	pCMB-Tag3B	none	Genentech
MCL-1 4A (*)	pCMB-Tag3B	MCL-1 4A	Genentech

(*): 4A = S64A/S121A/S159A/T163A

VIII.7 Reagents, Kits and Chemicals

Table 20: Reagents and Kits

Reagent/Kit	Supplier
Caspase 3/7 Green Detection Kit	ThermoFisher
Casyton	Roche
Dynabeads anti-mouse IgG	Life Technologies
FACS Clean / Rinse solution	BD Biosciences
FACS Flow sheath fluid	BD Biosciences
FACS Shutdown solution	BD Biosciences
Lipofectamine 2000	Life Technologies
Opti-MEM transfection medium	Life Technologies
Page Ruler Plus Prestained Protein Ladder	ThermoScientific
Pierce BCA protein assay	ThermoScientific
Pierce ECL Western Blotting Substrate	ThermoScientific
Protease Inhibitor Cocktail (PIC), 25x	Roche Diagnostics
RNAiMAX reagent	Life Technologies
SUPERFIX-MRP x-ray fixer	TETENAL

Table 21: Chemicals

Chemical/Compound	Supplier
2-propanol	Carl Roth
Acrylamide mix, 30% (Rotiphorese)	Carl Roth
Agar	Carl Roth
Albumin fraction V (BSA)	Carl Roth
Ammonium persulfate (APS)	Carl Roth
Ampicillin	Carl Roth
Bromophenol Blue	Carl Roth
Cholamidopropyldimethyl ammonio propane sulfonate (CHAPS)	Sigma-Aldrich
Crystal violet	Carl Roth
Dithiothreitol (DTT)	Millipore
Dimethyl sulfoxide (DMSO)	Sigma-Aldrich
3-(4,5-dimethylthiazol-2-yl)-2,5-diphenyltetrazolium bromide (MTT)	Roche Diagnostics
Disodium hydrogen phosphate dihydrate (Na_2HPO_4)	Carl Roth
Ethanol	Carl Roth
Ethylene diamine tetraacetic acid (EDTA)	Carl Roth
Formaldehyde	Carl Roth
Glycine	Carl Roth
Hoechst-33342	Sigma Aldrich
Hydrochloric acid (HCl)	Carl Roth
Hydroxyethyl piperazinylethane sulfonic acid (HEPES)	Carl Roth
Kanamycin	Carl Roth
LB medium	Carl Roth
Methanol	Carl Roth
Milk powder (skimmed milk powder, SMP)	Carl Roth
PMSF	Carl Roth
Potassium chloride (KCl)	Carl Roth
Potassium dihydrogen phosphate (KH_2PO_4)	Carl Roth
Propidium iodide (PI)	Sigma Aldrich
Sodium chloride (NaCl)	Carl Roth
Sodium dodecyl sulfate (SDS)	Carl Roth
Sodium hydroxide (NaOH)	Carl Roth
Tetramethylethylenediamine (TEMED)	Carl Roth
Tetramethylrhodamin-methylester ($TMRM^+$)	Sigma-Aldrich
TrisBase	Carl Roth
TrisHCl	Carl Roth
Triton X-100	Carl Roth
Tween-20	Carl Roth

VIII.8 Consumables

Table 22: Consumables

Product	Supplier
Aluminium foil	Carl Roth
Casy cups	Roche
Cell culture dishes (6 cm, 10 cm or 14.5 cm diameter)	Greiner Bio-One
Cell culture flasks (25 cm^2; 75 cm^2; 175 cm^2)	Greiner Bio-One
Cell culture plates (6-well; 24-well; 96-well)	Greiner Bio-One
Cell scraper	BD Biosciences
Combitips (0.25 ml; 0.5 ml; 5 ml; 10 ml)	Eppendorf
Centrifuge tubes (15 ml; 50 ml)	Greiner Bio-One
Cryogenic vials (1.8 ml)	Starlab
Disposal bags	Carl Roth
Dynabeads (pan-mouse IgG)	Dako
Filter tips (10 µl; 200 µl; 1 000 µl)	Starlab
Filter paper	Carl Roth
Hybond ECL nitrocellulose membrane	GE Healthcare
Hyperfilm ECL	GE Healthcare
Microcentrifuge tubes (0.5 ml; 1.5 ml; 2 ml)	Starlab
Nitrile gloves, sterile, powder-free	Kimberly-Clark
Parafilm	VWR
Pasteur pipettes (15 cm; 30 cm)	Carl Roth
Pipette tips (10 µl; 200 µl; 1,000 µl)	Starlab
Round-bottom tubes	BD Biosciences
Scalpels	B.Braun
Sterile culture vials	Carl Roth
Sterile filters (0.22 µm)	Millipore
Sterile pipettes (2 ml; 5 ml; 10 ml; 25 ml)	Greiner Bio-One
Syringes (5 ml; 10 ml; 20 ml)	B. Braun

VIII.9 Buffers

Table 23: Buffers

Buffer	Ingredients
Antibody dilution buffer	0.9% NaCl, 10 mM TrisHCl pH 7.5, 5 mM EDTA, 1 mg/ml BSA
Blocking buffer (5% SMP in PBS-T)	25 g milk powder in 500 ml PBS-T
Blotting buffer, 1x	11.6 g TrisBase, 5.8 g Glycine, 7.5 ml 10% SDS, and 400 ml methanol, add 2 liters ddH_2O
CHAPS lysis buffer	10 mM HEPES pH 7.4, 150 mM NaCl, 1% CHAPS
LB agar	15 g agar dissolved in 800 ml LB medium
Lysis buffer	30 mM TrisHCl, 150 mM NaCl, 1% Triton X-100, 10% Glycerol, 0.5 mM PMSF, 2 mM DTT, 1x PIC
MTT solution, 1x	10 ml MTT stock solution 5 mg/ml, 40 ml white RPMI (phenol-free)
Phosphate-buffered saline (PBS), 10x	400 g NaCl, 10 g KCl, 10 g KH_2PO_4, 72 g Na_2HPO_4 in 5 liters of ddH_2O, pH 7.4
PI buffer, hypotonic	0.05% Trisodium citrate dihydrate pH 7.4, 0.05% Triton X-100, 50 µg/ml PI
PI solution	1 µg/ml PI in PBS
PBS with 0.1% Tween 20 (PBS-T)	1 ml Tween 20 in 1,000 ml 1x PBS
Running buffer, 5x	30.2 g TrisBase, 188 g Glycine, and 100 ml 10% SDS in 2 liters of ddH_2O
SDS loading buffer, 6x	360 mM TrisBase pH 6.8, 30% Glycerol, 120 mg/ml SDS, 93 mg/ml DTT, 12 µg/ml bromophenol blue

VIII.10 Equipment

Table 24: Equipment

Equipment	Supplier
ARE heating magnetic stirrer	VELP Scientifica
Avanti J-26 XP ultracentrifuge	Beckman Coulter
Casy Cell Counter	Roche
Centrifuge MIKRO 200 R	Hettich
Centrifuge ROTIXA 50 RS	Hettich
Centrifuge ROTANTA 460 R	Hettich
CO_2 incubator	SANYO
Easypet (3)	Eppendorf
Electronic analytical balance EW	Kern
Electronic precision balance 770	Kern
FACSCanto II	BD Biosciences
HeraSafe class II biological safety cabinet	Kendro
ImageXpress Micro XLS system	Molecular Devices
Infinite M100 microplate reader	Tecan
Innova 4230 bacteria shaker	New Brunswick Scientific
Microcentrifuge	Benning
Microscope CKX41, cell culture	Olympus
Mini-PROTEAN Tetra Cell electrophoresis system	Bio-Rad
Multipette plus	Eppendorf
NanoDrop 1000 spectrophotometer	PEQLAB
Odyssey infrared imaging system	LI-COR
PerfectBlue Dual Gel Twin L electrophoresis system	PEQLAB
pH meter inoLab pH7310	WTW
Pipettes Research plus (2.5 µl; 10 µl; 20 µl; 100 µl; 200 µl; 1 000 µl)	Eppendorf
Power Pac HC high-current power supply	Bio-Rad
Rocking shaker	MS-L
Roller mixer	Ratek
SANYO incubator MIR-262	New Brunswick Scientific
Sunrise microplate reader	Tecan
Thermomixer comfort	Eppendorf
Trans-Blot SD semi-dry transfer cell	Bio-Rad
V-150 autoclave	SysTec
Vacuum pump HLC	Ditabis
Vortex mixer (ZX classic; wizard X)	VELP Scientifica
Water bath SWB20	Medingen

VIII.11 Software

Table 25: Software

Software	Company
CalcuSyn version 2.0	Biosoft
FACSDiva version 6.1.3	BD Biosciences
FlowJo version 7.6.5	Tree Star
i-control version 1.10	Tecan
ImageJ version 1.48v	National Institutes of Health
Image Studio version 2.1.10	LI-COR
ImageXpress 2015	Molecular Devices
Magellan Data Analysis version 7.2	Tecan
Mendeley Desktop version 1.15.1	Mendeley
MS-Office 2013	Microsoft Deutschland GmbH
Origin 9.0	OriginLab
Paint.NET v4.0.5.	dotPDN LLC
SigmaPlot 12.5	Systat software

List of figures

List of tables

Zusammenfassung

Die beiden häufigsten primäre Knochenmalignome sind Osteosarkom (OS) und Ewing Sarkom (ES). Beide Krebsarten gelten als aggressiv, stark metastasierend und treten vor allem bei Kindern, Jugendlichen und jüngeren Erwachsenen auf. Jedoch unterscheiden sich ES und OS deutlich in ihrer Pathogenese. Im OS, als stark heterogene Krankheit, reicht meist eine Zelle mit mutiertem p53 Protein aus, um in Expansion von diesem Zellklon den Tumor zu formen. Charakteristisch für das OS ist die hohe Instabilität des Genoms dessen Neuanordnungen und die Umgestaltung der Chromosomen zur Tumorgenese führen. ES entsteht in 85% aller Fälle durch Translokationen zwischen Chromosom 11 und Chromosom 22 resultierend in einem chimären Fusionsgen *EWS-FLI1*, t(11;22)(q24:q12) und in mehr als 10% durch Translokationen zwischen Chromosom 21 mit Chromosom 22 *EWS-ERG*, t(21;22)(q22;q12). Diese Fusionsgene exprimieren ein Fusionsprotein. Dieses Fusionsprotein EWS-FLI1, oder auch EWS-ERG, fungiert als Transkriptionsfaktor, der den Zellmetabolismus beeinflusst und so zur Tumorgenese führt. Trotz deutlicher Unterschiede in der Entstehung beider Tumorarten, teilen sich beide Krankheiten wesentliche Tumorcharakteristika. Dazu zählen, schnelle Progression und Metastasierung, einschließlich Neovaskularisation, hohe Invasionsbereitschaft, Resistenz gegenüber Chemotherapeutika und Umgehung der körpereigenen Immunantwort. Da OS, als sowohl ES mesenchymalen Ursprungs sind, ist die epithelialen zur mesenchymalen Transition in Knochensarkomen weitestgehend vernachlässigbar. Ein Vorgang, der in Knochensarkomen weniger ausführlich beschrieben ist, ist die Bildung von Mikrometastasen in tumorfernen Geweben, vor allem der Lunge. Lange nach der Entfernung des primären Tumors, können solche Metastasen zu der Rückkehr des Tumors führen (Rezidiv). Die Entstehung der Metastasen wirkt sich negativ auf die Überlebensraten in beiden Tumorentitäten aus. Während ohne Metastasen die Überlebensrate nach fünf Jahren sowohl im OS, als auch im ES bei 70% - 75% liegt, wird diese deutlich durch Metastasen in der Lunge auf 30% verringert. Das zeigt die Notwendigkeit weiterer Forschung, um die biologischen Grundlagen beider Krebsarten besser zu verstehen. Weiterhin gilt es bestehende Behandlungsmethoden zu verbessern und zu erweitern, um das Überleben von Kindern die unter OS oder ES leiden zu verlängern.

Die Funktion von poly(ADP)-ribose polymerase (PARP), DNA Schäden zu reparieren und die Möglichkeit, dass PARP Inhibitoren die zytotoxische Aktivität von alkylierenden Chemotherapeutika erhöhen, wurde zuerst in den 1980er Jahren gezeigt. In ersten Studien wurde demonstriert, dass *BRCA1* oder *BRCA2* defiziente Tumorzellen Sensitivität gegenüber PARP Inhibitoren aufweisen. BRCA1/2 sind zentrale Proteine des Homologen Rekombination (HR) Reparatur Signalweges. Die Mutation von *BRCA1/2* und sowohl der Verlust ihrer Funktion, als auch der Verlust weiterer Gene, die mit BRCA in dem HR Signalweg

assoziiert sind und im HR Defekt enden, wird als BRCAness bezeichnet. Tumorzellen welche BRCAness aufweisen wurden als sensitiv gegenüber PARP Inhibitoren beschrieben. Fehlende Reparatur von DNA Schäden durch HR erzeugt eine Abhängigkeit der Zellen von einem anderen Reparatursignalweg, dem so genannten Basen Exzisionsreparaturweg (BER). In BER nimmt PARP eine zentrale Rolle bei der Reparatur von Basenschäden ein. Wird PARP in der Folge inhibiert, so sterben Zellen welche BRCAness aufzeigen durch synthetische Letalität. Synthetische Letalität liegt dann vor, wenn mehrere Mutationen in zwei oder mehr Genen zum Zelltod führen, wohingegen eine Mutation in nur einem dieser Gene für die Zelle kompensierbar ist. Eine weitere Eigenschaft die Sensitivität gegenüber PARP Inhibitoren erzeugt, ist die erhöhte Expression des PARP Proteins. Vermittelt durch das Fusionsprotein ESW-FLI1 oder EWS-ERG weist ES hohe PARP Expressionslevel auf. Aus diesem Grund konnte bereits in früheren Studien im ES gezeigt werden, dass für diese Krebsart eine Sensitivität gegenüber PARP Inhibitoren besteht. Jedoch, blieb in diesen Studien unklar welche molekularen Zelltodmechanismen dieser PARP Inhibitor vermittelten Zytotoxizität zu Grunde liegen.

Sowohl in präklinischen, als auch in klinischen Studien werden PARP Inhibitoren meist zusammen mit Chemotherapeutika verabreicht, da diese die Aktivität von PARP Inhibitoren steigern können. Diese Steigerung beruht auf den unterschiedlichen Wirkmechanismen von PARP Inhibitoren. Neben der Inhibition der enzymatischen Aktivität von PARP, sind PARP Inhibitoren in der Lage an DNA gebundene PARP Proteine zu binden. Diesen Vorgang nennt man „PARP-trapping“. PARP-trapping von PARP Molekülen an die DNA und die darauf folgende Beeinträchtigung der DNA Replikation, stellen den zentralen Mechanismus der von PARP Inhibitoren vermittelten Zytotoxizität dar. Dies wurde in verschiedenen Studien demonstriert. So weisen unterschiedliche PARP Inhibitoren verschieden starke Aktivitäten bei der Unterdrückung von Tumorzellwachstum auf, wobei alle neuartigen PARP Inhibitoren die enzymatische Aktivität mit vergleichbarer Dissoziationskonstante von PARP hemmen ($K_i \approx 1 – 5$ nM). Es wurde gezeigt, dass PARP-trapping dieses Phänomen erklärt. Konsequenterweise zeigen PARP Inhibitoren mit der stärksten PARP-trapping Aktivität die niedrigsten IC_{50} Konzentrationen die nötig sind, um die Viabilität von Capan-1 Zellen zu inhibieren. Folgende IC_{50} Konzentrationen für PARP Inhibitoren in Capan-1 Zellen wurden beschrieben: 5 nM Talazoparib, 259 nM Olaparib, 609 nM Rucaparib, 650 nM Niraparib oder > 10 000 nM Veliparib. Dazu passend untersuchte Murai *et al.* in einer Studie die PARP-trapping Aktivität der unterschiedlichen PARP Inhibitoren. Sie riefen in gleicher Reihenfolge der PARP Inhibitoren PARP-trapping hervor wie sie zuvor für Zytotoxizität in Capan-1 Zellen gezeigt wurde. Talazoparib wurde als stärkster PARP Inhibitor gezeigt (≈ 100-fach stärker als Olaparib, Rucaparib oder Niraparib), während Veliparib als schwächster PARP Inhibitor beschrieben wurde (≈ 100-fach schwächer

als Olaparib, Rucaparib oder Niraparib). In diesen Ergebnissen wurde dargestellt, dass die Inhibition der enzymatischen Aktivität von PARP eine sekundäre Rolle bei der Vermittlung der Zytotoxizität spielt und die Intensität des PARP trappings die Wirksamkeit eines PARP Inhibitors bestimmt.

Mögliche Behandlungsstrategien zur Bekämpfung von Knochensarkomen sind Bestrahlung, Operation und Chemotherapie. Die Chemotherapie beinhaltet Substanzen welche die DNA schädigen oder deren Reparatur verhindern. Dadurch werden besonders schnell replizierende Krebszellen gegenüber Chemotherapeutika sensitiviert. Es gibt mehrere Klassen von Chemotherapeutika die sich aus deren Wirkmechanismen ergeben. Dies sind z.B. alkylierende Substanzen, Anthrazykline, Antimetabolite, Topoisomerase Inhibitoren I und II, Mirkotubuli Inhibitoren und Kortikosteroide. Um in unseren Studien einen kombinatorischen Effekt, also die Reduktion der Zellviabilität durch PARP Inhibitoren in gleichzeitiger Behandlung mit Chemotherapeutika zu untersuchen, haben wir unterschiedliche Substanzklassen von Chemotherapeutika zusammen mit PARP Inhibitoren getestet Bei der Auswahl der Chemotherapeutika haben wir uns vor allem auf jene Substanzen konzentriert, die bereits für die Therapie des jeweiligen Tumors in der Klinik eingesetzt werden.
Für OS haben wir Kombinationen der alkylierenden Substanz Temozolomid (TMZ), dem Topoisomerase I Inhibitor SN-38, der alkylierenden Substanz Cisplatin (Cis), dem Topoisomerase II Inhibitor Doxorubicin (Doxo), dem Antimetabolit Methotrexat (MTX) und eine Kombination aus der alkylierenden Substanz Carboplatin (Carbo) zusammen mit dem Topoisomerase II Inhibitor Etoposid (Etop) zusammen mit dem stärksten PARP Inhibitor Talazoparib in fünf verschiedenen OS Zelllinien getestet. Die Kombination Etop/Carbo wurde getestet um die Behandlung im Rezidiv bei OS widerzuspiegeln.
Für ES haben wir zusammen mit vier unterschiedlichen PARP Inhibitoren (Talazoparib, Olaparib, Niraparib und Veliparib), die Kombinationen mit den Chemotherapeutika TMZ, SN-38, Etop, die alkylierende Substanz Ifosfamid, Doxo, den Mikrotubuli Inhibitor Vincristin (VCR) und das Anthrazyklin Actinomycin D (AMD) in zwei unterschiedlichen ES Zelllinien getestet. Anschließend haben wir untersucht, welche Signalwege des programmierten Zelltods von der potentesten Kombination aus PARP Inhibitor und Chemotherapeutika ausgelöst wurden.

Programmierter Zelltod ist ein kontrollierter Mechanismus der von Organismen genutzt wird, um alte, beschädigte oder überflüssige Zellen, zum Beispiel während der Embryonalentwicklung, zu beseitigen. Eine Form von programmiertem Zelltod ist Apoptose. Charakteristika dieses Zelltods sind unter anderem das Schrumpfen der Zelle, Kondensation/Fragmentation der DNA und Verlust der Membranintegrität. Mechanistisch ist Apoptose in zwei Signalwege unterteilt, der intrinsische, mitochondriale Signalweg und

der extrinsische, Todesrezeptor Signalweg. Beide Signalwege lassen sich durch Bestrahlung oder Chemotherapie induzieren und konvergieren am Mitochondrium mit dem Verlust des mitochondrialen Membranpotentials und der Aktivierung von Caspasen als Effektormoleküle. Der mitochondriale Signalweg ist dabei streng durch pro- und anti-apoptotische Proteine der BCL-2-Familie reguliert. Die Proteine der BCL-2 Familie lassen sich anhand ihrer BCL-2 Homologie Domäne (BH Domäne) in drei unterschiedliche Gruppen einteilen. BCL-2, BCL-X_L und MCL-1 sind die Vertreter der anti-apoptotischen Proteine die alle vier BH Domänen aufweisen und pro-apoptotischen Proteine binden. Pro-apoptotische Proteine die ebenfalls alle vier BH Domänen aufweisen sind BAK, BAX und BOK. BAK und BAX unterlaufen nach ihrer Aktivierung eine Konformationsänderung und bilden eine Pore in der äußeren Mitochondrienmembran. Dies ist verantwortlich für die Depolarisation des Mitochondriums. Pro-apoptotische Proteine welche nur die BH3 Domäne aufweisen sind unter anderem BID, BIM, PUMA oder NOXA. Alle Proteine der BCL-2 Familie bilden ein komplexes Zusammenspiel, um das Mitochondrium in der lebenden Zelle vor Depolarisation zu schützen oder während der Apoptose zu depolarisieren. Oftmals weisen Krebszellen erhöhte Level an anti-apoptotischen Proteinen auf, was Stressresistenz erzeugt und Tumorwachstum fördern kann. Depolarisiert das Mitochondrium, z.B. in der Folge BAK und BAX Aktivierung, so werden Faktoren aus dem Mitochondrium in das Zytoplasma freigesetzt die Caspasen aktivieren und zu Zelltod führen.

In unseren Untersuchungen von PARP-Inhibitoren zusammen mit Chemotherapeutika im Ewing Sarkom, sowie Osteosarkom haben wir systematisch, klinisch relevante Kombinationsbehandlungen getestet um die besten kombinatorischen Behandlungsmöglichkeiten zu bestimmen. Für ES haben wir vier verschiedene PARP-Inhibitoren (Talazoparib, Olaparib, Niraparib und Veliparib) in Kombination mit sieben verschiedenen Chemotherapeutika getestet. Solch ein ausführliches Screening nach einem kombinatorischen Effekt konnte bisher noch nicht gezeigt werden. Darüber hinaus haben die der Synergie zwischen PARP Inhibitor und Chemotherapeutika zugrunde liegenden, molekularen Zelltodmechanismen aufzuklären. Das Osteosarkom weist, wie wir durch Exon-Sequenzierung primärer Tumorproben zeigen konnten, unterschiedliche Mutationsprofile auf, welche charakteristisch für BRCAness sind. Deshalb war es zunächst unser Ziel die Sensitivität von OS Zelllinien gegenüber dem PARP Inhibitor Talazoparib zu testen. Zweitens, komplementär zu ES, untersuchten wir die synergistische Wirkung, von im OS klinisch relevanten Chemotherapeutika in Kombination mit Talazoparib. Zuletzt haben wir versucht unsere zuvor gezeigten Zelltodmechanismen aus dem ES Projekt im OS zu validieren, da OS einen unterschiedlichen genetischen Hintergrund besitzt.

In unserem Screening von ES Tumorzelllinien haben wir vier verschiedene PARP-Inhibitoren verwendet die bereits ausführlich in klinischen Studien (Phase I – III) untersucht werden. In Kombination mit einer Auswahl von Chemotherapeutika konnten wir unterschiedliche Wirksamkeiten in der Kombination der Substanzen feststellen. Im ES waren PARP Inhibitoren besonders geeignet die Zytotoxizität von TMZ oder SN-38 zu potenzieren. Weiterhin konnten wir eine schwache Steigerung der Zytotoxizität von Doxorubicin, Etoposid oder Ifosfamid nachweisen. Im Gegensatz dazu waren die Kombinationen mit AMD und VCR die additiv oder antagonistisch zusammen mit PARP Inhibitoren reagierten nicht geeignet für eine Kombinationsbehandlung. Bei der Untersuchung der molekularen Mechanismen des Zelltods wurde die zentrale Rolle der mitochondrialen, intrinsischen Apoptose deutlich, die die Wirkung von PARP Inhibitoren zusammen mit TMZ vermittelt. Unsere Experimente haben gezeigt, wie durch TMZ vermittelte Methylierung und gleichzeitiges PARP-trapping, DNA-Strangbrüche erzeugt werden. Diese DNA Schäden lösen die Aktivierung der Checkpoint Kinasen 1 und 2 aus und die Zelle arretiert in der G_2-Zellzyklusphase. Die Kombination von Olaparib und TMZ führte darüber hinaus zur proteasomalen Degradierung von MCL-1 und der Aktivierung der pro-apoptotischen BCL-2 Proteine BAK und BAX. Durch BAK/BAX Aktivierung wurde der Verlust des mitochondrialen Membranpotentials und die Aktivierung der Caspasen ausgelöst. Die Bedeutung des intrinsischen Apoptose Signalwegs für die Kombination von Olaparib und TMZ konnten wir mit weiteren Experimenten bestätigen. Durch Zugabe des Caspase Inhibitor zVAD.fmk, Herrunterregulation von *NOXA* oder *BAK/BAX* mittels siRNA, die Überexpression von BCL-2 oder die Expression einer nicht abbaubaren, für Phosphorylierungen defekten MCL-1 Mutante führten allesamt zu einer signifikanten Reduktion der durch Olaparib/TMZ-induzierten Apoptose.

In unseren Experimenten mit Talazoparib im OS haben wir die Korrelation zwischen BRCAness und PARP Inhibitor Sensitivität in verschiedenen Zelllinien validiert. Weiterhin haben wir Talazoparib mit sechs verschiedenen, für das OS klinisch relevanten chemotherapeutischen Substanzen kombiniert und auf synergistische Effekte untersucht. Als erstes konnten wir klar zeigen, wie der genetische Hintergrund von OS Ziellinien zur Sensitivität gegenüber PARP Inhibitoren führt. Dazu haben wir die genomische Instabilität via homologe Rekombination Defizienz (HRD) – Verlust der Heterozygosität (LOH) als Marker für BRCAness und die Genmutationen HR assoziierter Proteine bestimmt. Zelllinien die positiv für HRD-LOH waren, (MG63 und ZK-58) zeigten konsequenterweise auch eine hohe Sensitivität gegenüber Talazoparib. Weniger Talazoparib sensitive Zelllinien (SaOS-2 und MNNG-HOS), waren weder positiv noch negativ, beziehungsweise positiv für HRD-LOH. Diese Zelllinien wiesen zwar eine hohe genomische Instabilität auf, aber auch einen triploiden Chromosomensatz welcher die Auswertung erschwerte. Die HRD-LOH negative Zelllinie, U2OS, zeigte keine Sensitivität gegenüber Talazoparib. Um die beste Kombination von PARP

Inhibitor und Chemotherapeutika zu bestimmen, haben wir den Kombinationsindex, sowie den Anteil der betroffenen Zellpopulation berechnet und als Kombinationsindex über den Anteil der betroffenen Zellpopulation dargestellt. Talazoparib zusammen mit TMZ zeigte den potentesten Synergismus und war den Kombinationen Talazoparib/Doxorubicin oder Talazoparib/Cisplatin in der Induktion von Zelltod in OS Zellen deutlich überlegen. Deshalb konzentrierten wir uns abschließend auf Schlüsselexperimente um den zuvor von uns beschrieben Zelltodmechanismus für einen PARP Inhibitor zusammen mit TMZ im OS zu validieren. Auch in diesem Modell kooperierte Talazoparib zusammen mit TMZ um mitochondriale Apoptose auszulösen. Das mitochondriale Apoptose in Talazoparib/TMZ-induzierten Zelltod eine wesentliche Rolle spielt, konnten wir durch weitere Experimente belegen. So führt die Behandlung von OS mit Talazoparib und TMZ zu einer Aktivierung von BAK und BAX, dem Verlust des mitochondrialen Membranpotentials und der Aktivierung von Caspasen.

Zusammen weisen diese Ergebnisse wichtige Implikationen für die Entwicklung neuer Behandlungsstrategien von OS mit PARP-Inhibitoren allein, oder in Kombination mit Chemotherapeutika (insbesondere TMZ) auf. Außerdem betonen sie deren wichtige Rolle für die Chemosensitivierung von ES und bieten eine neue Behandlungsoption für BRCAness positive OS Tumore.

Eidesstaatliche Erklärung

Ich erkläre hiermit an Eides Statt, dass ich die vorgelegte Dissertation mit dem Titel „PARP inhibitors in combination with chemotherapeutics target the underlying genetic phenotype of Ewing's sarcoma and osteosarcoma to induce cell death or synthetic lethality" selbstständig angefertigt und mich anderer Hilfsmittel als der in ihr angegebenen nicht bedient habe, insbesondere, dass alle Entlehnungen aus anderen Schriften mit Angabe der betreffenden Schrift gekennzeichnet sind.

Ich versichere, nicht die Hilfe einer kommerziellen Promotionsvermittlung in Anspruch genommen, sowie die Grundsätze der guten wissenschaftlichen Praxis beachtet zu haben.

Frankfurt, den 9. August 2016 *Florian Engert*